WYLE LABORATORIES
SCIENTIFIC SERVICES AND SYSTEMS GROUP
EASTERN OPERATIONS
FACILITIES LOCATED IN
HUNTSVILLE, ALA. AND HAMPTON, VA.

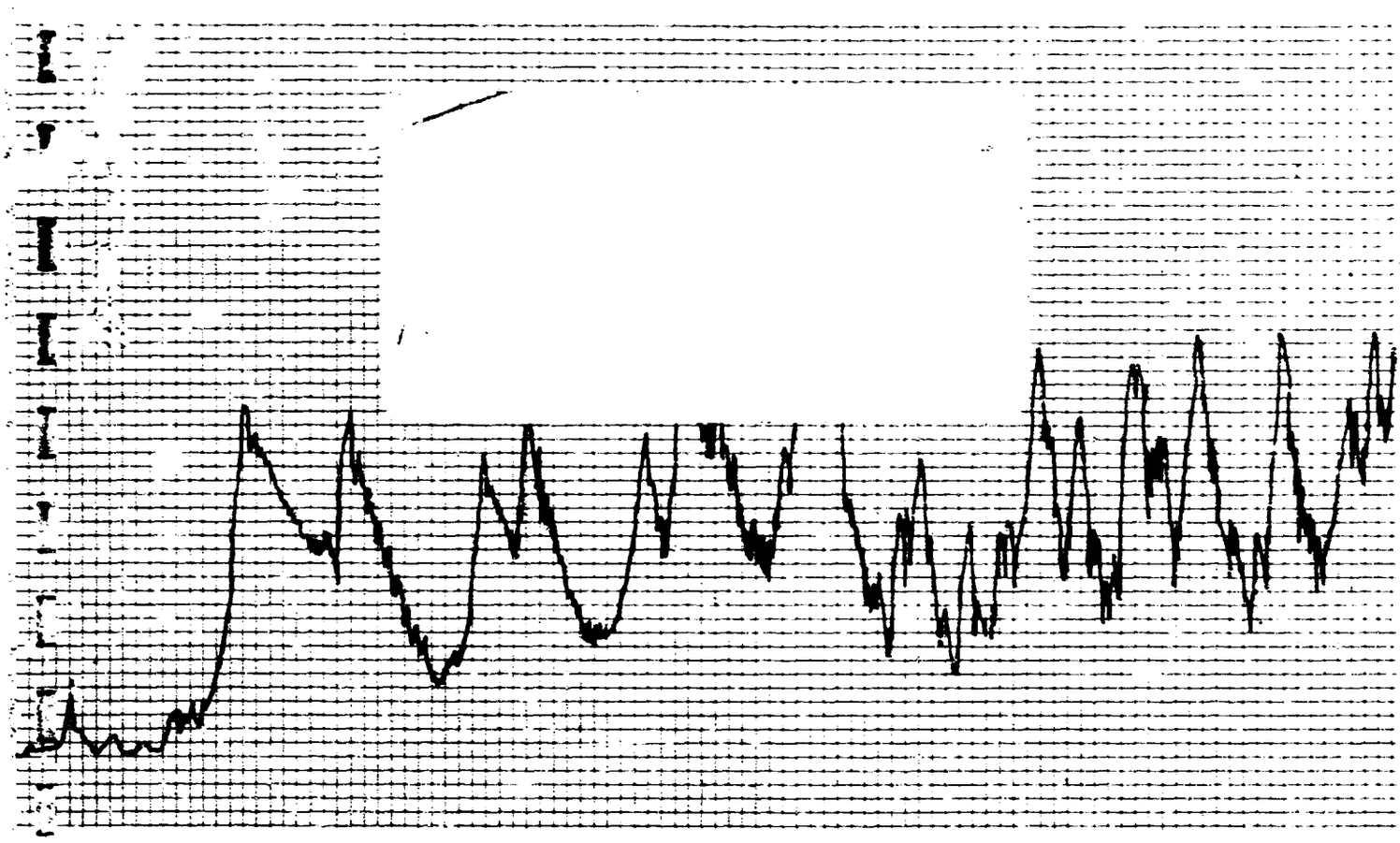

(NASA-CR-124347) PREDICTION OF SPACE SHUTTLE FLUCTUATING PRESSURE ENVIRONMENTS, INCLUDING ROCKET PLUME EFFECTS Final Report (Wyle Labs., Inc.) 156 p HC $10.00 CSCL 22B G3/31

N73-29885

Unclas 15228

research REPORT

WYLE LABORATORIES — RESEARCH STAFF

REPORT WR 73-6

PREDICTION OF SPACE SHUTTLE FLUCTUATING PRESSURE ENVIRONMENTS, INCLUDING ROCKET PLUME EFFECTS

By

Kenneth J. Plotkin
J. E. Robertson

June 1973

FINAL REPORT

of

Work Performed Under Contract NAS8-26919

WYLE LABORATORIES

Copy No. 08

ABSTRACT

Preliminary estimates of Space Shuttle fluctuating pressure environments have been made based on prediction techniques developed by Wyle Laboratories. Particular emphasis has been given to the transonic speed regime during launch of a parallel-burn Space Shuttle configuration. A baseline configuration consisting of a lightweight orbiter and monolithic SRB, together with a typical flight trajectory, have been used as models for the predictions. Critical fluctuating pressure environments are predicted at transonic Mach numbers with the following maximum overall fluctuating pressure levels: 1) shoulder-induced flow separation (157 dB), 2) terminal shock-wave oscillation (164 dB), 3) protuberance flows (168 dB), 4) compression-corner induced separated flow (148-157 dB), 5) shock-induced interference flow (161 dB), 6) shock-free interference flow (150 dB), and 7) attached turbulent boundary layer flow (137 dB). Comparisons between predicted environments and wind tunnel test results, in general, showed good agreement. Predicted one-third octave band spectra for the above environments were generally one of three types: 1) attached turbulent boundary layer spectra (typically high frequencies), 2) homogeneous separated flow and shock-free interference flow spectra (typically intermediate frequencies), and 3) shock-oscillation and shock-induced interference flow spectra (typically low frequencies). Predictions of plume induced separated flow environments were made. Only the SRB plumes are important, with fluctuating levels comparable to compression-corner induced separated flow and shock oscillation.

TABLE OF CONTENTS

		Page
ABSTRACT		ii
TABLE OF CONTENTS		iii
LIST OF FIGURES		iv
1.0	INTRODUCTION	1
2.0	FLUCTUATING PRESSURE ENVIRONMENTS	3
3.0	GENERAL PREDICTION FORMULAE	6
3.1	Overall Fluctuating Pressure Level	6
3.2	Power Spectra	8
3.3	Cross-Power Spectra	10
4.0	FLUCTUATING PRESSURE ENVIRONMENTS FOR SPACE SHUTTLE	12
4.1	Description of Space Shuttle Vehicles	12
4.2	Description of Flow Fields	12
4.3	Predicted Fluctuating Pressure Levels	18
4.4	Predicted Power Spectra	23
5.0	ANALYSIS OF CRITICAL SPACE SHUTTLE FLIGHT CONDITIONS	28
5.1	Maximum Dynamic Pressure, MAX Q	30
5.2	Critical Expansion-Induced Separated Flows	32
5.3	Critical Transonic Shock-Oscillation Environments	32
5.4	Critical Interference-Flow Environments	32
5.5	Comparison of Predictions with Experimental Measurements	33
6.0	CONCLUDING REMARKS	34
REFERENCES		36
FIGURES		39
APPENDIX A	— Summary of Prediction Methods for In-Flight Fluctuating Pressure Environments	A-1
APPENDIX B	— Shock Wave Oscillation Driven by Turbulent Boundary Layer Fluctuations	B-1
APPENDIX C	— Mathematical Properties of the Empirical Spectra	C-1
APPENDIX D	— Computer Program Descriptions	D-1

LIST OF FIGURES

Figure		Page
1.	Comparison of Pressure Fluctuation Measurements by Various Investigators for Attached Turbulent Boundary Layers	39
2.	Variation of Fluctuating Pressure Level for Homogeneous Separated Flow with Mach Number	40
3.	Variation of Fluctuating Pressure Level for Shock-Wave Oscillation with Mach Number	41
4.	Power Spectra for Turbulent Boundary Layer Fluctuating Pressures	42
5.	Power Spectrum of Fluctuating Pressures within Homogeneous Separated Flow Regions	43
6.	Comparison of Predicted and Measured Power Spectra for Shock-Wave Oscillation Upstream of Two- and Three-Dimensional Separated Flow Fields	44
7.	Longitudinal Distribution of Pressure Fluctuations and Typical Power Spectra in Vicinity of Supersonic Flow Separation Ahead of a 45° Wedge	45
8(a).	Narrow Band Longitudinal Space Correlation Coefficient for Boundary Layer Fluctuating Pressures	46
8(b).	Narrow Band Lateral Space Correlation Coefficient for Boundary Layer Fluctuating Pressures	46
9.	Typical Longitudinal Cross-Spectra of Pressure Fluctuations for Separated Flow (Reference 14)	47
10.	Schematic of Baseline Shuttle Launch Configuration	48
11.	Trajectory Parameters for Baseline Shuttle Configuration	49
12.	Schematic of Interference-Free Flows Over a Cone-Cylinder Body	50
13.	Location of Plume-Induced Separation Points on Baseline Shuttle	51
14.	Basic Attached Flow Fluctuating Pressure Level, Shuttle Launch Trajectory	52

LIST OF FIGURES (Concluded)

Figure		Page
15.	Maximum Fluctuating Pressure Coefficient for Separated Flow Behind a Cone-Cylinder Shoulder for Transonic Flight ($0.6 \leq M_\infty \leq M_a$)	53
16.	Variation of Terminal Shock-Wave Location with Free-Stream Mach Number for Interference-Free Flow Over Cone-Cylinder Bodies	54
17.	Variation of Terminal Shock-Wave Location, Interpolated for 17.5° and 22.5°	55
18.	Variation of Transonic Shock-Induced Pressure Fluctuations With Free-Stream Mach Number for Various Cone-Cylinder Configurations (Reference 18)	56
19.	Basic Compression Corner Fluctuating Pressure Level, Shuttle Launch Trajectory	57
20.	Basic Compression Corner Shock Oscillation Fluctuating Pressure Environment, Shuttle Launch Trajectory	58
21.	One-Third Octave Band Spectra for Typical Fluctuating Pressure Environments at MAX Q	59
22.	One-Third Octave Band Spectrum for Shoulder-Induced Separated Flow on the SRB at Low Transonic Mach Number	60
23.	One-Third Octave Band Spectra for Terminal Shock-Wave Oscillation on the SRB at Transonic Mach Numbers	61
24.	One-Third Octave Band Spectra for Critical Interference-Flow Environments	62
25.	Comparison of Measured and Predicted Overall Fluctuating Pressure Levels for a Typical Parallel-Burn Space Shuttle Launch Configuration at Transonic Mach Numbers	63

1.0 INTRODUCTION

During launch and flight through the atmosphere, the external surfaces of the Space Shuttle vehicles will be exposed to high intensity acoustic and fluctuating pressure environments. These environments will be critical to the design and success of the complete Space Shuttle system. Definition of the environments is necessary, therefore, in order to insure structural integrity, reliability and the economic operational requirements of the Space Shuttle. In order to arrive at an optimized Space Shuttle system, accurate definition of the critical acoustic environments which will be encountered during Space Shuttle flight is required at the earliest possible time during the development stage.

Wyle Laboratories is engaged in a research program under NASA-MSFC Contract NAS8-26919 to develop reliable methods of predicting critical acoustic environment trends during Space Shuttle flight. The primary objective of this study is to perform a critical analysis of the acoustic and fluctuating pressure environments for the complete flight envelope of the Space Shuttle. Particular emphasis is to be directed to the area of fluctuating pressure environments as encountered during flight through the atmosphere. Key features of this investigation have been the bringing together of data from disparate sources, combining the results to show general trends for the various unsteady phenomena, the development of prediction methods based on the combined results, and the application of the prediction methods in the final assessment of critical environments for the Space Shuttle vehicle.

In early phases of this program, effort was devoted to a study of basic aerodynamic and acoustic environments for the purpose of: 1) formulating prediction methods for the basic fluctuating pressure environments which are encountered by aerospace vehicles; and 2) definition of the fluctuating pressure environments which are unique to the Space Shuttle vehicles. During this phase of the study, emphasis was given to the transonic speed regime during launch. During the past year, work was continued on the development of prediction techniques. Prediction schemes were refined and incorporated into computer programs.

During the past year, flow field analysis and fluctuating environment prediction schemes were extended to include effects of rocket exhaust plume-induced separation. An extensive investigation of plume-induced separation was undertaken for the purpose of: 1) developing a scheme to predict the extent of plume-induced separation regions, and 2) evaluating the fluctuating environment associated with such regions. The results of this study were the subject of a recent report, and are incorporated into the predictions of the present report.

This report presents the latest predictions for a Space Shuttle launch configuration. Selection of the vehicle booster and orbiter design and specification of trajectory parameters is presently in progress. Although these vital criteria have not been finalized, it is necessary to proceed with engineering studies to arrive at preliminary estimates of both steady and unsteady aerodynamic loads which will be encountered during atmospheric flight by the Space Shuttle vehicle. This report provides a cursory analysis of the fluctuating pressure environments which may be anticipated during launch, and predicted fluctuating pressure levels and spectra for critical flight conditions. These predictions are based on a typical Space Shuttle configuration and launch trajectory, and therefore, should be considered as preliminary estimates.

Section 2.0 contains a brief description of various types of fluctuating pressure environments which may be experienced by the Space Shuttle vehicle. Section 3.0 presents a description of the prediction methods developed by Wyle Laboratories for various fluctuating pressure environments together with comparisons of the predictions with experimental data. A description of anticipated unsteady flow fields and attendant fluctuating pressure environments which will be experienced by the mated Space Shuttle launch configuration is presented in Section 4.0. Section 5.0 presents an assessment of critical Space Shuttle flight conditions and anticipated overall pressure levels and spectra. Particular emphasis is given to the transonic Mach number range and the condition of maximum dynamic pressure. Finally, Section 6.0 summarizes the more significant conclusions reached during this study.

2.0 FLUCTUATING PRESSURE ENVIRONMENTS

When a vehicle moves through air there are two basic means by which it can produce noise: 1) by its propulsion mechanisms (motor-jet, rocket, etc.,) and 2) by its interaction with its surroundings. At low speeds, for example, during and immediately after lift-off, the first of these is by far the dominant one, while near or above the speed of sound the second becomes important.

During any flight cycle for an aerospace vehicle, there are four important phases of the flight which should be investigated in order to assess the environmental trends due to acoustic and fluctuating pressures. These are listed in the chronological order in which they occur.

- Lift-off phase during which acoustic excitation results from the exhaust noise.
- Launch flight to orbit phase, during which rocket exhaust noise diminishes and aerodynamic fluctuating pressures (pseudo-sound) start to dominate. From an aerodynamic noise viewpoint, this phase becomes most critical at transonic Mach numbers ($0.60 \leq M \leq 1.6$).
- Re-entry phase during which only aerodynamic fluctuating pressures are present.
- Flyback phase during which the noise from flyback engines dominate.

This report is devoted to the specification of surface fluctuating pressures resulting from unsteady aerodynamic flows which occur during the launch phase of flight since this is considered to be the primary area of study for this contractual effort. Inflight surface fluctuating pressures are distinctly different from acoustic disturbances originating from rocket exhaust flows and engine noise. Inflight disturbances, as considered herein, arise from several modes of disturbances — the principle source being the passage of a turbulence environment over the external surface. One other important source to be discussed is shock-wave oscillation which is characterized by both turbulence (in close proximity to the foot of the shock wave) and pseudo-static disturbances resulting from the modulation of the pressure gradient through the shock wave. Thus, inflight fluctuating pressure phenomena are near-field mechanisms acting on the surface of a vehicle with the distinction that the disturbances are generally convected at some fraction of the local mean flow velocity. On the other hand, rocket noise and engine noise are acoustic mode disturbances which generally originate away from the surface. Furthermore, acoustic mode disturbances consist of sound waves which propagate at the local speed of sound with a direction independent of the local velocity.

Two specific areas are considered in the present study: 1) "basic" fluctuating pressure environments which will occur on virtually all aerospace vehicles during some phase of flight, and 2) "special" fluctuating pressure environments which are unique to the Space Shuttle

configuration and mission parameters. Under the first category fall such environments as attached turbulent boundary layers, separated flows and certain shock-oscillation environments. Other environments which are more dependent on configuration and mission parameters are certain types of shock-wave impingement, protuberance flows, wake and base flows, rocket plume interference, and rocket exhaust impingement. Distinction is made between the two areas since the "basic" fluctuating pressure environments are dictated by the aerodynamic flow field of the overall vehicle; whereas, the "special" fluctuating pressure environments are relatively localized flow fields which are essentially superimposed upon the basic flow field.

There are an infinite number of possible vehicle configurations and any discussion of their fluctuating pressure environments must be general. Even simple vehicle shapes, such as cone-cylinder bodies, produce complex and highly nonhomogeneous unsteady flow fields — particularly at subsonic and transonic Mach numbers. Unsteady flow phenomena are of particular importance at transonic speeds, since in this range, fluctuating pressures reach maximum levels due to their proportionality to dynamic pressure (q). However, peak fluctuating pressures do not necessarily occur at maximum dynamic pressure for certain regions of a vehicle due to the nonhomogeneous nature of the flow field. For example, regions of the vehicle exposed to separated flow and the impingement of oscillating-shock waves will experience fluctuating pressures at least an order of magnitude greater than regions exposed to attached flow. Thus, if separated flow and oscillating-shock waves are present, say at Mach numbers other than the range of maximum dynamic pressure, then peak fluctuating pressures will also be encountered at conditions other than at maximum q. Thus, it is easily seen that vehicle configuration is very important in the specification of fluctuating pressure levels since the source phenomena are highly configuration dependent in addition to varying with Mach number and angle of attack.

In light of the foregoing discussion, one general statement can be made in regard to aerodynamic fluctuating pressures. Regions exposed to the same unsteady phenomenon will experience fluctuating pressure levels which are proportional to dynamic pressure. Thus, it can be readily seen that a fundamental parameter in the specification of the surface excitation is free-stream dynamic pressure and its variation with Mach number. For a given configuration, Mach number and angle of attack define the phenomena, and dynamic pressure defines the fluctuating pressure levels associated with the phenomena.

In order to assess the fluctuating pressure environments for a vehicle of arbitrary geometry, such as the Space Shuttle vehicle, it is convenient to develop prediction formula for the statistical properties of the fluctuating pressures for each basic type of unsteady flow field. From previous wind tunnel tests and flight data, the following unsteady flow fields have been identified as sources of fluctuating pressures:

a) Attached turbulent boundary layers

b) Separated flows

   1) Expansion Corners
   2) Compression Corners

c) Oscillating shock waves

   1) Transonic terminal shock
   2) Supersonic compression shock
   3) Supersonic impinging shock

d) Wake and base flows

e) Jet/rocket exhaust flow interaction with the vehicle aerodynamic flow field

f) Protuberance flows

g) Rocket exhaust impingement

During past research programs, not all of these phenomena have been studied in sufficient detail to enable prediction methods to be developed (for example, items d and g). However, the other flow fields have been examined sufficiently to provide at least a first order analysis of the attendant fluctuating pressure environments.

The surface fluctuating pressures for each of the above flow conditions may be expected to exhibit different statistical characteristics due to dissimilarities in the mechanisms at work. For example, attached flow pressure fluctuations result from the disturbances within turbulent boundary layers. Separated flow pressure fluctuations result from disturbances within the separated shear layer and instabilities associated with the separation and reattachment points. Pressure fluctuations for shock-wave oscillation result from the movement of the shock wave and the static pressure discontinuity associated with the shock wave. Generally, shock-wave impingement occurs in the presence of either attached or separated flow and added disturbances result due to the combined environments. Thus, in order to develop prediction techniques for the many unsteady flow fields which a vehicle may encounter, it is necessary to examine each flow field independently, and to define, at least empirically, the statistical properties of the attendant fluctuating pressure environment.

The statistical characteristics of each fluctuating pressure environment that are important in the analysis of structural response may be classified under three parameters:

- The overall fluctuating pressure level
- The power spectra
- The cross-power spectra (or narrow band cross-correlation)

In the following section, a summary of the prediction formula is presented together with typical comparisons of the predictions with existing experimental data.

3.0 GENERAL PREDICTION FORMULAE

Analyses of various unsteady flow environments have been performed under this contract for the purpose of defining empirical formulae for estimating the statistical properties of the attendant fluctuating pressures. This work is based on the results contained in References 1 through 25, and the findings are presented in References 26-29. A detailed summary of the basic findings and prediction formulae is presented in Appendix A. The surface fluctuating pressures for both "basic" unsteady flows and certain "special" unsteady flows unique to the Space Shuttle vehicles have been reviewed. The resulting empirical formulae have been generalized for the various environments in order to achieve 1) simplicity in their mathematical formulation, 2) a relationship to the physical parameters of the flow, and 3) good agreement with the available experimental data. As noted in the previous section, complete definition of a fluctuating pressure environment requires that the overall level, power spectra, and cross-power spectra be defined. A brief summary of prediction methods for each of these statistical parameters is given in the following subsections for attached flow, separated flow, and shock-wave oscillation.

3.1 Overall Fluctuating Pressure Level

The correct method of presenting overall fluctuating pressure levels for surfaces beneath the convected turbulence in boundary layers is in terms of the root-mean-square fluctuating pressure level, $\sqrt{\overline{P^2}}$. Free-stream dynamic pressure, q_∞ , local dynamic pressure, q_ℓ , and wall shear stress, τ_ω , have been used to normalize $\sqrt{\overline{P^2}}$ so that meaningful data collapse can be realized throughout the Mach number range. The most generally accepted normalizing parameter is q_∞ and, thus, it will be used in the current expressions.

The effects of Mach number on the normalized rms intensities of the fluctuating pressures in attached flows are shown in Figure 1. There is significant scatter in the data which may be attributed to several factors: 1) background noise and free-stream turbulence in the testing medium; 2) instrumentation quality and the precision of the experimental technique, and 3) data acquisition and reduction techniques, etc. For the range of Mach numbers covered in the data of Figure 1, the normalized rms value of the fluctuating pressure varies from $\sqrt{\overline{P^2}}/q_\infty \approx 0.006$ at subsonic Mach numbers to 0.002 at supersonic Mach numbers. Lowson, Reference 1, proposed the following semi-empirical prediction formula which appears to agree with the general trend in the data:

$$\sqrt{\overline{P^2}}\Big/ q_\infty = 0.006\Big/\left(1 + 0.14\, M_\infty^2\right) \tag{1}$$

It is important to note that this formula has some theoretical basis and is not strictly an empirical approximation of measured results (see Reference 1). The use of this formula at high supersonic and hypersonic Mach numbers should be done so with the understanding that it has not been verified in this Mach number range and may lead to significant error. Predictions for

high supersonic and hypersonic Mach numbers have been developed under this program and are presented in Reference 27. However, in the Mach number range up to, say $M_\infty = 3.0$, the above equation is in good agreement with experimental results.

It should be noted that the results presented in Figure 1, particularly the wind tunnel results, were obtained for both homogeneous and stationary flows at free-stream conditions and in the absence of external pressure gradients. Consideration should be given to local conditions which deviate from free-stream conditions. This work is currently in progress.

The variation of fluctuating pressure level, normalized by free-stream dynamic pressure, with local Mach number for various separated flow environments is presented in Figure 2. These data represent both expansion and compression corners. For expansion corners, the largest levels occurred at low Mach numbers and decreased as local Mach number increased. These data represent the region of plateau-static pressure and the tolerance brackets on the data represent the variations in fluctuating pressure level within the region of constant static pressure rather than scatter in the measurements. A good empirical approximation to the expansion induced separated flow disturbances is:

$$\sqrt{\overline{P^2}} \Big/ q_\infty = \frac{0.045}{1 + M_\ell^2} \qquad (2)$$

This equation is similar in form with that previously proposed for attached turbulent boundary layers.

Fluctuating pressure measurements for the region of plateau-static pressure upstream of compression corners exhibited a somewhat different trend with Mach number. In general, the compression corner data showed an increase in fluctuating pressure level with increasing free-stream Mach number in the range, $1.0 \leq M_\infty \leq 2.0$ — reaching a constant level at Mach numbers above 2.0. Free-stream Mach number is used here because adequate data is not available for determining the local Mach number in the vicinity of the compression-induced separated flow region. Derivation of an empirical prediction formula for the fluctuating pressure level within compression-induced separated flows will require further study.

Generally, shock-wave oscillation produces the most intense fluctuating pressure levels that are usually encountered by a vehicle. Typical shock waves encountered by vehicles are:

- Terminal shock waves for regions of transonic flow
- Displaced oblique shock waves as induced by the separated flow in compression corners at local supersonic speeds

- Reattachment shock waves in the vicinity of the reattachment point for separated flows generated by both compression and expansion corners

- Impingement shock waves as caused by local bodies such as strap-on rockets

- Oblique shock waves associated with separated flow induced by highly expanded rocket plume at high altitudes.

All shock waves may be expected to produce generally similar fluctuating pressure environments since the pressure fluctuations arise from motion of the shock wave. The mechanism of this motion was investigated under this contract, and it was found that the oscillations are driven by velocity fluctuations in the incoming turbulent boundary layer. The maximum displacement is governed by mean flow conditions. Except for alternating flow conditions, where oscillation distance is much larger than shock thickness and the power spectrum is therefore a Poisson distribution, spectra and overall levels for various shock environments are quite similar. A discussion of shock oscillation and results of analytical investigation are presented in Reference 28, and are summarized in Appendix B. The overall level is a strong function of Mach number in the transonic regime; typical overall levels for terminal shock wave oscillation are presented in Figure 3.

3.2 Power Spectra

Power spectra represent the distributions of the mean-square fluctuating pressure with frequency. Power spectra for the various fluctuating pressure environments are found to scale on a Strouhal number basis; that is, the frequency is normalized by multiplying by a typical length and dividing by a typical velocity. Normalized spectra enable similar, stationary flows to be represented by a single spectrum regardless of the scale of the flow field or the free-stream velocity.

Numerous studies have been conducted to determine the proper parameters to be used to nondimensionalize the spectra for various aero-acoustic environments. Unfortunately, the choice of parameters which best collapses the data appear to be dependent on the nature of the fluctuating pressure environment. In general, free-stream velocity is used as the normalizing velocity parameter, although a typical eddy convection velocity (itself a function of frequency) has been used occasionally. The local convection velocity appears to correspond more closely with the physical situation for fluctuating pressures due to turbulent eddies. Selection of a typical length is more difficult. Boundary layer thickness, δ, displacement thickness, δ^*, wall shear stress, τ_w, and momentum thickness, θ, have all been used by various investigators for attached flow. For separated flow and shock-wave oscillation, local boundary layer thickness and separation length have also been used.

Generally, prior knowledge of the overall fluctuating pressure level is required to predict the power spectra; however, prediction formula for the overall levels have been developed to a limited degree as discussed in Section 3.1.

Prediction formulae for the power spectra for the various unsteady flows, with the exception of shock-wave oscillation, have the following form:

$$\frac{\Phi(f)\,U}{q_\infty^2\,L} = \frac{\overline{P^2}/q_\infty^2}{\frac{f_0 L}{U}\left\{1+\left(f/f_0\right)^n\right\}^k} \tag{3}$$

where U = characteristic velocity

L = characteristic length

f_0 = characteristic frequency

n, k = spectrum shape factor

Some mathematical properties of Equation (3), in particular the relationship between n, k and overall level, are discussed in Appendix C.

For shock-wave oscillation, the power spectrum is a combination of power spectra for inviscid shock-wave motion as well as contributions from the separated flow near the foot of the shock wave. The prediction formula has the following form:

$$\left(\frac{\Phi(f)\,U}{q_\infty^2\,L}\right)_{SW} = \left(\frac{\Phi(f)\,U}{q_\infty^2\,L}\right)^{I}_{SW} + k_1\left(\frac{\Phi(f)\,U}{q_\infty^2\,L}\right)_{S} \tag{4}$$

where $k_1 \approx 0.25$, the subscripts SW and S denote shock wave and separated flow respectively, and the superscript I denotes the absence of viscous effects. A complete discussion of the power spectra predictions for the various fluctuating pressure environments are presented in Reference 26. Comparisons of predicted power spectra with experimental data are presented for attached flow, separated flow, and shock-wave oscillation in Figures 4, 5 and 6. Also, power spectra predictions have been developed for nonhomogeneous attached and separated flows (see Reference 26). Comparisons of these predictions with experimental data are shown in Figure 7 together with attached flow, separated flow and shock-wave oscillation.

3.3 Cross-Power Spectra

The final requirement in determining the characteristics of the fluctuating pressure environment of an unsteady flow field is to define the narrow band, space correlation function or co-power spectral density. This parameter is the key function needed to describe an impinging pressure field on a structure in order to calculate the induced mean-square response of the structure (see, for example, Reference 17 for the structural response computational technique). The spatial correlation properties of a fluctuating pressure field can be obtained only from a careful and detailed examination of the flow field at a large number of points.

Measurements by several investigators have shown that the co-power spectral density of the turbulent boundary layer pressure fluctuations in the direction of the flow can be approximated by an exponentially damped cosine function, and the lateral co-spectral density can be approximated by an exponential function.

The spatial coherence of the fluctuating pressure environments as defined by the co-power spectra have been evaluated for the various unsteady flows. The cross-power spectra for attached turbulent boundary layers, two- and three-dimensional separated flows and protuberance-induced wake flows appear to be fairly well defined at least in the longitudinal direction. Much uncertainty remains for transverse cross-power spectra in upstream separated flows, and protuberance wake flows. Both longitudinal and transverse cross-power spectra for the regions beneath oscillating shock waves require additional study.

In general, the normalized co-power spectra for the various fluctuating pressure environments can be defined as exponentially damped sinusoids for the longitudinal axis as follows:

$$C(\xi, f) = e^{-a\omega\xi/U_c} \cos \frac{\omega\xi}{U_c} \tag{5}$$

Along the transverse axis, the normalized co-spectra may be defined by an exponential decay as follows:

$$C(\eta, f) = e^{-b\omega\eta/U_c} \tag{6}$$

where ω is the circular frequency, U_c is the convection velocity, and ξ and η are the longitudinal and transverse separation distances, respectively, and a and b are the coefficients of exponential decay.

The coefficient of exponential decay is a function of the particular environment under study and may also depend on free-stream Mach number as well as local flow conditions. Derivations of the coefficient of exponential decay are presented in Reference 26 for each unsteady flow condition where the data was sufficiently well defined to merit an analysis. For attached boundary layer flow, the coefficient of exponential decay in the longitudinal direction was found to be $a = 0.10$. For two-dimensional and axisymmetric separated flows, the values ranged from 0.13 at $M_\infty = 2.5$ to 0.33 at $M_\infty = 1.60$. The coefficient of exponential decay in the inner and outer regions of three-dimensional separated flows upstream of cylindrical protuberances were approximately the same in the longitudinal direction with a value of $a \approx 0.7$. In the protuberance wake, the spatial decays were clearly defined only in the neck and far-wake regions with a value of $a \approx 0.19$. Typical co- and quad-spectra are presented in Figures 8 and 9 for attached flow and separated flow, respectively.

4.0 FLUCTUATING PRESSURE ENVIRONMENTS FOR SPACE SHUTTLE

4.1 Description of Space Shuttle Vehicles

Space Shuttle studies over the past three years have considered a wide variety of system configurations. The final concept will consist of an Orbiter vehicle with an external, expendable, liquid hydrogen/liquid oxygen system (H/O) tank. Two solid rocket boosters (SRB) will be used for the shuttle booster in a strap-on configuration similar to the Titan III concept. Selection of solid rocket diameter is still under study with a 144 inch diameter segmented motor or a 142 inch diameter monolithic motor being strong contenders. Orbiter design is still under study, with the most likely candidate being a lightweight double delta wing configuration with a target gross weight of 150,000 lb.

Power for the Orbiter will be supplied by three high-pressure engines which will burn in parallel with the solid rocket motors during launch. One concept for the Space Shuttle is the baseline configuration shown in Figure 10. The detail geometry of the mated Space Shuttle configuration has certainly not been finalized; however, the concept has progressed to the point that reasonable estimates can be made in regard to the fluctuating pressure environments which may be anticipated during launch. The baseline configuration shown in Figure 10, consisting of a lightweight Orbiter and 142 inch diameter monolithic SRB's will be used in this report as a baseline model for arriving at preliminary estimates of the Space Shuttle fluctuating pressure environments.

4.2 Description of Flow Fields

The Space Shuttle launch configuration is a complex combination of several bodies — with each major body having a different geometry. The flow field for the mated launch vehicle will consist of the individual flow fields of each major body of the vehicle with modified regions as generated by the interference and interactions among the flow fields of the various bodies. An extensive experimental/theoretical study will be required to accurately define the resulting flow over the mated configuration. The problem at the present time is to arrive at some feasible means of defining the aerodynamic flow field so that preliminary estimates of surface fluctuating pressure environments can be made. The approach to be taken is to analyze, first, the interference-free flow field for each major body of the mated Space Shuttle vehicle, and to modify the individual flow fields according to predicted flow interference effects. Only a cursory description of the flow fields for the mated configuration is thus obtained; however, the analysis does point out representative fluctuation pressure environments which may be anticipated during Space Shuttle flight.

The fluctuating pressure environments are, of course, a function of launch trajectory. For the purpose of this report, predictions will be made for a due east trajectory. Flight parameters for this trajectory are shown in Figure 11. It should be noted that the basic fluctuating environments are functions of Mach number and scale with dynamic pressure; therefore, the present predictions can generally be corrected for other trajectories. An important exception to this scaling rule is plume induced separation, where the geometry of the separated flow, as well as overall level depends on dynamic pressure. Plume effects must therefore be calculated for each specific trajectory.

4.2.1 Interference-Free Flow Environments — The solid rocket motors are basically cone-cylinder missile configurations with a 17.5 degree cone half angle. Cone-cylinder geometries have been studied extensively in past years and their unsteady flow fields are fairly well defined. For these bodies, the following environments may be anticipated.

- Attached turbulent boundary layer flow
- Shoulder-induced separated flow (subsonic Mach numbers)
- Terminal shock-wave oscillation (transonic Mach numbers below 1.0)
- Exhaust plume-induced flow separation with shock-wave oscillation for high altitude supersonic flight.

For a cone-cylinder body, the types of unsteady flow conditions which will occur at a given Mach number depend on cone-angle, angle of attack, and Reynolds number. Typical flow fields for cone-cylinders are shown for the zero angle of attack, interference-free case in Figure 12.

For all Mach numbers, the flow over the nose cones will be attached with the location of boundary layer transition occurring as a function of Reynolds number. Flow characteristics in the vicinity of the cone-cylinder juncture will vary depending on free-stream Mach number, angle of attack, and shoulder angle. For cones having half angles (shoulder angles) greater than approximately 10 degrees, the flow will not fully expand over the shoulder at subsonic speeds but will separate at the shoulder. A separation bubble is thus formed, with reattachment occurring a short distance aft of the shoulder with the axial extent of the bubble depending primarily on cone-angle. At high subsonic Mach numbers, the flow negotiates the shoulder without separating, reaches supersonic speed immediately aft of the shoulder, and produces a near-normal, terminal-shock wave at some point along the cylinder. The boundary layer becomes extremely thin at the shoulder due to the strong expansion fan and a new boundary layer is essentially formed at the shoulder. The boundary layer remains attached between the shoulder and the shock wave. At the shock location, the boundary layer may undergo separation depending on the strength of the shock wave. The shock strength is at a maximum corresponding to the initial attachment of the flow at the shoulder and decreases in strength as it moves aft with increasing Mach number. At sonic speed, the terminal-shock wave will move aft of the body and will be reduced to zero strength.

For Mach numbers above 1.0, the interference-free flow fields for the SRB will consist of attached boundary layer flow and possible shock-oscillation environments corresponding to surface protuberances and other geometric irregularities. At supersonic, high altitude, conditions, spreading of the rocket exhaust plume will induce separated flow over the aft portion of the total Space Shuttle vehicle. This will be discussed in Section 4.2.3, Plume-Induced Separated Flow Environments.

H/O Tank — The H/O tank is basically an ogive-cylinder configuration. The configuration shown in Figure 10 has a sphere-cylinder at the nose housing a de-orbit engine. Design of the H/O tank is still in a fluid state, with such details as de-orbit engine location and precise nose geometry not finalized at the present time. Latest concepts call for de-orbit engines to be located flush along the sides of the H/O tank, rather than in the sphere-cylinder as shown. Therefore, for the purposes of this report the H/O tank will be treated as an ogive-cylinder.

Ogive-cylinders have been studied in the past, although not as extensively as the more basic cone-cylinder configuration. A key factor in this type of body is the configuration of the shoulder.

Robertson (Reference 30) investigated the effect of introducing a radius at the shoulder of a cone-cylinder, with geometry ranging from a sharp corner to an ogive-cylinder. It was found that flow separation decreases as shoulder radius increases, with no separation observed for ogive-cylinders. Static pressure measurements indicate that the terminal shock wave on an ogive-cylinder is generally weaker and occurs at a higher Mach number than on an equivalent cone-cylinder. Interference-free flow environments for the H/O tank will therefore consist of attached boundary layer flow and terminal shock wave oscillation (though not as severe as for a cone-cylinder) at subsonic speeds, and attached boundary layer flow for Mach numbers above 1.0. As with the SRB, there may also be separated flow and shock oscillation environments corresponding to surface protuberances and other irregularities.

Orbiter Vehicle — The Space Shuttle Orbiter is a fairly clean vehicle from an aerodynamic viewpoint; however, there are several specific areas of concern which should be noted as regions of potentially severe fluctuating pressure environments. In general, a major portion of the upper surface area of the Orbiter will experience attached flow with relatively small fluctuating pressure levels. The lower surface area will experience attached flow also; however, the lower surface will be affected largely by interference flow due to the close proximity of the SRB and H/O Tank. The following exceptions to attached flow over the upper surface of the Orbiter should be noted:

1) Separated flow and shock-wave oscillation in the vicinity of the crew compartment.

2) Terminal shock-wave oscillation aft of the crew compartment over the upper surface of the fuselage.

3) Protuberance-induced separated flow and shock-wave oscillation in the vicinity of the OMS Engines.

4) Exhaust plume-induced separated flow and shock-wave oscillation at high altitude supersonic flight.

A detailed analysis of the crew compartment and protuberance-induced fluctuating pressure environments will not be presented in this report since the final design of the Orbiter will likely be altered from the design of these components as shown in Figure 10. However, certain general features of these components may be expected in the final design.

Crew-Compartment — Due to the location of the crew compartment and the requirements for pilot visibility, the flow over the upper fuselage will be perturbed to a significant degree. The angle between the pilot's window and fuselage will form a compression corner and the flow in this area will resemble a forward facing step or wedge characterized by compression-induced separated flow. At supersonic Mach numbers, shock-wave oscillation may be expected at the flow separation and reattachment points. Also, if the shoulder above the pilot's station is a sharp angle, over-expansion at transonic Mach numbers similar to that observed at cone-cylinder junctures may be expected. Finally, terminal shock-wave oscillation will occur over the upper surface of the fuselage at high subsonic Mach numbers for some distance aft of the crew compartment. For the baseline configuration, the shoulder above the crew compartment is rounded and shoulder-induced separated flow is not anticipated. However, terminal shock-wave oscillation will occur but with reduced fluctuating pressure levels as compared to a sharp-shoulder configuration (see Reference 30).

OMS Pods — The OMS units are three-dimensional protuberances that will induce separated flow. Relatively severe fluctuating pressures are anticipated in the vicinity of these units. Most of the aft fuselage and wing root section on the upper surface will be affected by the OMS engines. Essentially, these engines are small strap-on rockets and many of the arguments presented in the next section for the SRB interference-induced flow field are pertinent to the OMS engine areas.

The flow field for the OMS engines will be characterized by compression-induced separated flow and shock-wave oscillation.

4.2.2 Mated Vehicle Interference-Flow Environments — The launch configuration of Space Shuttle vehicles will be comprised of four approximately parallel bodies. Such vehicles have regions of flow interference between the various bodies which will result in relatively severe fluctuating pressure environments. For other similar configurations such as Titan III, shock-induced pressure fluctuations have been observed at the location of shock impingement from one body onto the surface of the other bodies. This phenomenon may be anticipated for Mach numbers starting at approximately 1.2 when the bow shock for the mated vehicle divides into separate bow shocks for each major body of the vehicle. Shock impingement will continue to produce severe fluctuating pressure levels until booster separation, H/O Tank separation, or until the q_∞ decreases to a level sufficiently low that the disturbances are no longer of concern. The following shock interference regions will occur:

1) Bow-shock impingement and shock-boundary layer interaction between the SRB and H/O Tank due to SRB bow shock.

2) Bow-shock impingement and shock-boundary layer interaction between the H/O Tank and Orbiter fuselage due to Orbiter bow shock.

3) Shock-boundary layer interaction between the Orbiter lower wing surfaces and SRB due to wing leading edge shocks.

4) Possible transonic shock-boundary layer interaction between SRB and H/O Tank and H/O Tank and Orbiter due to transonic terminal shock waves.

The most severe interference flow regions are anticipated to be in the vicinity of the cone-cylinder juncture of the SRB, in the region between the SRB and H/O Tank, and in the vicinity of the H/O Tank and the underside of the Orbiter nose. The most critical Mach number range is anticipated to be in the transonic region ($0.80 \leq M_\infty \leq 1.6$) corresponding to maximum dynamic pressure, transonic buffet phenomena and near-normal shock wave impingement. Downstream of the shock-interaction regions, the flow may become choked and a shock-free interference flow environment will occur. This type environment will be referred to as shock-free interference flow and fluctuating-pressure levels on the order of those experienced in homogeneous separated flow may be expected.

4.2.3 Plume-Induced Separated Flow Environments -- At high altitudes, a rocket exhaust plume expands to form an effective flared afterbody larger than the vehicle itself. Under supersonic conditions, flow over the vehicle may be separated due to this effective flare. The onset of plume-induced separation, and the extent of the separated region, is highly dependent on vehicle design parameters and flight conditions. Plume diameter increases with diminishing dynamic pressure; the onset of plume-induced separation therefore will generally occur at times after conditions of maximum dynamic pressure. As altitude increases after the onset of separation, the separation region grows. Pressure fluctuations within the separated region are similar to those for an equivalent rigid flare; however, the non-rigid nature of the plume boundary leads to some important differences. The most important difference due to motion of the plume interface is an increase in shock oscillation distance and attendant fluctuating pressure level. Effects of plume-induced separation have been investigated as part of this program. Prediction schemes for both separation length and fluctuating environments on axisymmetric vehicles are presented in Reference 29. Plume-induced separation has been computed for axisymmetric representations of the SRB and of the Orbiter. Tables 1 and 2 summarize vehicle and engine parameters pertinent to plume-induced separation on the baseline shuttle configuration. Approximations involved are similar to those made in Reference 29 for the PRR configuration.

Figure 13 shows the predicted separation point on the shuttle SRB and Orbiter. Separation on the SRB begins shortly after maximum q_∞, and extends over most of the SRB by SRB cut-off. Separation on the Orbiter does not occur until well past maximum q_∞, so that separation due to the Orbiter engine plume will not be an important environment. Separation due to the Orbiter engines occurs at a much later time than that due to the SRB's because the Orbiter's high p_c H/O engines are much less underexpanded (through both higher area ratio and higher exhaust gamma) than the SRB solid fuel engines.

TABLE 1. SRB PARAMETERS

Vehicle Radius	71 Inches
Thrust	2.5×10^6 Lb
γ_{ex}	1.145
Nozzle Area Ratio	7.0
Exhaust Mach Number	2.9
Chamber Pressure	730 psia

TABLE 2. ORBITER PARAMETERS

Vehicle Radius	131 Inches
Thrust	1.41×10^6 Lb
γ_{ex}	1.23
Nozzle Area Ratio	35
Exhaust Mach Number	4.05
Chamber Pressure	3000 psia

4.3 Predicted Fluctuating Pressure Levels

The following summary presents estimates of overall fluctuating pressure levels, as a function of free-stream Mach number and dynamic pressure, typical of those which may be anticipated for the various unsteady flow environments for the Space Shuttle bodies.

4.3.1 Attached Turbulent Boundary Layer Flow —

$$\frac{\sqrt{\overline{p^2}}}{q_\infty} = \frac{0.006}{1 + 0.14\, M_\infty^2} \tag{7}$$

H/O Tank

- Ogive Nose — All Mach numbers and surface area except interference-flow region
- Cylinder — $X_s/D \gtrsim 0$, $M_\infty \lesssim 0.9$
  — $0 \leq X_s/D \leq X_{sw}/D$, $0.9 \lesssim M_\infty < 1.0$
  — $X_s/D > 0$, $M_\infty \geq 1.0$

SRB

- Nose Cone — All Mach numbers and surface area except interference-flow region
- Cylinder — $X_s/D \gtrsim 0.2$, $M_\infty \lesssim 0.78$
  — $0 \leq X_s/D \leq X_{sw}/D$, $0.78 \lesssim M_\infty < 1.0$
  — $X_s/D > 0$, $M_\infty \geq 1.0$

Orbiter

- All surface areas except:
  - Crew Compartment Canopy — All Mach numbers
  - Upper Fuselage aft of Crew Compartment for $0.86 \lesssim M_\infty \lesssim 1.0$ (See Section 4.3.3 for discussion approximate X_{sw}/D)

— Protuberance-Flow Fields — All Mach numbers

— Interference-Flow Fields — All Mach numbers

Figure 14 shows the basic root mean square boundary layer fluctuating pressure, both in pounds per square foot and dB, for the launch trajectory shown in Figure 11. Maximum level for this environment is 137.5 dB at TALO = 50 sec, for which $M_\infty = 1.05$ and altitude is 24,400 ft. Note that this occurs before conditions of maximum Q, at 60 seconds.

4.3.2 Shoulder-Induced Separated Flow — For the shoulder-induced separated flow environment, there are two sources of fluctuating pressures which should be noted. First, immediately aft of the shoulder and within the separation bubble, the pressure fluctuations appear to be fairly homogeneous with levels similar to those observed immediately downstream of a rearward facing step or in the wake of bulbous payload configurations. However, further aft, the flow reattaches and higher level fluctuating pressures have been observed in the vicinity of the reattachment point. Also, even though the flow separates at the shoulder, the flow may reach local supersonic conditions as it expands over the separation bubble, in which case, reattachment aft of the shoulder will produce a recompression shock wave and relatively severe fluctuating pressure levels. Measurements presented in References 18 and 31 indicate fluctuating pressure levels ranging up to $\sqrt{\overline{P^2}}/q_\infty = 0.16$ for reattachment aft of cone-cylinder junctures with shoulder angles ranging up to 30 degrees. Most of the results presented in References 18 and 31 show considerable scatter with variations in both cone angle and free-stream Mach number. A prediction curve which appears to be representative of the maximum fluctuating pressure levels for shoulder-induced separated flow on cone-cylinder bodies is given in Figure 15. This curve is attributed to Stevens in Reference 32, and it will be employed in the present predictions for shoulder-induced separated flow. Results from References 18 and 31 are also shown in Figure 15.

For the Mach number range from 0.60 to the attachment Mach number (M_a), the homogeneous region of separated flow will produce fluctuating pressure levels in the range from $\sqrt{\overline{P^2}}/q_\infty =$ 0.02 to 0.04 (Figure 2). The fluctuating pressure levels given by Steven's prediction are greater than those for homogeneous separated flow and the difference can be attributed to the disturbances in the reattachment region (see Figure 12). For cone-cylinders with shoulder angles less than approximately 10 degrees, shoulder separation does not occur and the fluctuating pressure levels will decrease to the levels observed in attached flow as indicated by the dashed portion of the prediction curve.

$$\sqrt{\overline{P^2}}\Big/q_\infty = f(\theta_N) \quad , \qquad \text{Figure 15}$$

H/O Tank

- None anticipated for the ogive-cylinder configuration.

SRB

- Cylinder — $X_s/D \lessapprox 0.2$, $\sqrt{\overline{P^2}}/q_\infty = 0.06$ } $M_\infty \lesssim 0.78$

Orbiter

- Crew Compartment — Shoulder angle unknown. Non[illegible]anticipated for baseline configuration with [illegible]d shoulder.

Expansion-induced separated environments occur over a limited transonic M[illegible]mber range. Basic fluctuating levels for the Shuttle are discussed in Section 5.0.

4.3.3 Transonic Shock-Wave Oscillation — Typical cone-cylinder data showing the attachment Mach number and the variation of shock location with free-stream Mach number is presented in Figure 16. Shown in Figure 17 is an interpolation of these data for two additional core angles. Shock-induced fluctuating pressure levels, normalized by free-stream dynamic pressure, are presented in Figure 18 for a range of cone angles. Curves for 17.5° and 22.5° are interpolated, 17.5° corresponding to the SRB. At this time, corresponding predictions have not been made for the H/O tank. Fluctuating levels and X_{sw}/D for an ogive-cylinder are generally less than for a cone-cylinder of similar nose angle; however, geometry of the H/O tank has not yet been finalized to a point where precise predictions are reasonable. The nose half angle of the ogive in Figure 10 is approximately 38° . As a preliminary estimate, fluctuating levels will be taken as corresponding to a 30° cone. This is a very conservative estimate, and will overpredict the level by at least several dB. X_{sw}/D is not estimated for the H/O Tank.

Transonic shock-wave oscillation will also occur aft of the Orbiter crew compartment canopy with characteristics similar to H/O tank and SRB. Because of unknowns associated with canopy geometry, precise estimates of fluctuating pressure levels and shock-wave locations as a function of Mach numbers are not made herein. However, the data for the H/O tank and SRB are indicative of the ranges expected for the Orbiter.

The prediction for shock oscillation is:

$$\sqrt{\overline{P^2}}/q_\infty = f(M_\infty, \theta_N) \quad , \qquad \text{Figure 17}$$

H/O Tank

• Cylinder	—	Narrow band of approximately 3 δ_ℓ width corresponding to X_{sw}/D in Figure 16.	$0.86 < M_\infty \leq 1.0$

SRB

• Cylinder	—	Narrow band of approximately 3 δ_ℓ width corresponding to X_{sw}/D in Figure 17.	$0.78 < M_\infty \leq 1.0$

Orbiter

• Fuselage	—	Location and Mach number range depend on crew compartment shoulder angle. Predictions for SRB and H/O Tank are reasonable approximations of the range of parameters for Orbiter terminal shock-wave oscillation.	$0.86 < M_\infty < 1.0$

Transonic shock oscillation occurs over a limited Mach number range. Fluctuating levels and shock location are easily obtained from Figures 16 through 18; levels and location for the shuttle are computed and discussed in Section 5.0.

4.3.4 Compression-Induced Separated Flow (Two-Dimensional)

$$\sqrt{\overline{P^2}}/q_\infty = 0.015 \text{ to } 0.025 \qquad \text{(Figure 2)}$$

H/O Tank	—	Protuberance-Flow Fields Interference-Flow Fields	All Mach Numbers
SRB	—	Protuberance-Flow Fields Interference-Flow Fields	All Mach Numbers

Orbiter	—	Crew Compartment Canopy Protuberance-Flow Fields Interference-Flow Fields	All Mach Numbers

Fluctuating levels for the launch trajectory are shown in Figure 19. Note that because $\sqrt{\overline{P^2}}/q_\infty$ is an increasing function of Mach number, the critical (maximum fluctuating level) compression-induced separation environment occurs at TALO = 72 seconds, a later time than maximum q_∞.

4.3.5 Supersonic Shock-Boundary Layer Interactions

$$\sqrt{\overline{P^2}}/q_\infty = 0.06 \text{ to } 0.08$$

H/O Tank	—	Protuberance-Flow Fieids Interference-Flow Fields	Local Mach Number > 1.0
SRB	—	Protuberance-Flow Fields Interference-Flow Fields	Local Mach Number > 1.0
Orbiter	—	Crew Compartment Canopy Protuberance-Flow Fields Interference-Flow Fields	Local Mach Number > 1.0

Fluctuating levels for the launch trajectory are shown in Figure 20. Because the prediction used here is not a function of Mach number (other than applying only for $M > 1$), the critical shock oscillation environment occurs at maximum q_∞.

4.3.6 Plume-Induced Separation — Plume-induced separated flow is not a basic environment as those discussed in Sections 4.3.1 through 4.3.5, but is rather a modification of compression corner basic environments. The modification is dependent on the particular vehicle and trajectory. Not only does the mean separated flow depend on vehicle parameters, but the response of the plume enters into the fluctuating environments. In Reference 29, it was shown that homogeneous separated flow fluctuations in plume-induced separation are essentially the same as for a rigid flare, while shock oscillation depended on plume parameters. The homogeneous environment is thus given by Figure 19, with the limitation that it applies only to flight conditions where plume-induced separated flow exists, as defined in Figure 13. Note that separation due to the orbiter engines occurs only at very high altitudes; the dynamic pressure at these altitudes is sufficiently small that orbiter plume-induced separation may be neglected relative to other environments. The SRB plumes induce separation at considerably

lower altitudes, and must be considered. In Reference 29, a prediction scheme was developed for the fluctuating pressure associated with the separation shock. Predictions made for the PRR configuration indicate that shock excursion and fluctuating pressure level for plume-induced separation is generally less than 25% greater than for a rigid flare. The baseline shuttle is similar; shock oscillation fluctuating pressure levels for plume-induced separation on the baseline shuttle SRB will therefore be no more than 2 dB greater than for the basic shock environment given in Figure 20. This environment occurs only at TALO greater than 62 seconds, the onset of plume-induced separation.

4.4 Predicted Power Spectra

The following empirical prediction equations, presented in normalized form, may be employed to compute the power spectra for the various fluctuating pressure environments.

4.4.1 Attached Turbulent Boundary Layer Flow — The following equations apply to the homogeneous regions of attached flow.

$$\frac{\Phi(\omega)\, U_\infty}{q_\infty^2\, \delta^*} = \frac{\left(\overline{P^2}/q_\infty^2\right)}{\dfrac{\omega_0\, \delta^*}{U_\infty}\left\{1 + (\omega/\omega_0)^{0.9}\right\}^{2.0}}$$

where

$$\omega_0 = 0.5\,\frac{U_\infty}{\delta^*}$$

$$\overline{P^2}/q_\infty^2 = \frac{(0.006)^2}{(1 + 0.14 M_\infty^2)^2}$$

$$\delta^* = \delta/8 \quad \text{for } M < 1.0$$

$$\delta^* = \frac{(1.3 + 0.43 M_\infty^2)\,\delta}{10.4 + 0.5 M_\infty^2\left[1 + 2.10^{-8}\, R_e\right]^{1/3}} \quad \text{for } M > 1.0$$

$$\delta = x \left[0.37\, R_e^{-0.2} \left\{ 1 + \left(\frac{R_e}{6.9 \cdot 10^7} \right)^2 \right\}^{0.1} \right]$$

x = Downstream distance from the leading edge

R_e = Reynolds number = $U_\infty\, x/\nu$

ν = Kinematic viscosity

4.4.2 Compression/Expansion-Induced Separated Flow and Shock-Free Interference Flow — The following equations apply to the homogeneous regions of separated flow.

$$\frac{\phi(f)\, U_\ell}{q_\infty^2\, \delta_\ell} = \frac{\overline{P^2}/q_\infty^2}{\dfrac{f_0\, \delta_\ell}{U_\ell} \left\{ 1 + \left(f/f_0 \right)^{0.83} \right\}^{2.15}}$$

where $f_0 = 0.17\, \dfrac{U_\ell}{\delta_\ell}$

$\overline{P^2}/q_\infty^2 = \dfrac{0.045}{1 + M_\ell^2}$, for expansion induced separated flows.

$\overline{P^2}/q_\infty^2$ = the results as determined in Figure 2 for compression induced separated flows.

and the subscripts ℓ and ∞ refer to local and free-stream conditions, respectively.

It is anticipated that the above equation can be used with good accuracy to predict the power spectra for fluctuating pressures within the homogeneous region of expansion-induced separated flows and shock-free interference flows although it was derived based on data taken in compression corners.

4.4.3 Shock-Oscillation Environments — To predict the power spectra for nonhomogeneous flows generated by shock-wave oscillation, prior knowledge of the overall fluctuating pressure levels is required. Under the assumption of statistical independence between the various contributing sources, the power spectra for nonhomogeneous environments may be written as the summation of power spectra of the contributing sources.

$$\left[\phi(f)\right]_A^{NH} = \left[\phi(f)\right]_A^{H} + c_1 \left[\phi(f)\right]_{SW}^{I,H}$$

$$\left[\phi(f)\right]_S^{NH} = \left[\phi(f)\right]_S^{H} + c_2 \left[\phi(f)\right]_{SW}^{I,H}$$

where c_1 and c_2 are given as

$$c_1 = \frac{\left(\frac{\overline{p^2}}{q_\infty^2}\right)_A^{NH} - \left(\frac{\overline{p^2}}{q_\infty^2}\right)_A^{H}}{\left(\frac{\overline{p^2}}{q_\infty^2}\right)_{SW}^{I,H}}$$

$$c_2 = \frac{\left(\frac{\overline{p^2}}{q_\infty^2}\right)_S^{NH} - \left(\frac{\overline{p^2}}{q_\infty^2}\right)_S^{H}}{\left(\frac{\overline{p^2}}{q_\infty^2}\right)_{SW}^{I,H}}$$

The power spectra for nonhomogeneous attached flow as caused by shock-wave oscillation in the vicinity of an attached flow region has the following form normalized by local conditions upstream of the shock wave:

$$\left[\frac{\phi(f)\ U_0}{q_\infty^2\ \delta_0}\right]_A^{NH} = \frac{\left(\frac{\overline{p^2}}{q_\infty^2}\right)_A^H}{\left(\frac{f_0\ \delta_0}{U_0}\right)_A \left\{1 + \left(f/f_0\right)^{0.9}\right\}^2} +$$

$$\frac{\left(\frac{\overline{p^2}}{q_\infty^2}\right)_A^{NH} - \left(\frac{\overline{p^2}}{q_\infty^2}\right)_A^H}{\left(\frac{f_0\ \delta_0}{U_0}\right)_{SW} \left\{1 + \left(f/f_0\right)^{1.55}\right\}^{1.7}}$$

where $\left(\frac{f_0\ \delta_0}{U_0}\right)_A \approx 0.40$ depending on Mach number

$$\left(\frac{f_0\ \delta_0}{U_0}\right)_{SW} = 0.01$$

The following expression has been derived for nonhomogeneous separated flow:

$$\left[\frac{\phi(f)\ U_0}{q_\infty^2\ \delta_0}\right]_S^{NH} = \frac{\left(\frac{\overline{p^2}}{q_\infty^2}\right)_S^H}{\left(\frac{f_0\ \delta_0}{U_0}\right)_S \left\{1 + \left(f/f_0\right)^{0.83}\right\}^{2.15}} + \frac{\left(\frac{\overline{p^2}}{q_\infty^2}\right)_S^{NH} - \left(\frac{\overline{p^2}}{q_\infty^2}\right)_S^H}{\left(\frac{f_0\ \delta_0}{U_0}\right)_{SW} \left\{1 + \left(f/f_0\right)^{1.55}\right\}^{1.7}}$$

where $\left(\frac{f_0\ \delta_0}{U_0}\right)_S = 0.075$

$$\left(\frac{f_0\ \delta_0}{U_0}\right)_{SW} = 0.01$$

also the subscripts and superscripts denote the following:

Subscripts:	SW	-	shock wave
	S	-	separated flow
	A	-	attached flow
Superscripts:	1	-	absence of viscosity (inviscid)
	H	-	homogeneous flow

Generally, shock-wave oscillation occurs in the presence of separated flow for critical environments, and examples are shock-induced interference flows, terminal shock-wave oscillation, the separation and reattachment points for compression corner flow at supersonic Mach numbers, and the reattachment point for expansion shoulder flows for local supersonic conditions. For terminal shock-wave oscillations at Mach numbers near 1.0, the flow does not separate and the nonhomogeneous attached flow equation is applicable.

5.0 ANALYSIS OF CRITICAL SPACE SHUTTLE FLIGHT CONDITIONS

The analysis presented in Section 4.0 revealed that many severe and complex fluctuating pressure environments may be experienced by the Space Shuttle vehicles. The most severe environments will occur at transonic and low supersonic Mach numbers, $0.60 \leq M_\infty \leq 2.0$. In terms of fluctuating pressure coefficient, transonic environments ($0.60 \leq M_\infty \leq 1.0$) are the most severe, while supersonic environments are critical because of high dynamic pressure. Although critical (maximum) fluctuating levels for each supersonic environment do not necessarily occur at conditions of maximum dynamic pressure (MAX Q) the levels at MAX Q are sufficiently close to maximum that for the purposes of this report critical supersonic environments have been computed at MAX Q. Transonic environments have been computed over a range of Mach numbers.

The various prediction schemes developed under this contract have been incorporated into several computer programs. Descriprions of the various programs are contained in Appendix D. All predictions contained in this report have been made utilizing these programs. Calculations are presented for overall levels and typical spectra. Although a computer program has been prepared for the calculation of correlation functions (see Appendix D for description), specific sample calculations are not presented. The scaled correlations shown in Figures 8 and 9 adequately illustrate these for the purposes of the present report.

Computations were performed for the following critical flight conditions:

1. Maximum Dynamic Pressure (MAX Q), $M_\infty = 1.31$

   - Attached Turbulent Boundary Layers

     - Typical H/O Tank, SRB and Orbiter Stations based on representative values of local boundary layer thickness and velocity.

   - Homogeneous Compression-Induced Separated Flows

     - Typical of the shock-free region of separated flow over the Crew Compartment and shock-free interference flow fields.

   - Shock-Boundary Layer Interactions

     - Typical of Boundary Layer Separation and reattachment areas and shock-induced interference flow fields.

   - Frotuberance Induced Flows

     - Typical of various H/O Tank, SRB and Orbiter protuberances

2. Critical Expansion-Induced Separated Flows

- SRB Worst-Case Shoulder Separation $\sim M_\infty \approx 0.75$

3. Critical Transonic Shock Oscillation Environments

- SRB Cylinder - $M_\infty = 0.78, 0.82, 0.86, 0.90, 0.94$
- H/O Tank Cylinder - $M_\infty = 0.90$
- Orbiter Upper Fuselage (in the range of SRB and H/O Tank data)

4. Critical Interference-Flow Environments

- Typical SRB, H/O Tank and Orbiter Stations
  - Shock-Induced Interference Flow - $M_\infty = 1.31, 1.6, 2.0, 3.0$
  - Shock-Free Interference Flow - $M_\infty = 0.60, 1.00, 1.31$

Primary emphasis has been given to the condition of maximum dynamic pressure since this flight condition will generally produce the most severe fluctuating pressure environments. However, it is equally important to consider certain critical flow conditions which are unique to Mach numbers below the condition of MAX Q, such as transonic shoulder-induced flow separation and transonic shock-wave oscillation. Finally, critical interference-flow environments will be generated due to bow-shock impingement which will occur at supersonic Mach numbers. For the latter case, a range of supersonic Mach numbers are considered, starting at $M_\infty = 1.31$ (MAX Q) and ranging up to $M_\infty = 3.0$.

The computations represent typical overall fluctuating pressure levels and one-third octave band spectra which may be anticipated within the perturbed flow region under analysis. It should be noted that the predictions are based on estimated average values of local flow parameters rather than actual measured values. The greatest uncertainty in the predictions is in the frequency scale rather than the amplitude scale since errors in the specification of local flow conditions (typical length scale and velocity scale) will cause a translation in frequency rather than amplitude. If actual local values of boundary layer thickness, flow separation length and velocity become available, the frequency scale for the predictions may be adjusted accordingly. The following relationship will apply for correcting the frequency scale of the predictions.

$$f = \frac{\delta_p}{\delta} \frac{U}{U_p} \cdot f_p \quad , \quad \text{Hz}$$

where the subscript p denotes the values used in the prediction.

Variations in overall fluctuating pressure levels and one-third octave band spectrum levels may be anticipated for full-scale dynamic pressures different from those employed in the predictions. An adjustment to the predicted values for different values of q_∞ can be made as follows:

$$\text{OAFPL} = (\text{OAFPL})_p + 20 \log_{10} \left[\frac{q_\infty}{(q_\infty)_p} \right], \text{ dB}$$

$$1/3 \text{ OBFPL} = (1/3 \text{ OBFPL})_p + 20 \log_{10} \left[\frac{q_\infty}{(q_\infty)_p} \right], \text{ dB}$$

In the following sections, the computed overall fluctuating pressure levels and one-third octave band spectra are discussed for the various fluctuating pressure environments which are expected to be encountered at critical Space Shuttle flight conditions.

5.1 Maximum Dynamic Pressure, MAX Q

The following trajectory parameters were employed in the predictions of MAX Q fluctuating pressure levels and spectra.

- Mach number, $M_\infty = 1.31$
- Dynamic Pressure, $q_\infty = 649.4$ lb/ft^2
- Altitude, h = 34,400 ft
- Free-Stream Velocity, $U_\infty = 1,296$ ft/sec

Representative spectra for the unsteady flow fields which will be encountered by the mated Space Shuttle vehicles at MAX Q are presented in Figure 21. The following environments were analyzed using a nominal value of local boundary layer thickness of 1.0 foot and a nominal value of local velocity equal to free-stream velocity.

- Attached Turbulent Boundary Layer Flow
- Homogeneous Compression-Induced Separated Flow
- Shock-Boundary Layer Interactions
- Three-Dimensional Protuberance Induced Flow

Attached turbulent boundary layer flow may be anticipated for much of the vehicle surface at MAX Q with overall fluctuating pressure levels near 137 dB. With the exception of interference flow regions between the various bodies, local protuberance flows, and exhaust plume—induced separated flow, all surfaces will experience fluctuating pressures characteristic of the attached flow environment.

Homogeneous separated flow regions (separated flow regions not affected by shock-wave oscillation) will experience fluctuating pressure levels near 148 dB. Typical areas are the interference flow region between the H/O Tank and SRB cylinders downstream of the shoulders, and between the H/O Tank and Orbiter fuselage well downstream of the Orbiter nose. Also, local surface irregularities such as the crew compartment canopy and two-dimensional type protuberances will have regions of homogeneous separated flow. Shock-boundary layer interaction regions will experience fluctuating pressure levels near 161 dB at MAX Q and typical areas are the interference regions in the vicinity of the nose cones and cone-cylinder shoulders on the SRB and the interference region between the Orbiter nose and H/O Tank. Also, boundary layer separation and reattachment points in a local supersonic environment, such as the crew compartment canopy and various protuberances, will experience shock-induced fluctuating pressures near 160 dB. Three-dimensional protuberances are defined as protuberances which will cause the perturbed flow to move around the protuberance transverse to the local unperturbed flow direction. Extremely large fluctuating pressures may be anticipated for these environments due to the large vortex action within the three-dimensional separated flow field (see Reference 22). Levels at MAX Q may be anticipated near 168 dB.

The frequency characteristics of the various fluctuating pressure environments are shown in Figure 21 and may be summarized as follows:

- Attached Turbulent Boundary Layers — HIGH FREQUENCIES
- Homogeneous Separated Flows (2-D and 3-D) — INTERMEDIATE FREQUENCIES
- Shock-Boundary Layer Interactions — LOW FREQUENCIES

Naturally, consideration must be given to local length and velocity scales when determining spectra for specific flow conditions. A composite of predicted spectra for various specific areas of the Space Shuttle is presented in Figure 19 of Reference 33 where consideration was given to anticipated local flow conditions and typical length and velocity scales; the present predictions are similar.

5.2 Critical Expansion-Induced Separated Flows

Expansion-induced separated flows will occur at the cone-cylinder junctures of the SRB, possibly above the crew compartment of the Orbiter (depending on shoulder geometry) and in the wake of certain protuberances and other surface irregularities. With the exception of bluff geometries, expansion-induced separated flow will be confined, primarily, to moderate and low subsonic Mach numbers. Typical examples are the cone-cylinder junctures of the SRB. For these cases, maximum disturbances will occur immediately prior to flow attachment. A typical spectrum is shown in Figure 22. Predicted levels are near 157 dB for the SRB. Disturbances in the vicinity of flow reattachment aft of the shoulder peak in the frequency range from 8 to 16 Hz.

5.3 Critical Transonic Shock-Oscillation Environments

Following flow attachment at the shoulders of the SRB and aft of the crew compartment on the Orbiter, local supersonic flow will result in a near normal, transonic, terminal shock wave. Typical spectra for the SRB are shown in Figure 23. Flow attachment is predicted at $M_\infty = 0.78$ for the SRB shoulder and corresponds to the condition of maximum transonic shock-induced pertubations with an overall level of 164 dB. As Mach number is increased, the shock wave will move aft on the SRB cylinders and decrease in strength with a predicted level of 143 dB at $M_\infty = 0.94$. The frequency of peak fluctuating pressure level also decreases as the shock moves aft due to: 1) the increase in inflowing boundary layer thickness upstream of the shock wave, and 2) the decrease in local velocity which results from the isentropic recompression between the shoulder and the shock wave. Peak frequencies of shock-induced disturbances are estimated to be 40 Hz at $M_\infty = 0.78$, decreasing to 4 Hz at $M_\infty = 0.94$. As Mach numbers approach 1.0, the shock is further weakened with surface disturbances approaching those of attached flow. Based on a 30° cone, as discussed earlier, critical terminal shock oscillation on the ogive-cylinder H/O tank is estimated to be 156.6 dB at $M_\infty = 0.90$. This level should be regarded as an upper bound, with the actual level several dB lower.

Without detailed knowledge of the Orbiter crew compartment geometry, it is difficult to determine the exact nature of terminal shock-oscillation on the Orbiter fuselage. However, it will occur and may be expected to exhibit characteristics similar to the H/O Tank and SRB environments.

5.4 Critical Interference-Flow Environments

It was previously noted in Section 4.0 that several regions of the mated Space Shuttle vehicles will experience interference flow environments caused by the close proximity of the various bodies composing the launch configuration. Interference-flow fields on the Space Shuttle will be caused, in general, by the impingement of shock waves from one body onto the surface of a neighboring body. Naturally, shock-wave impingement is possible only in a local supersonic flow environment. At local subsonic Mach numbers, say downstream of shock-boundary layer interaction regions for supersonic free-stream conditions, the perturbed flow field will not contain shock waves even though the flow field is caused by interference between flow fields. Thus, it is convenient to define two basic types of interference flow fields:

- Shock-Induced Interference Flows
- Shock-Free Interference Flows

With the exception of possible transonic terminal shock-wave impingement* , shock-induced interference flows will occur only at supersonic free-stream conditions whereas shock-free interference flows may occur at all Mach numbers. Typical spectra for shock-induced interference flows typical of the interference regions between the H/O Tank and SRB (due to SRB bow shock impingement) between H/O Tank and Orbiter fuselage (due to Orbiter bow shock impingement) and between the SRB and the lower surface of the Orbiter wings (due to the impingement of the Orbiter wing leading edge shocks) are shown for a range of supersonic Mach numbers in Figure 24. Also shown in Figure 24 are representative spectra for shock-free regions of the interference-flow field areas which are predicted to be affected by this environment and are the neighboring surfaces of the SRB and H/O Tank cylinders (downstream of the shoulders), the neighboring surfaces between the H/O Tank and Orbiter well downstream of the Orbiter nose, and the lower surface of the Orbiter wings and aft cylinders of the SRB.

5.5 Comparison of Predictions with Experimental Measurements

In Reference 33, a detailed comparison was made between predictions for the MSC - 049 Shuttle configuration with measurements reported in Reference 34. The same general discussion applies to the present predictions, and will not be repeated herein. Shown in Figure 25 is a comparison of present predicted levels to measured levels at critical transonic conditions.

---

* Recently published data (Reference 34, discussed in Reference 33) indicates that shock-induced interference flow due to a blocked terminal-shock wave between the H/O Tank and Orbiter nose does occur at near-sonic Mach numbers.

6.0 CONCLUDING REMARKS

Preliminary estimates of Space Shuttle fluctuating pressure environments have been made based on prediction techniques developed by Wyle Laboratories. Particular emphasis has been given to the transonic speed regime during launch of a parallel-burn Space Shuttle configuration. The baseline configuration, together with a typical flight trajectory, have been used as models for the predictions. Analyses have consisted of the following:

- Description of Flow Fields and Attendant Fluctuating Pressure Environments for the Space Shuttle Launch Configuration. In most cases, these analyses are sufficiently general to be applicable to any parallel-burn launch configuration consisting of a reusable Orbiter vehicle, external H/O Tank and two strap-on solid rocket motors.

- Specification of Interference-Free and Interference-Induced Flow Fields and Empirically Determined Attendant RMS Fluctuating Pressure Levels and Power Spectral Densities. Particular emphasis has been given to the transonic Mach number regime during launch.

- Prediction and Evaluation of Plume-Induced Separated Flow Environments.

- Analyses of Overall Fluctuating Pressure Levels (Expressed in Decibels) and One-Third Octave Band Spectra of Various Fluctauting Pressure Environments which are Expected to be Encountered at Critical Space Shuttle Flight Conditions.

- Comparison of Analytical Predictions with Wind Tunnel Measurements for Various Regions of a Typical Space Shuttle Vehicle.

The results of this study have resulted in the following conclusions·

1) The following critical flow environments together with typical overall fluctuating pressure levels are predicted:

   - Cone-Cylinder Shoulder-Induced Separated Flow on the SRB with OAFPL Peaks Near 157 dB for Zero Angle of Attack

   - Terminal Shock-Wave Oscillation on the SRB, H/O Tank and Orbiter Fuselage Upper Surface Aft of Crew Compartment with OAFPL Peaks Near 164 dB

   - Three-Dimensional Protuberance Flows Representative of Various Space Shuttle Protuberance Environments with OAFPL Peaks Near 168 dB

   - Compression-Corner Induced Separated Flow in the Vicinity of the Orbiter Crew Compartment with OAFPL Ranging up to 148 dB and Peaks Near Flow Separation and Reattachment Ranging up to 157 dB

- Interference-Flow Environments Between the SRB and H/O Tank, Between the H/O Tank and Orbiter Nose, and Between the Orbiter Wind and SRB with Peak OAFPL Ranging up to 161 dB

- General Attached Flow Environments with OAFPL Ranging up to 137 dB

2) One-third octave band spectra for the above environments were generally one of three types:

   - Attached Turbulent Boundary Layer Spectra — Typically High Frequencies

   - Homogeneous Separated Flow and Shock-Free Interference Flow Spectra — Typically Intermediate Frequencies

   - Shock-Oscillation and Shock-Induced Interference Flow Spectra — Typically Low Frequencies

3) Flow separation due to the SRB engine exhaust plumes will occur shortly after MAX Q. Fluctuating environments will be comparable to those associated with compression corners. Separation due to the Orbiter engine exhaust plume occurs at high enough altitude such that it does not represent an important fluctuating pressure environment.

4) Comparisons between predicted and experimentally measured OAFPL showed good agreement except over aft portions of the Orbiter fuselage. In general, the agreement between OAFPL values for experiment and predictions was within 3 dB.

REFERENCES

1. Lowson, M. V., "Prediction of Boundary Layer Pressure Fluctuations," Wyle Laboratories Research Staff Report WR 67-15, October 1967.

2. Speaker, W. V. and Ailman, C. M., "Spectra and Space-Time Correlations of the Fluctuating Pressures at a Wall Beneath a Supersonic Turbulent Boundary Layer Perturbed by Steps and Shock Waves," NASA CR-486, May 1966.

3. Bull, M.K., "Properties of the Fluctuating Wall Pressure Field of a Turbulent Boundary Layer," AGARD Report 455, April 1963.

4. Bull, M.K., et al., "Wall Pressure Fluctuations in Boundary Layer Flow and Response of Simple Structure to Random Pressure Fields," University of Southampton, AASU Report 243, 1963.

5. Kistler, A. L. and Chen, W. S., "The Fluctuating Pressure Field in a Supersonic Turbulent Boundary Layer," Jet Propulsion Laboratory Technical Report No. 32-277, August 1962.

6. Belcher, P. M., "Prediction of Boundary Layer Turbulence Spectra and Correlations for Supersonic Flight," Presented at the 5th International Acoustic Congress, Liege, Belgium, September 1965.

7. Serafini, J. S., "Wall Pressure Fluctuations and Pressure Velocity Correlations in a Turbulent Boundary Layer," NASA TR R-165, December 1963.

8. Bakewell, H.P. Jr., et al., "Wall Pressure Correlation in Turbulent Pipe Flow," U. S. Navy Sound Laboratory Report No. 559, August 1962.

9. Shattuck, R. D., "Sound Pressures and Correlations of Noise on the Fuselage of a Jet Aircraft in Flight," NASA TN D-1086, August 1961.

10. Willmarth, W. W. and Roos, F. W., "Resolution and Structure of the Wall Pressure Field Beneath a Turbulent Boundary Layer," J. Fluid Mech., Vol. 22, Part 1, pp. 81-94, 1965.

11. Maestrello, L., "Measurement of Noise Radiated by Boundary Layer Excited Panels," J. Sound Vib., 2 (2), 1965.

12. Hilton, D. A., "In-Flight Aerodynamic Noise Measurements on a Scout Launch Vehicle," NASA TN D-1818, July 1963.

13. Williams, D.J.M., "Measurements of the Surface Pressure Fluctuations in a Turbulent Boundary Layer in Air at Supersonic Speeds," University of Southampton, AASU Report No. 162, Department of Aeronautics and Astronautics, December 1960.

14. Chyu, W. J. and Hanly, R. D., "Power and Cross-Spectra and Space Time Correlation of Surface Fluctuating Pressures at Mach Numbers Between 1.6 and 2.5," AIAA Preprint No. 68-77, January 1968.

15. Maestrello, L., "Measurement and Analysis of the Response Field of Turbulent Boundary Layer Excited Panels," J. Sound and Vib., 2 (3), July 1965.

16. Willmarth, W. W. and Woolridge, C. E., "Measurements of the Fluctuation Pressure at the Wall Beneath a Thick Turbulent Boundary Layer," J. Fluid Mech., Vol. 14, pp. 187-210, 1962.

17. Bozich, D. J. and White, R. W., "Study of the Vibration Responses of Shells and Plates to Fluctuating Pressure Environments," Wyle Laboratories Research Staff Report WR 69-19, September 1969.

18. Robertson, J. E., "Wind Tunnel Investigation of the Effects of Reynolds Number and Model Size on the Steady and Fluctuating Pressures Experienced by Cone Cylinder Missile Configurations at Transonic Speeds," AEDC-TR-66-266, March 1967.

19. Coe, Charles F., "Surface Pressure Fluctuations Associated with Aerodynamic Noise," Basic Aerodynamic Noise Research Conference Proceedings, NASA SP-207.

20. Coe, Charles F., and Rechtien, R. D., "Scaling and Spatial Correlation of Surface Pressure Fluctuations in Separated Flow at Supersonic Mach Numbers," Paper presented at the AIAA Structural Dynamics and Aeroelasticity Specialist Conference, New Orleans, La., April 16-17, 1969.

21. Rechtien, Richard D., "A Study of the Fluctuating Pressure Field Regions of Induced Flow Separation at Supersonic Speeds," University of Missouri - Rolla UMR Research Report, May 1970.

22. Robertson, J. E., "Characteristics of the Static- and Fluctuating-Pressure Environments Induced by Three-Dimensional Protuberances at Transonic Mach Numbers," Wyle Laboratories Research Staff Report WR 69-3, June 1969.

23. Robertson, J. E., "Fluctuating Pressures Induced by Three-Dimensional Protuberances," Wyle Laboratories Research Staff Report WR 70-10, April 1970.

24. Chapman, D.R., Kuehn, D.M., and Larson, H.K., "Investigation of Separated Flows in Supersonic and Subsonic Streams with Emphasis on the Effects of Transition," NACA Report 1356.

25. Incompressible Aerodynamics, Oxford at the Claredon Press, 1960.

26. Robertson, J. E., "Prediction of In-Flight Fluctuating Pressure Environments Including Protuberance Induced Flow," Wyle Laboratories - Research Staff Report WR 71-10, March 1971.

27. Tu, Bo-Jang, "Prediction of Wall Pressure Fluctuations Beneath a Turbulent Boundary Layer Flow at Supersonic and Hypersonic Speeds," Wyle Laboratories Research Staff Report TM 71-3, September 1971.

28. Plotkin, Kenneth J., "Shock Wave Oscillation Driven by Turbulent Boundary Layer Fluctuations," Wyle Laboratories Research Staff Report WR 72-12, September 1972.

29. Plotkin, Kenneth J., "Prediction of Fluctuating Pressure Environments Associated with Plume-Induced Separated Flow Fields," Wyle Laboratories Research Staff Report WR 73-3, May 1973.

30. Robertson, J. E., "Steady and Fluctuating Pressures on Cone-Cylinder Missile Configurations at Transonic Speeds," AEDC-TR-65-269, February 1966.

31. Coe, Charles F. and Koskey, Arthur J., "The Effects of Nose Bluntness on the Pressure Fluctuations Measured on 15° and 20° Cone-Cylinders at Transonic Speeds," NASA TM X-779, January 1963.

32. Himelblau, Harry, "Aeroacoustic, Vibration and Shock Environments for the Space Shuttle Orbiter," Paper presented at Space Shuttle Dynamics and Aeroelasticity Technology Working Group Meeting, Ames Research Center, Moffet Field, California, November 8-9, 1971.

33. Robertson, J. E., "Preliminary Estimates of Space Shuttle Fluctuating Pressure Environments," Wyle Laboratories Research Staff Report WR 72-10, August 1972.

34. Dobs, Jules B., Jr., and Hanly, Richard D., "In-Flight Aeroacoustic Environments on Prospective Space Shuttle Vehicles," Published in Proceedings of NASA Space Materials, San Antonio, Texas, April 12-14, 1972, NASA TM X-2570.

FIGURES

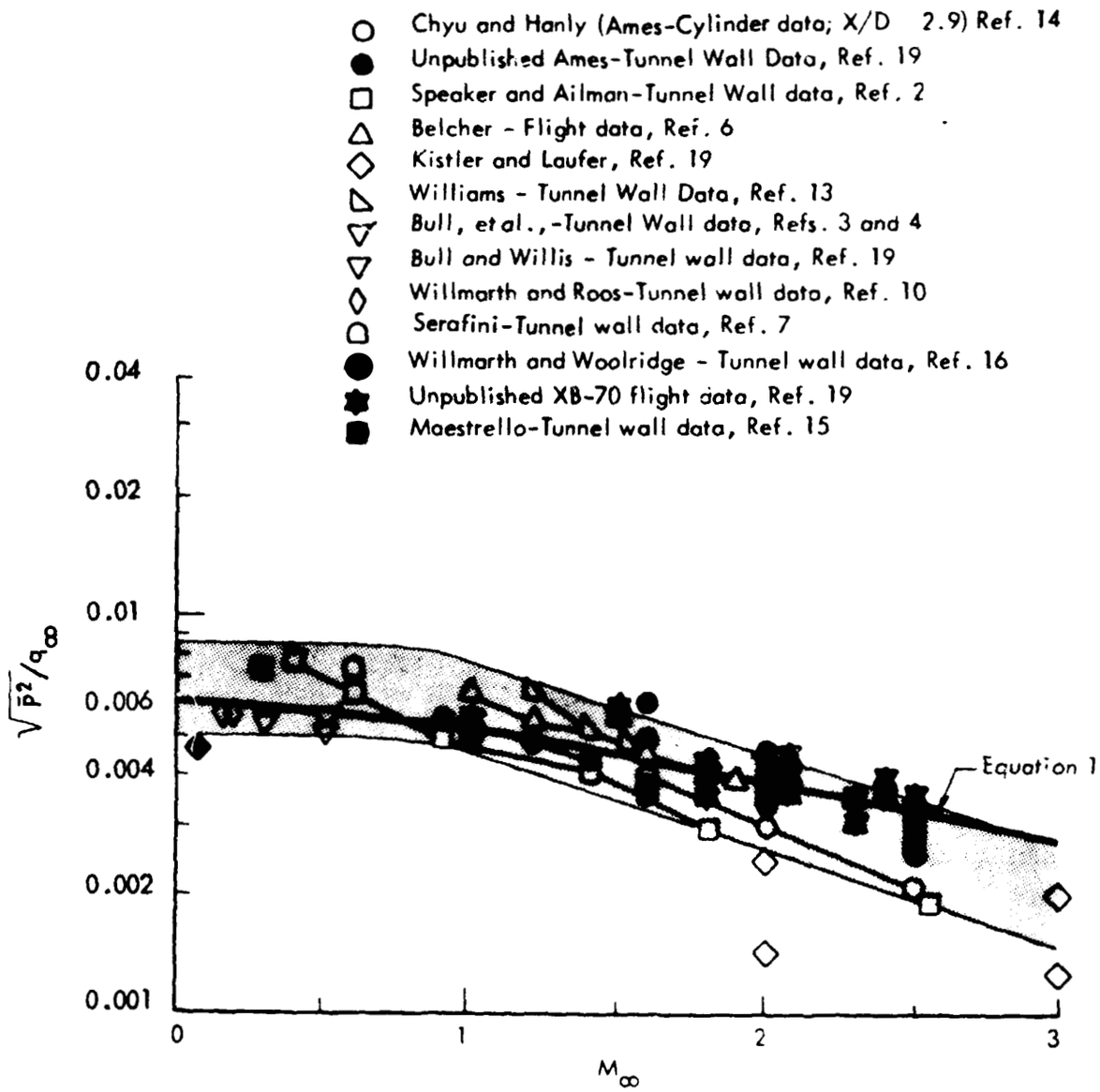

Figure 1. Comparison of Pressure Fluctuation Measurements by Various Investigators for Attached Turbulent Boundary Layers

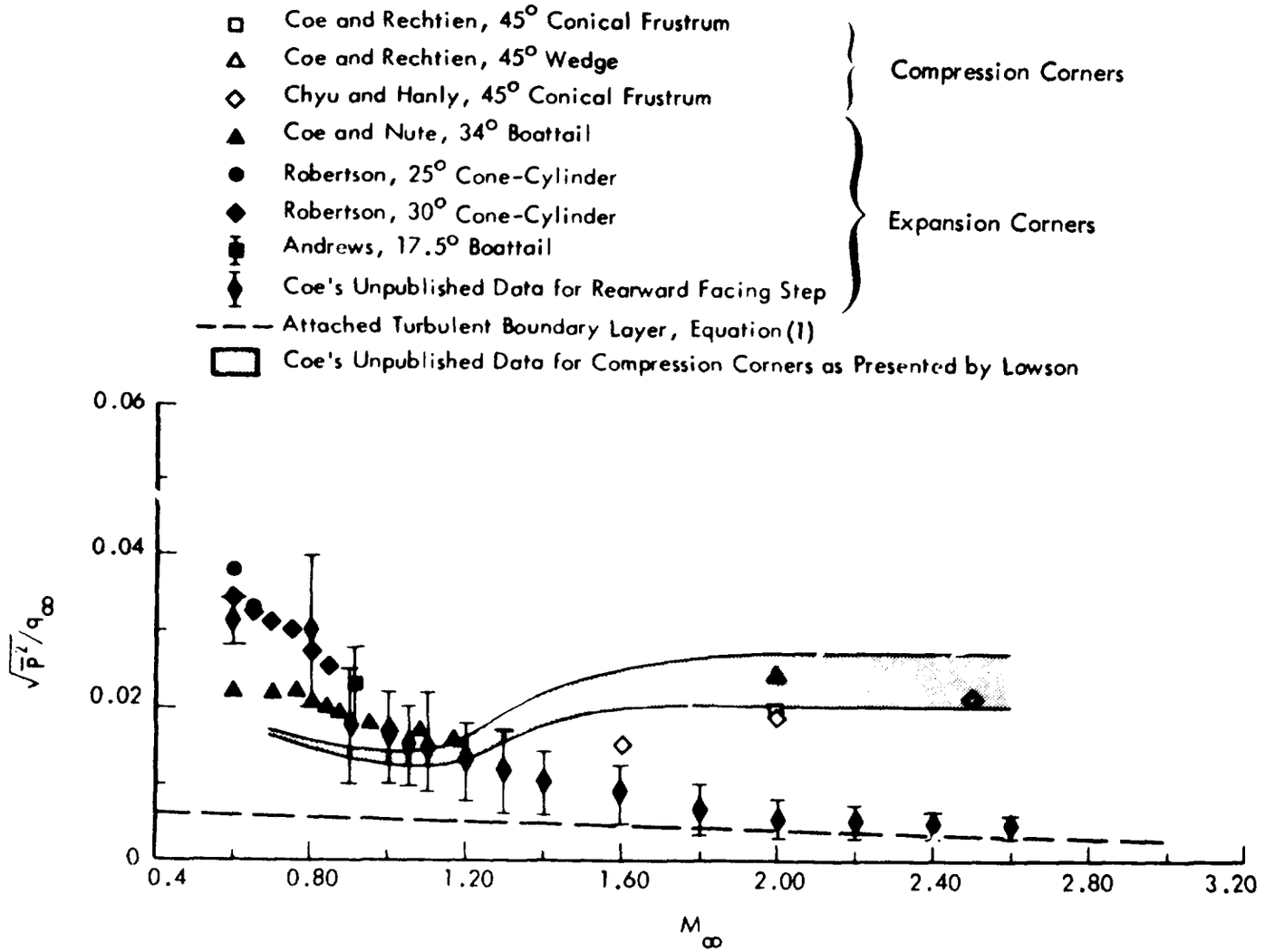

Figure 2. Variation of Fluctuating Pressure Level for Homogeneous Separated Flow with Mach Number

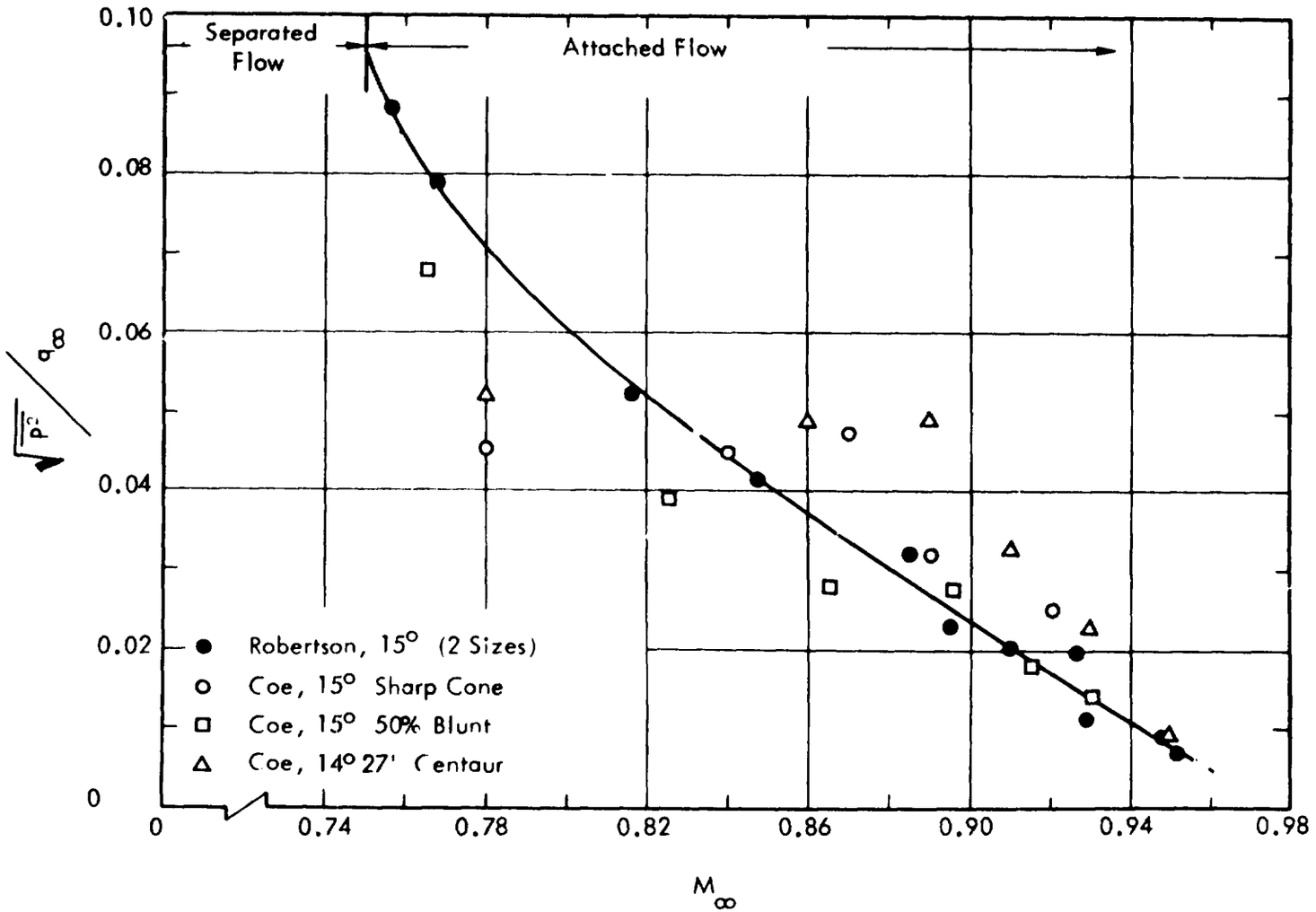

Figure 3. Variation of Fluctuating Pressure Level for Shock-Wave Oscillation with Mach Number

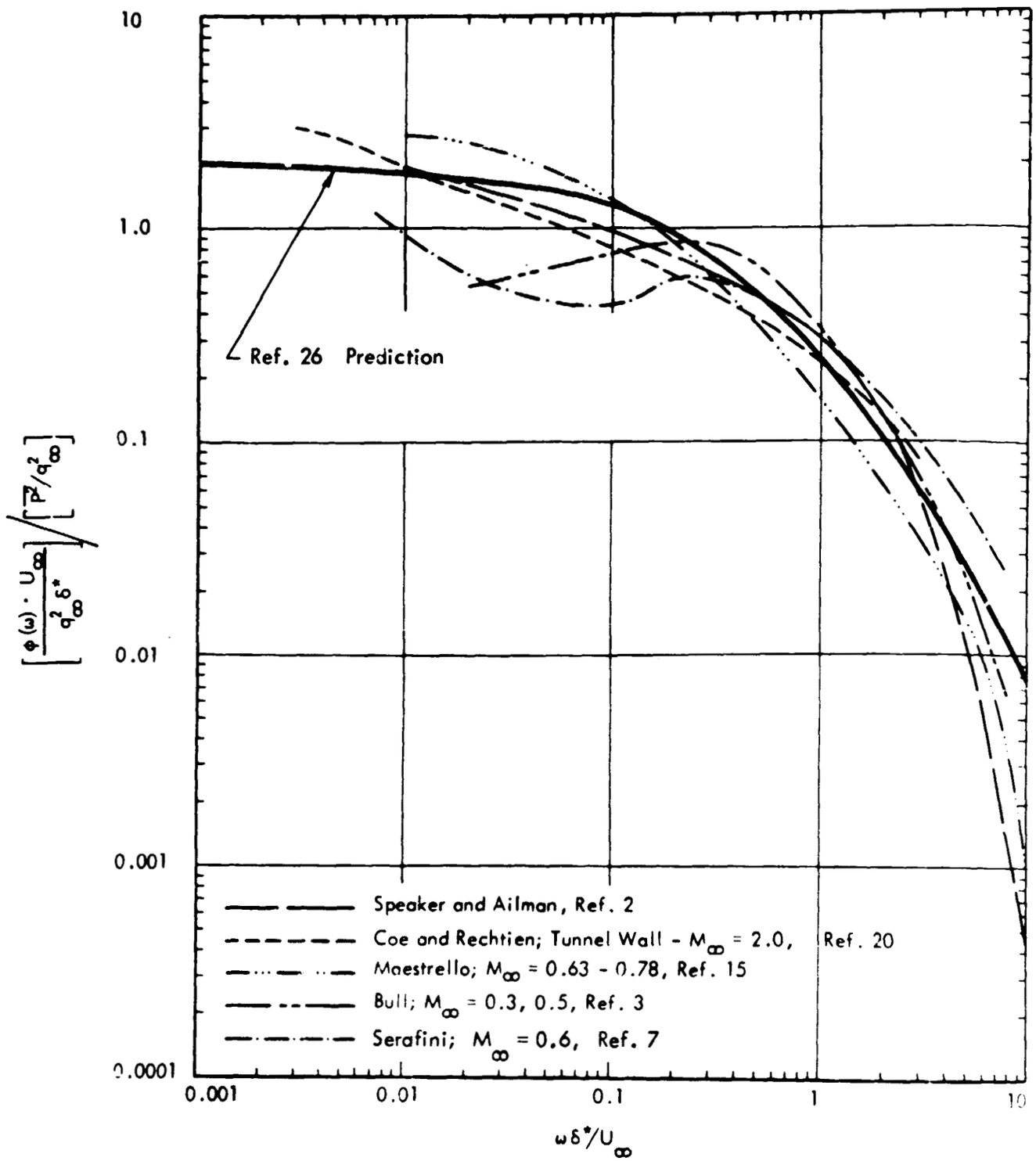

Figure 4. Power Spectra for Turbulent Boundary Layer Fluctuating Pressures

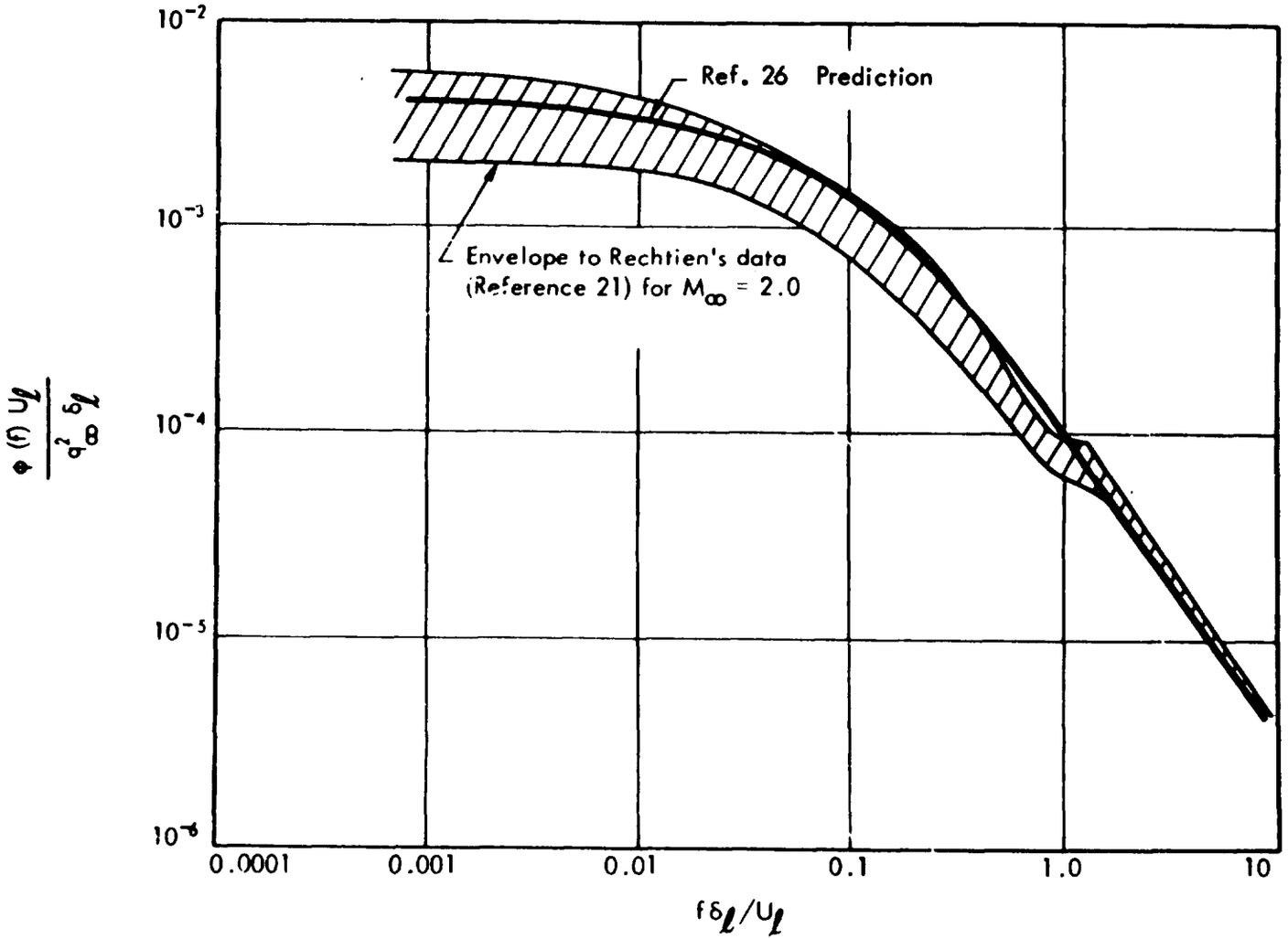

Figure 5. Power Spectrum of Fluctuating Pressures within Homogeneous Separated Flow Regions

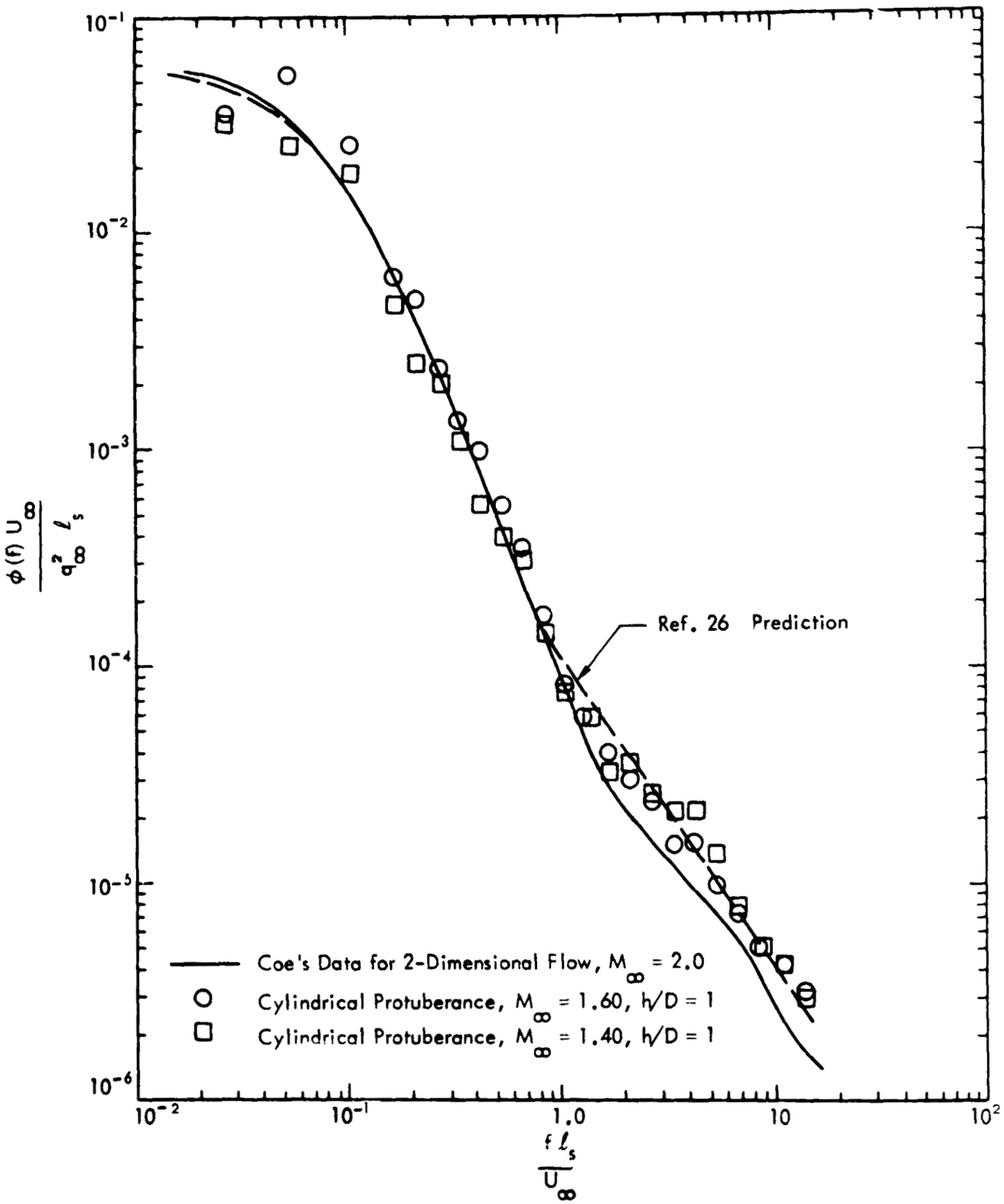

Figure 6. Comparison of Predicted and Measured Power Spectra for Shock-Wave Oscillation Upstream of Two- and Three-Dimensional Separated Flow Fields

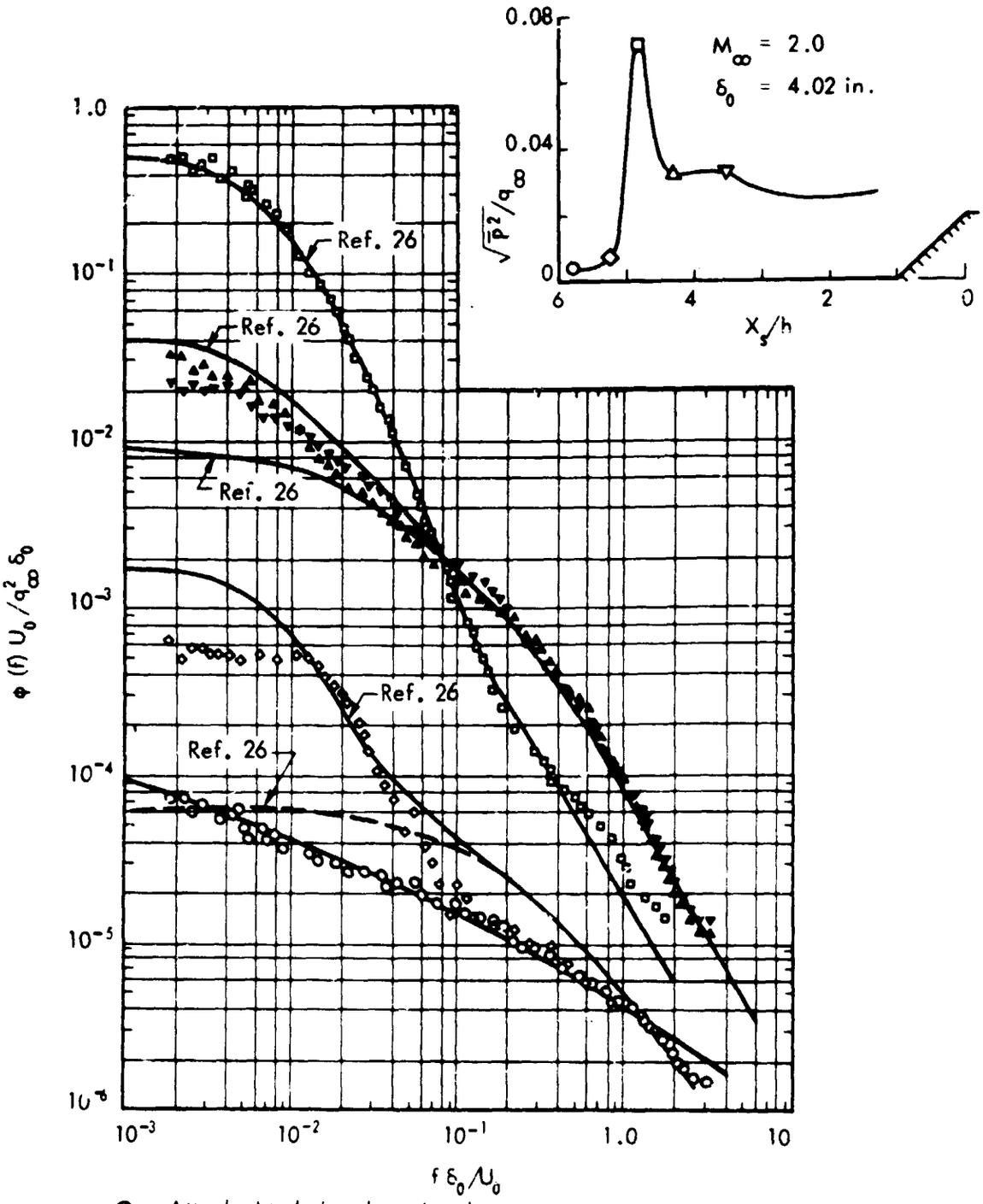

○ Attached turbulent boundary layer

◇ Non-homogeneous attached turbulent boundary layer

▽ △ Non-homogeneous separated flow

□ Shock wave oscillation

Figure 7. Longitudinal Distribution of Pressure Fluctuations and Typical Power Spectra in Vicinity of Supersonic Flow Separation Ahead of a 45° Wedge

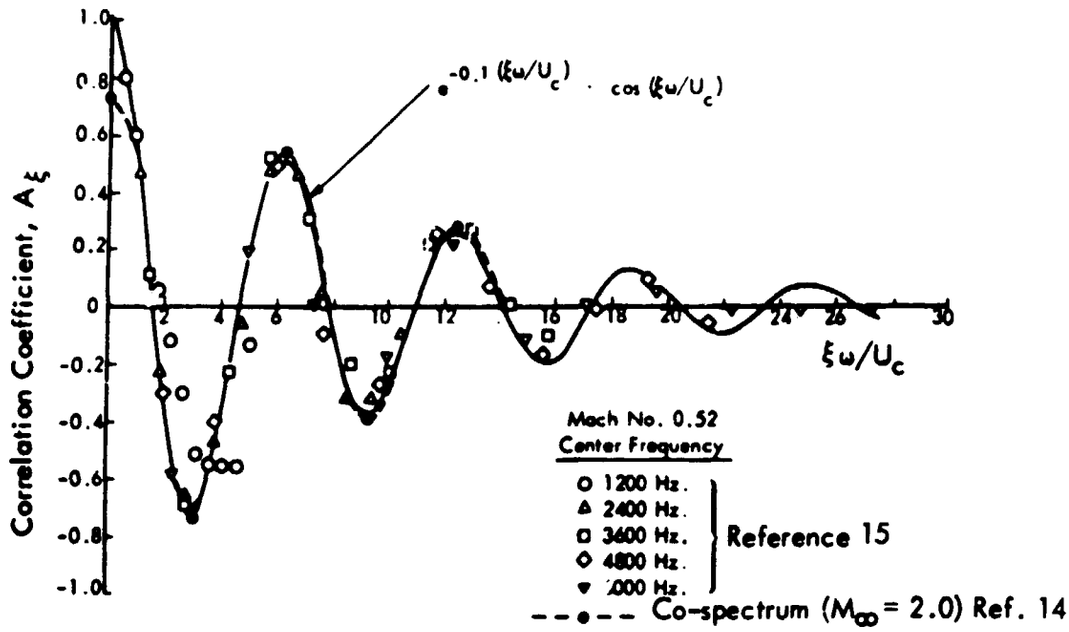

Figure 8(a). Narrow Band Longitudinal Space Correlation Coefficient for Boundary Layer Fluctuating Pressures

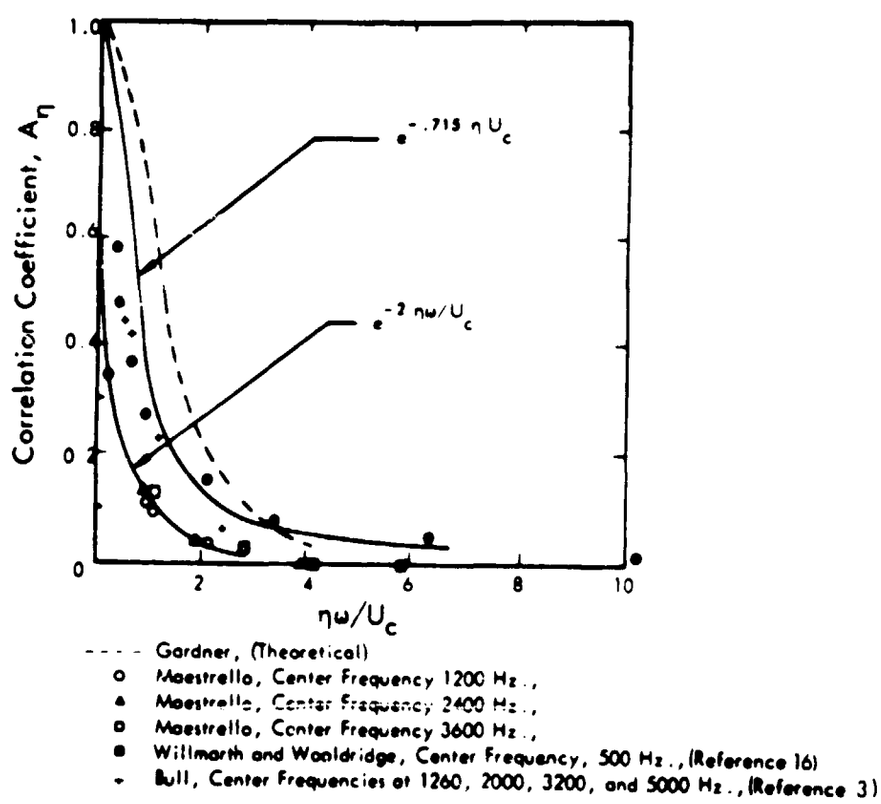

Figure 8(b). Narrow Band Lateral Space Correlation Coefficient for Boundary Layer Fluctuating Pressures

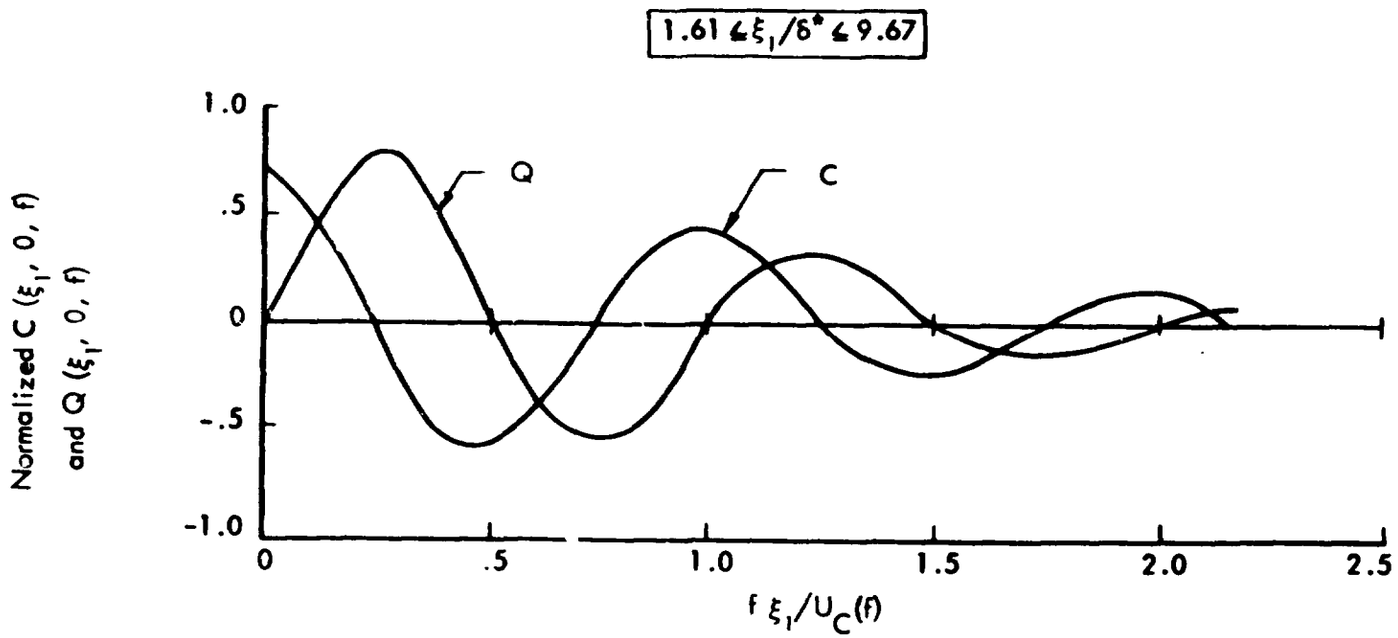

Figure 9. Typical Longitudinal Cross-Spectra of Pressure Fluctuations for Separated Flow (Ref. 14)

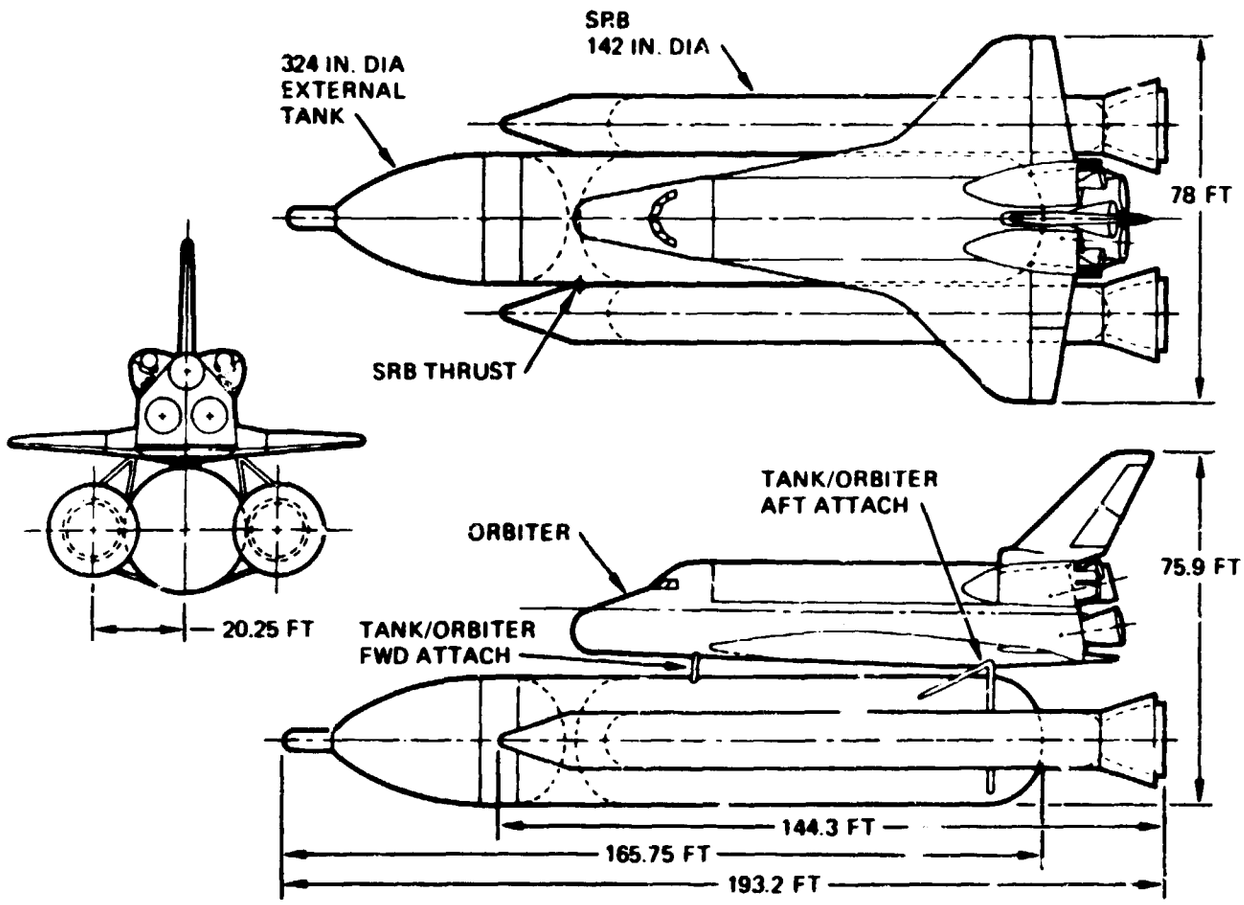

Figure 10. Schematic of Baseline Shuttle Launch Configuration

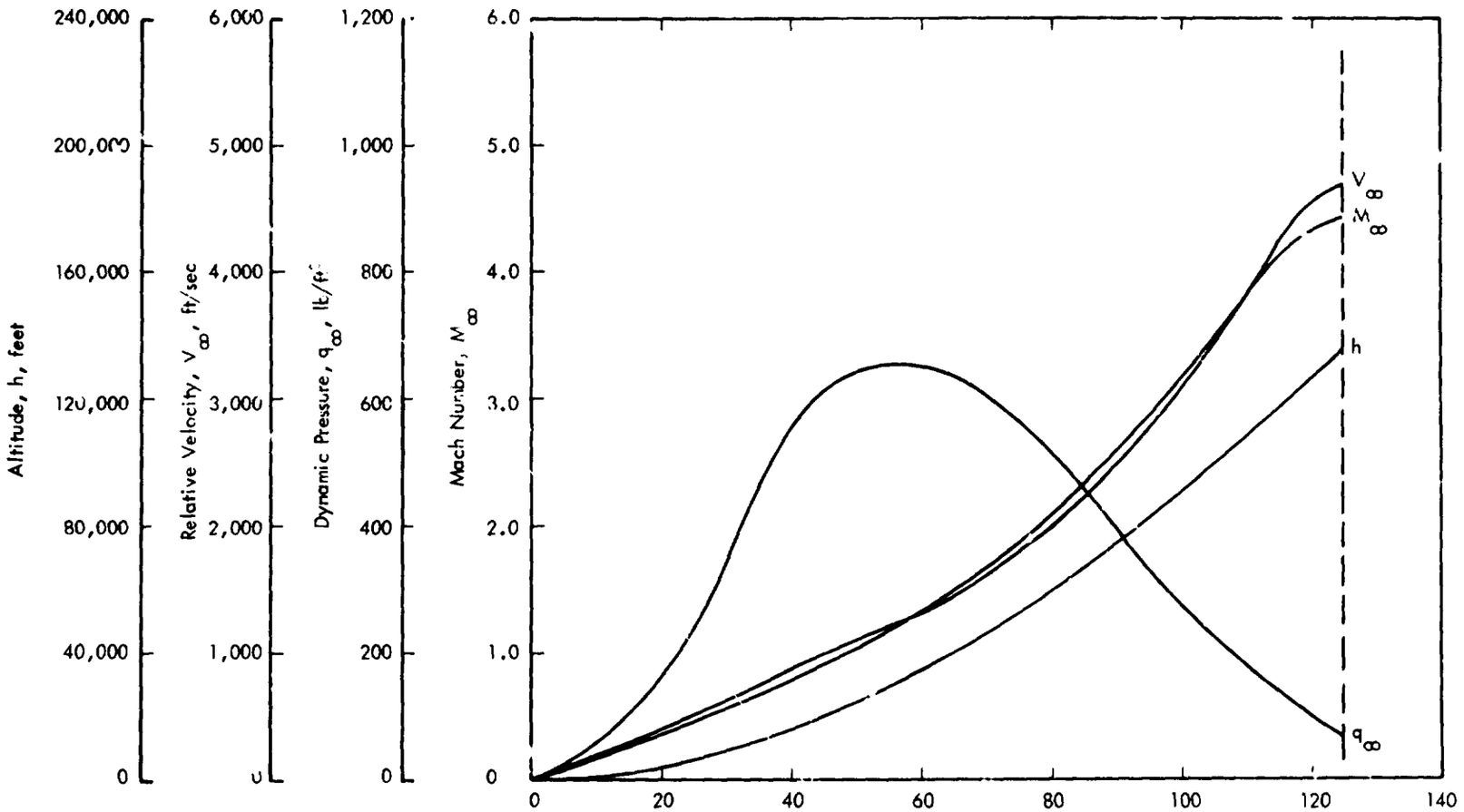

Figure 11. Trajectory Parameters for Baseline Shuttle Configuration

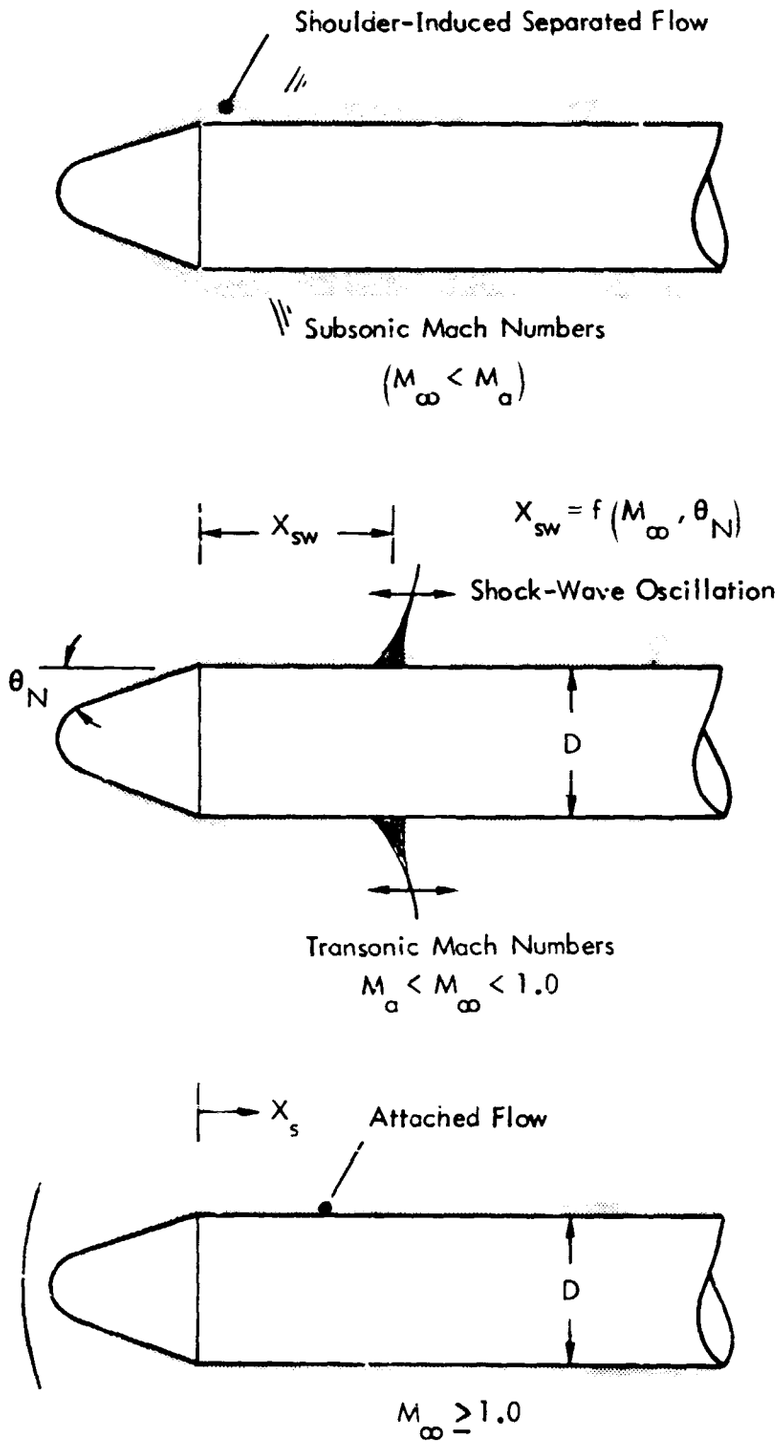

Figure 12. Schematic of Interference-Free Flows Over a Cone-Cylinder Body

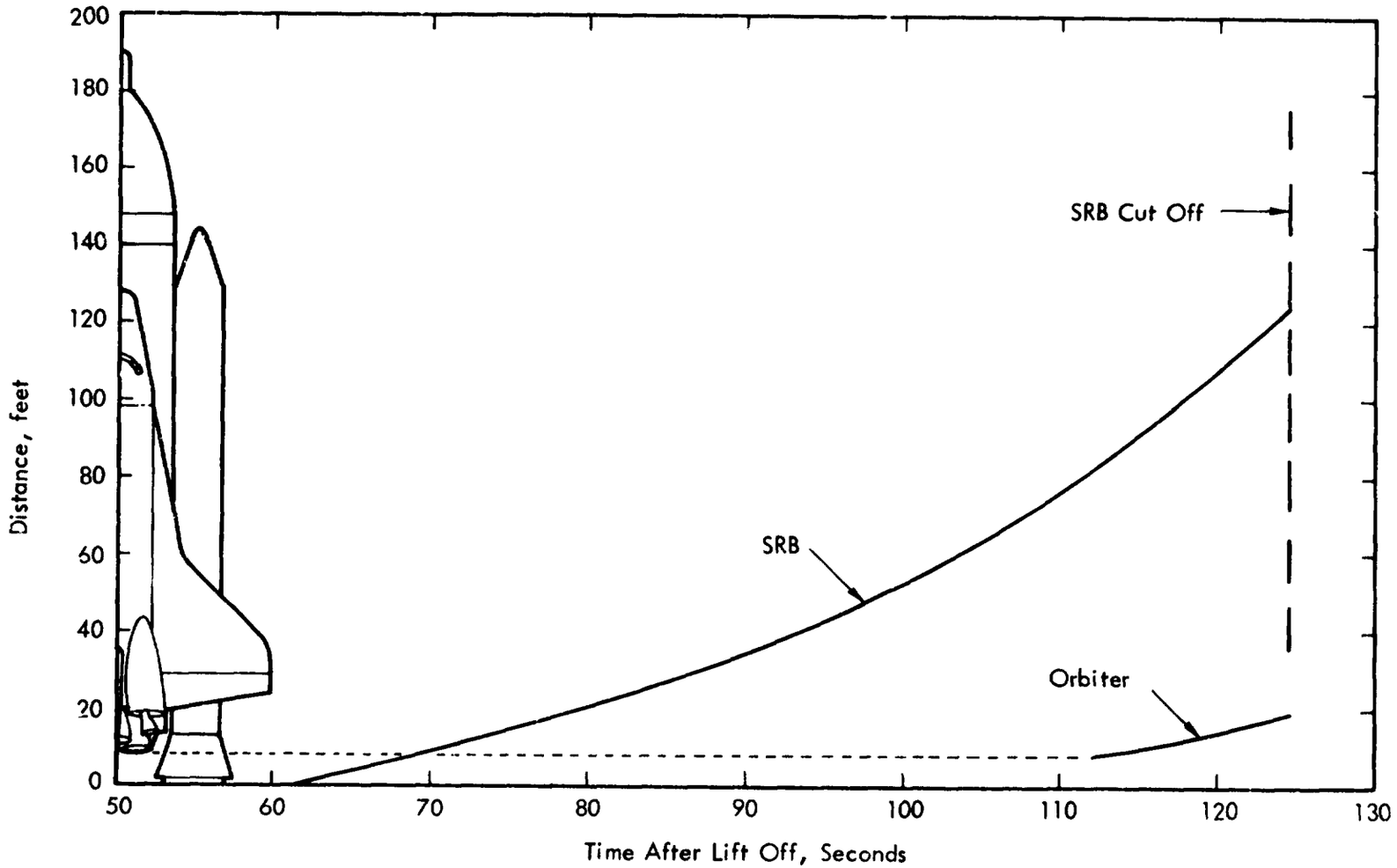

Figure 13. Location of Plume-Induced Separation Points on Baseline Shuttle

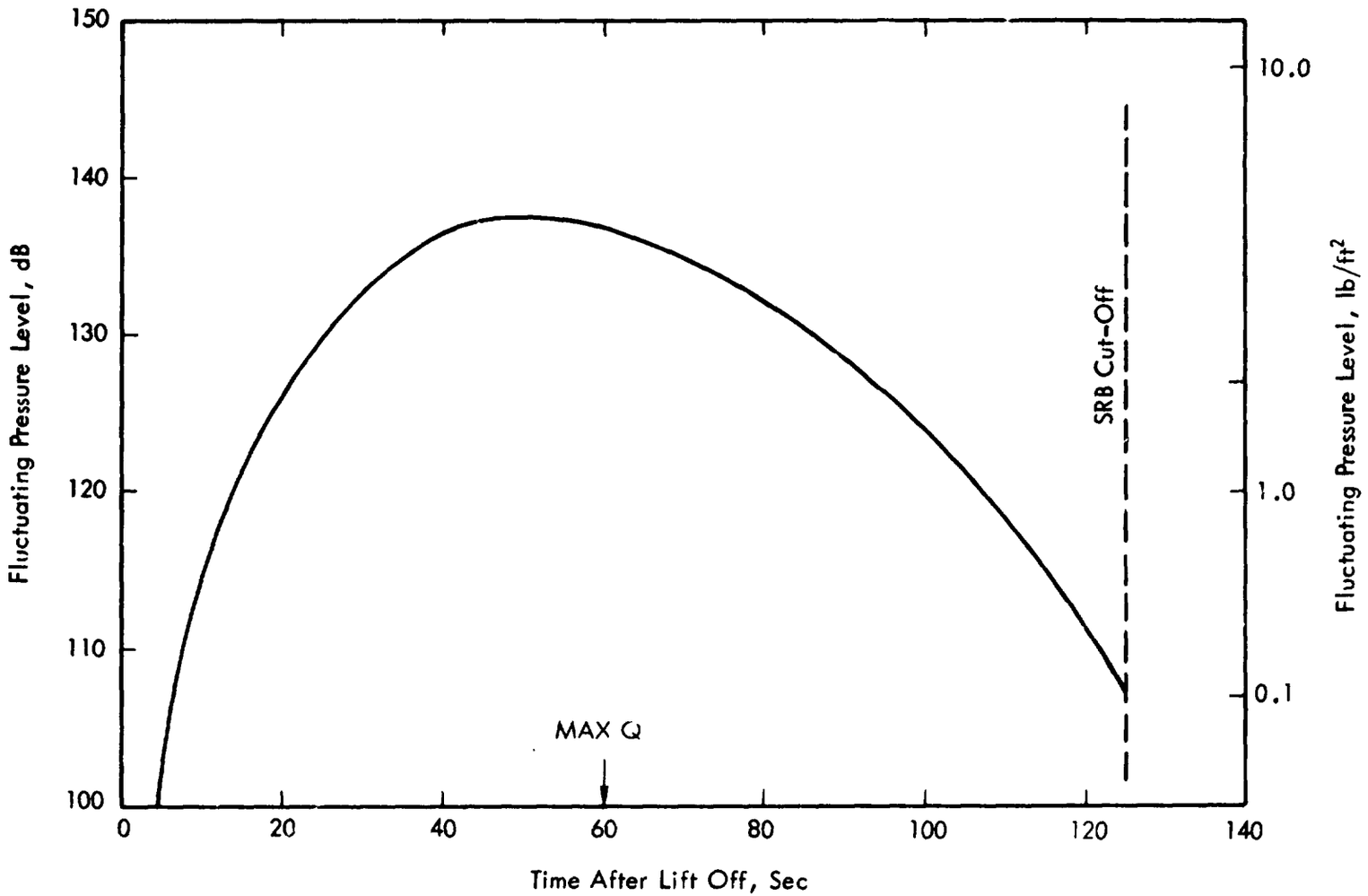

Figure 14. Basic Attached Flow Fluctuating Pressure Level, Shuttle Launch Trajectory

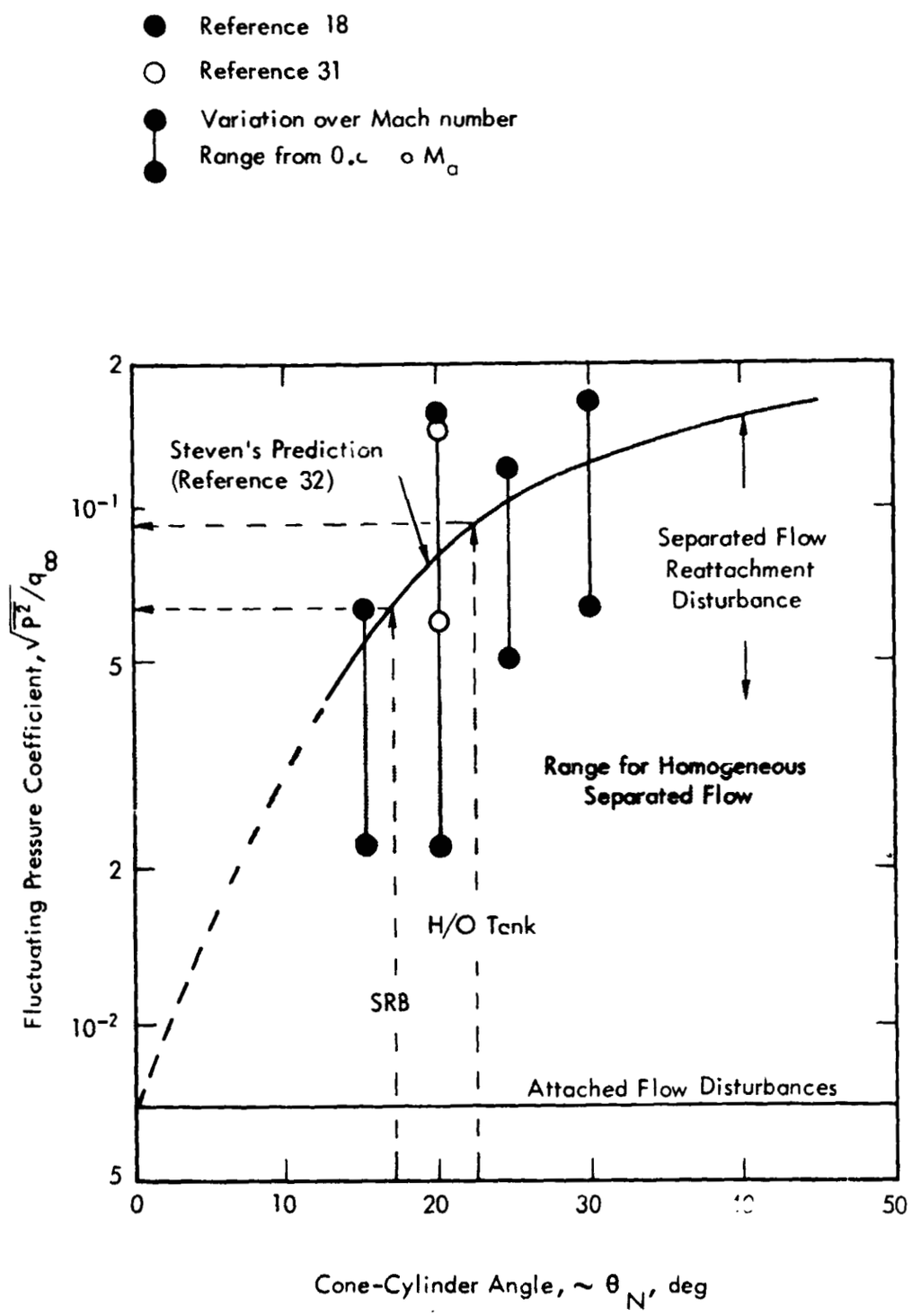

Figure 15. Maximum Fluctuating Pressure Coefficient for Separated Flow Behind a Cone-Cylinder Shoulder for Transonic Flight ($0.6 \leq M_\infty \leq M_a$)

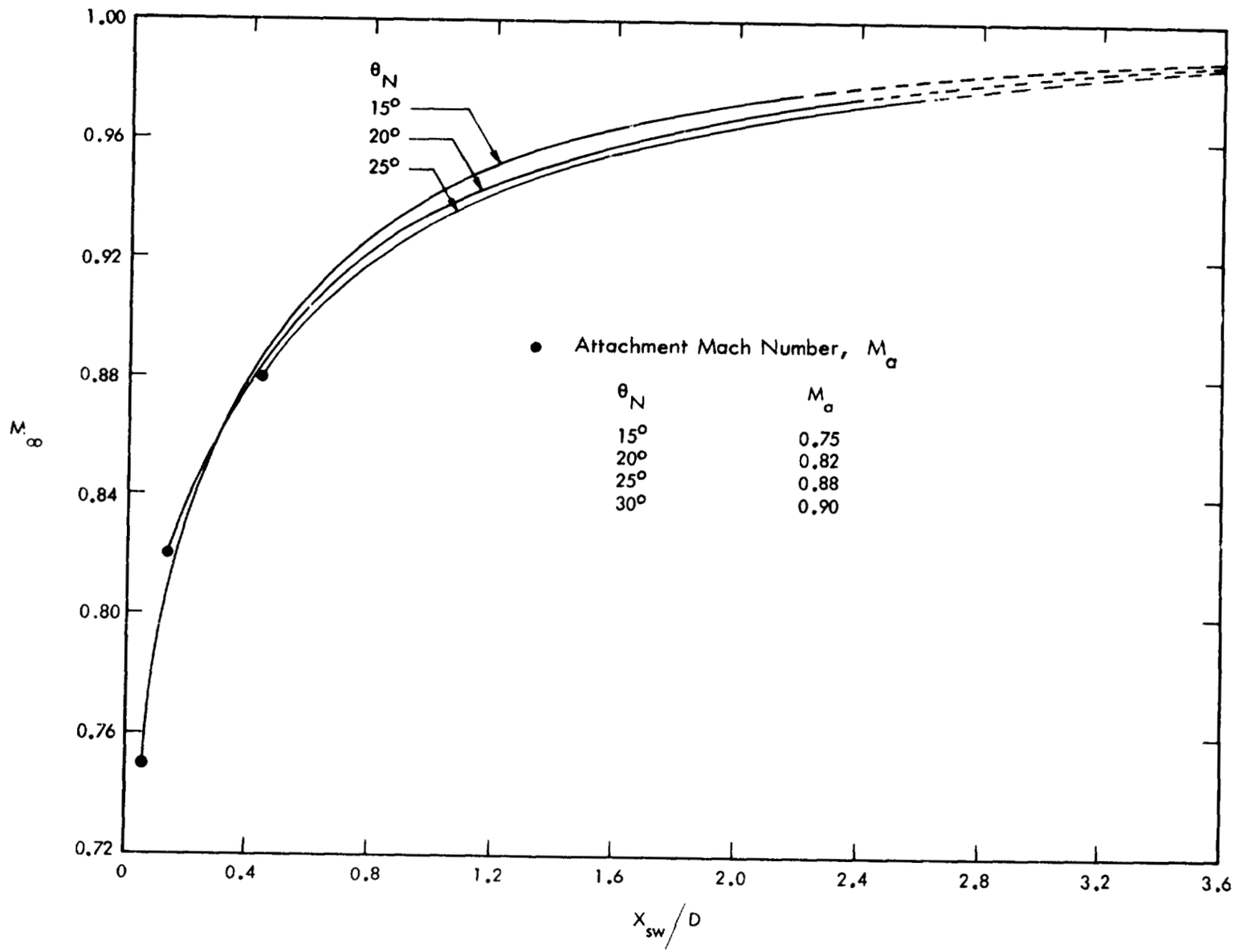

Figure 16. Variation of Terminal Shock-Wave Location with Free-Stream Mach Number for Interference-Free Flow Over Cone-Cylinder Bodies

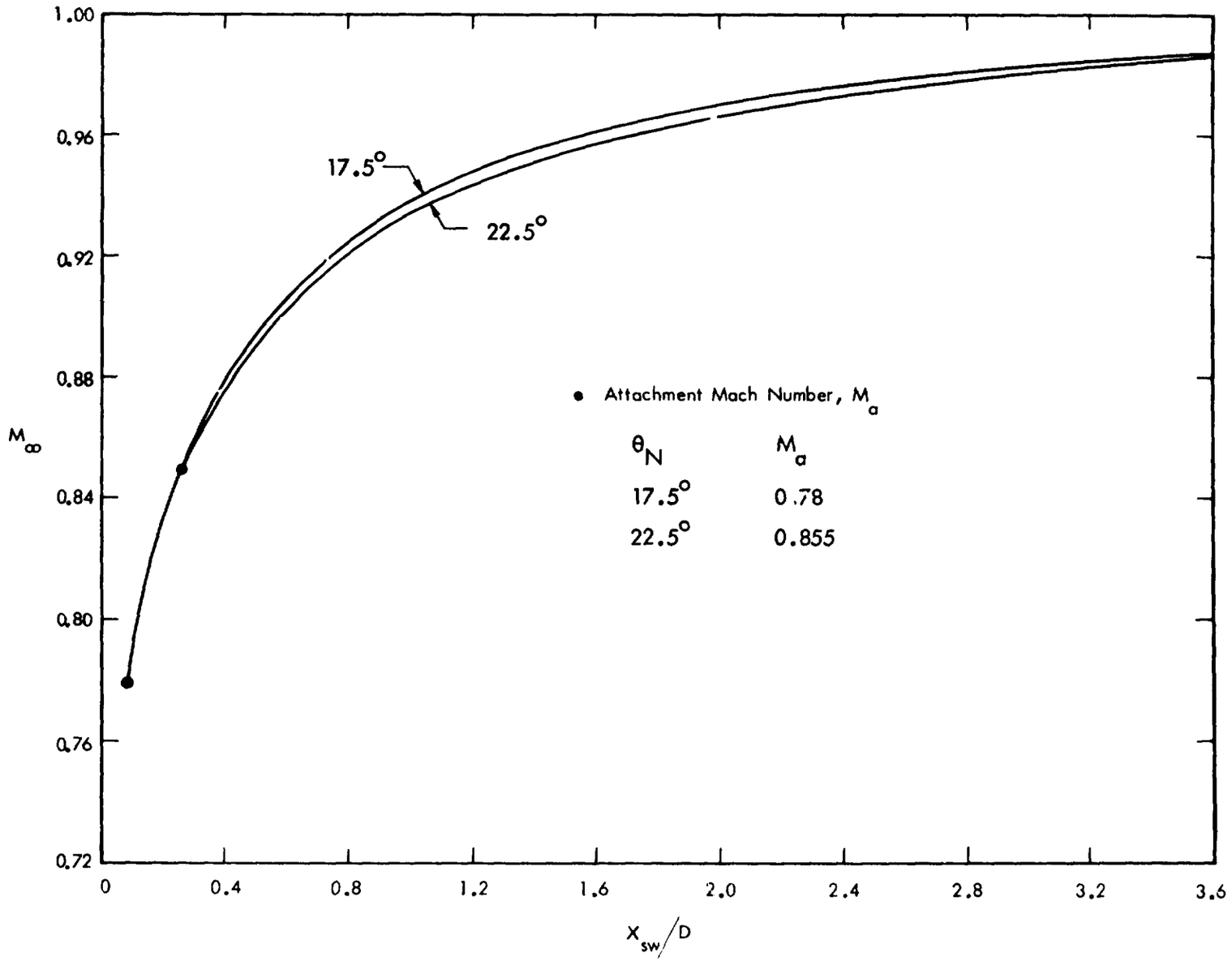

Figure 17. Variation of Terminal Shock-Wave Location, Interpolated for 17.5° and 22.5°

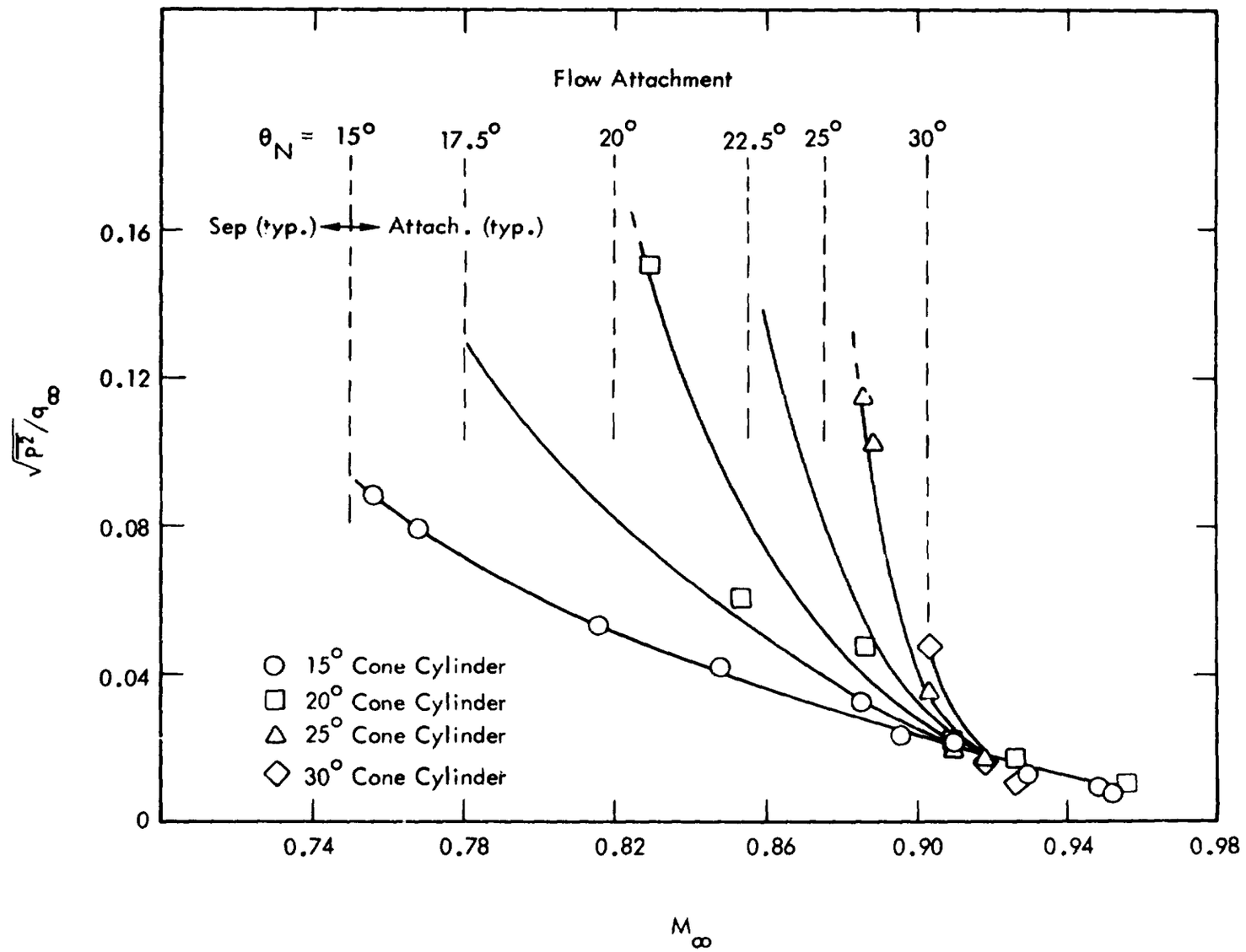

Figure 18. Variation of Transonic Shock-Induced Pressure Fluctuations With Free-Stream Mach Number for Various Cone-Cylinder Configurations (Reference 18)

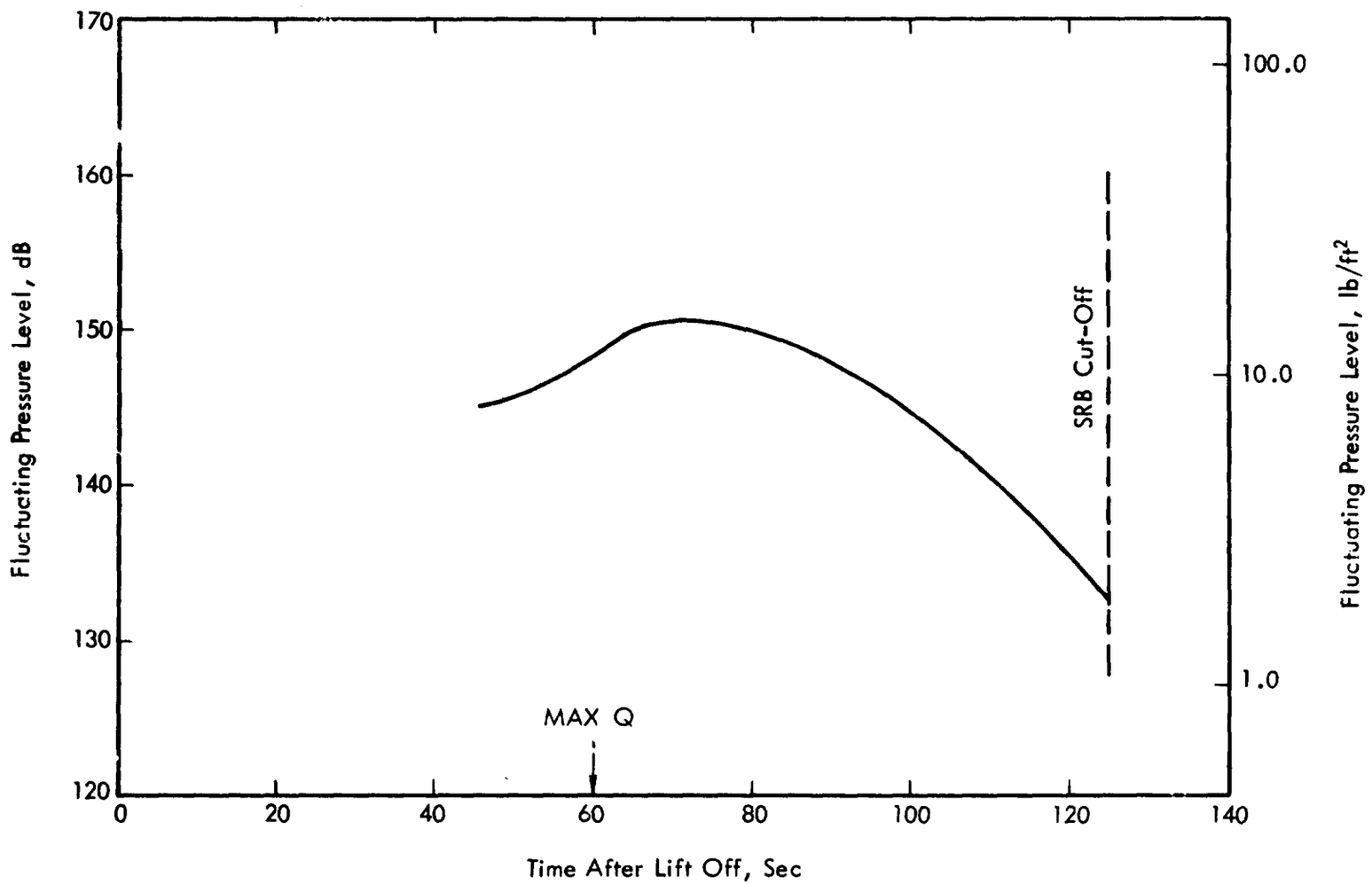

Figure 19. Basic Compression Corner Fluctuating Pressure Level, Shuttle Launch Trajectory

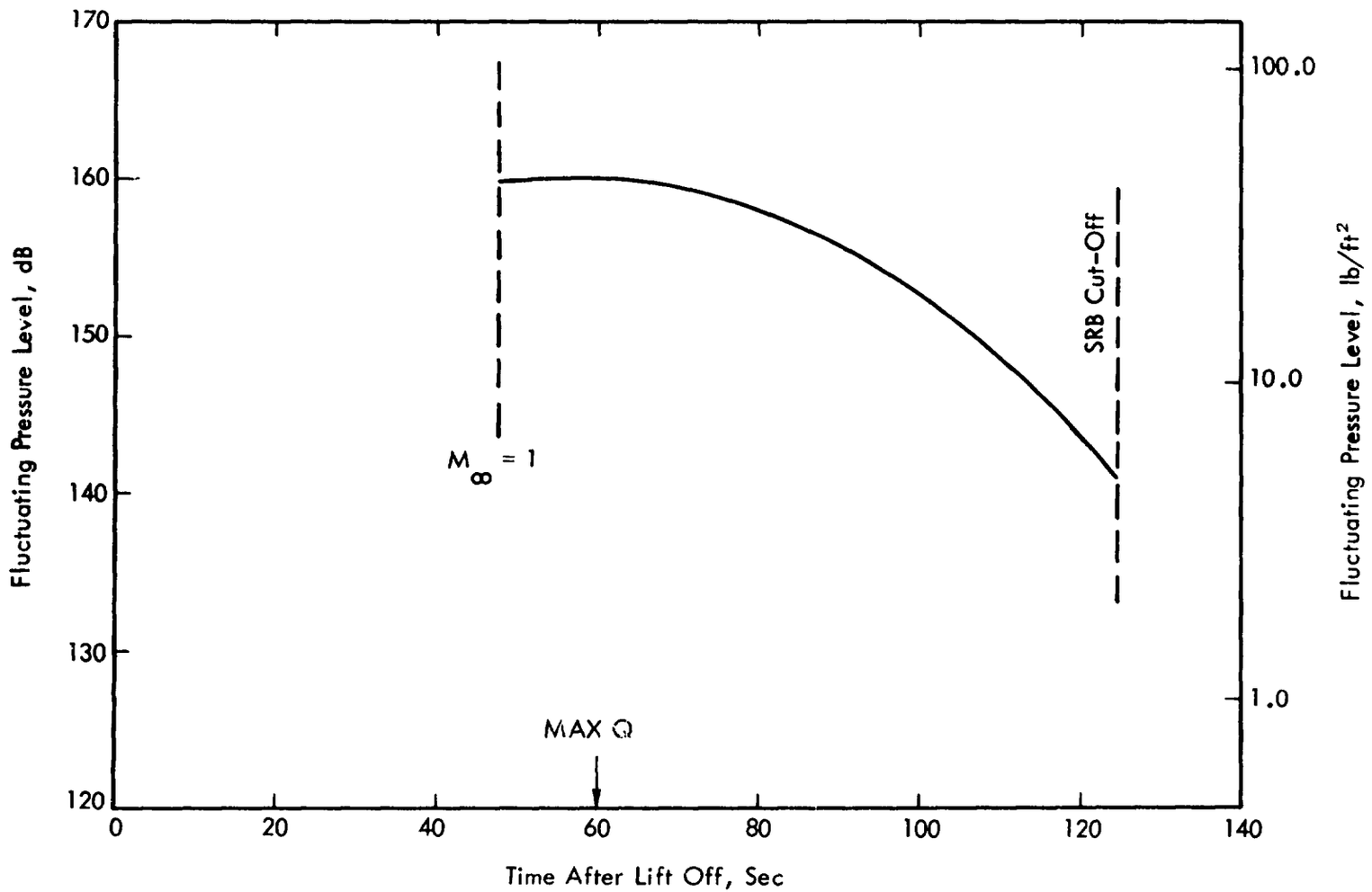

Figure 20. Basic Compression Corner Shock Oscillation Fluctuating Pressure Environment, Shuttle Launch Trajectory

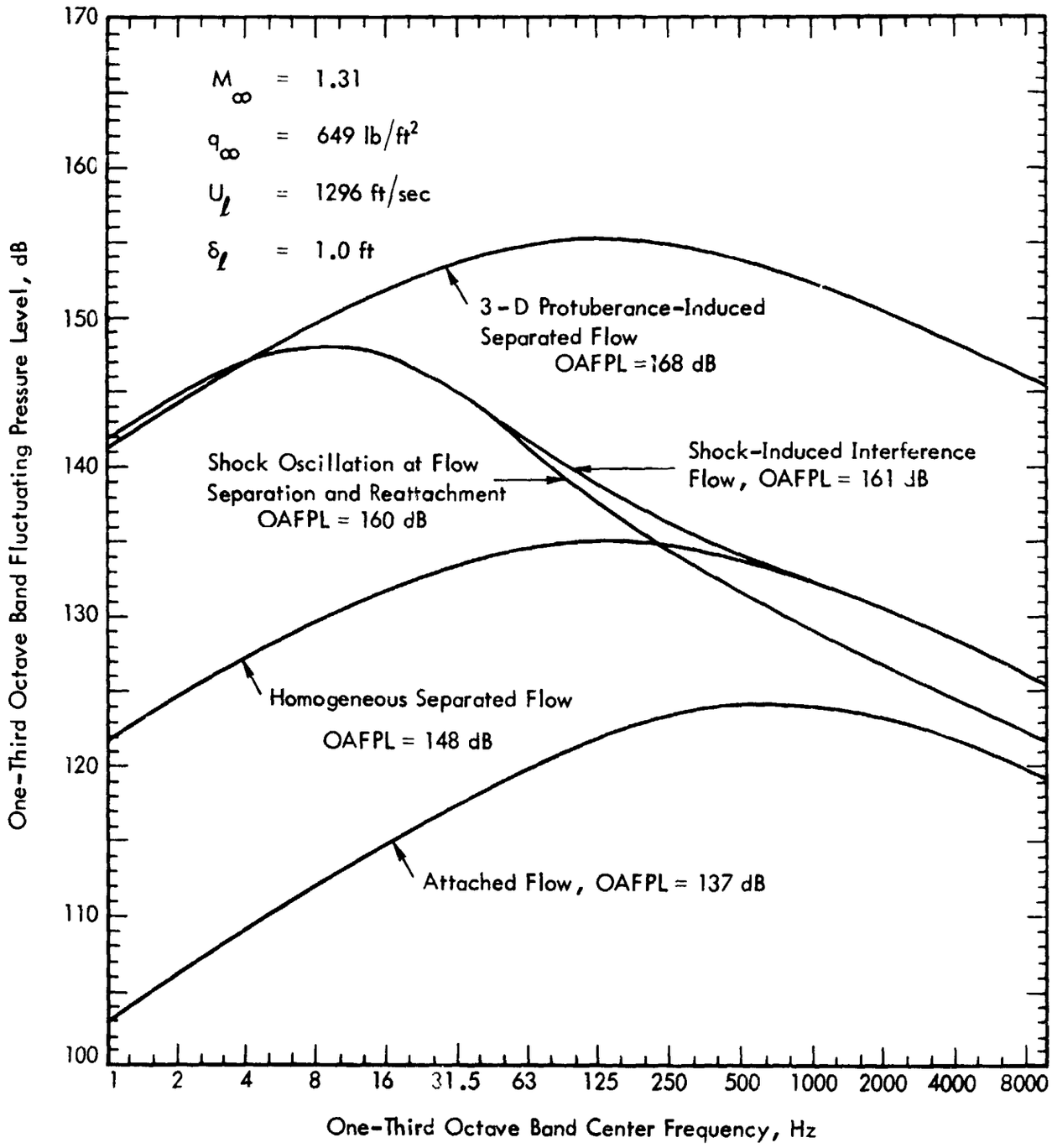

Figure 21. One-Third Octave Band Spectra for Typical Fluctuating Pressure Environments at MAX Q

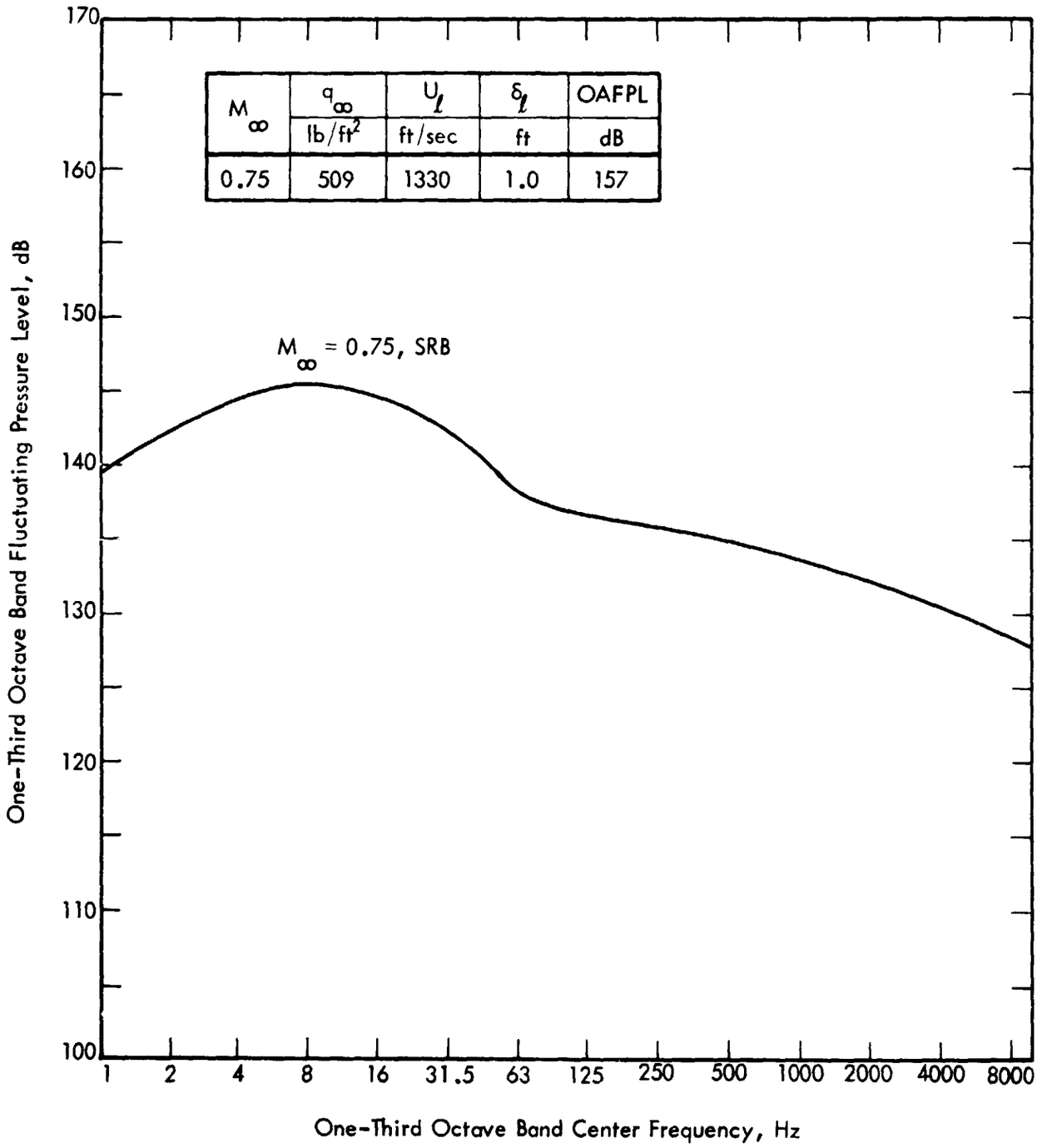

M_∞	q_∞	U_ℓ	δ_ℓ	OAFPL
	lb/ft^2	ft/sec	ft	dB
0.75	509	1330	1.0	157

Figure 22. One-Third Octave Band Spectrum for Shoulder-Induced Separated Flow on the SRB at Low Transonic Mach Number

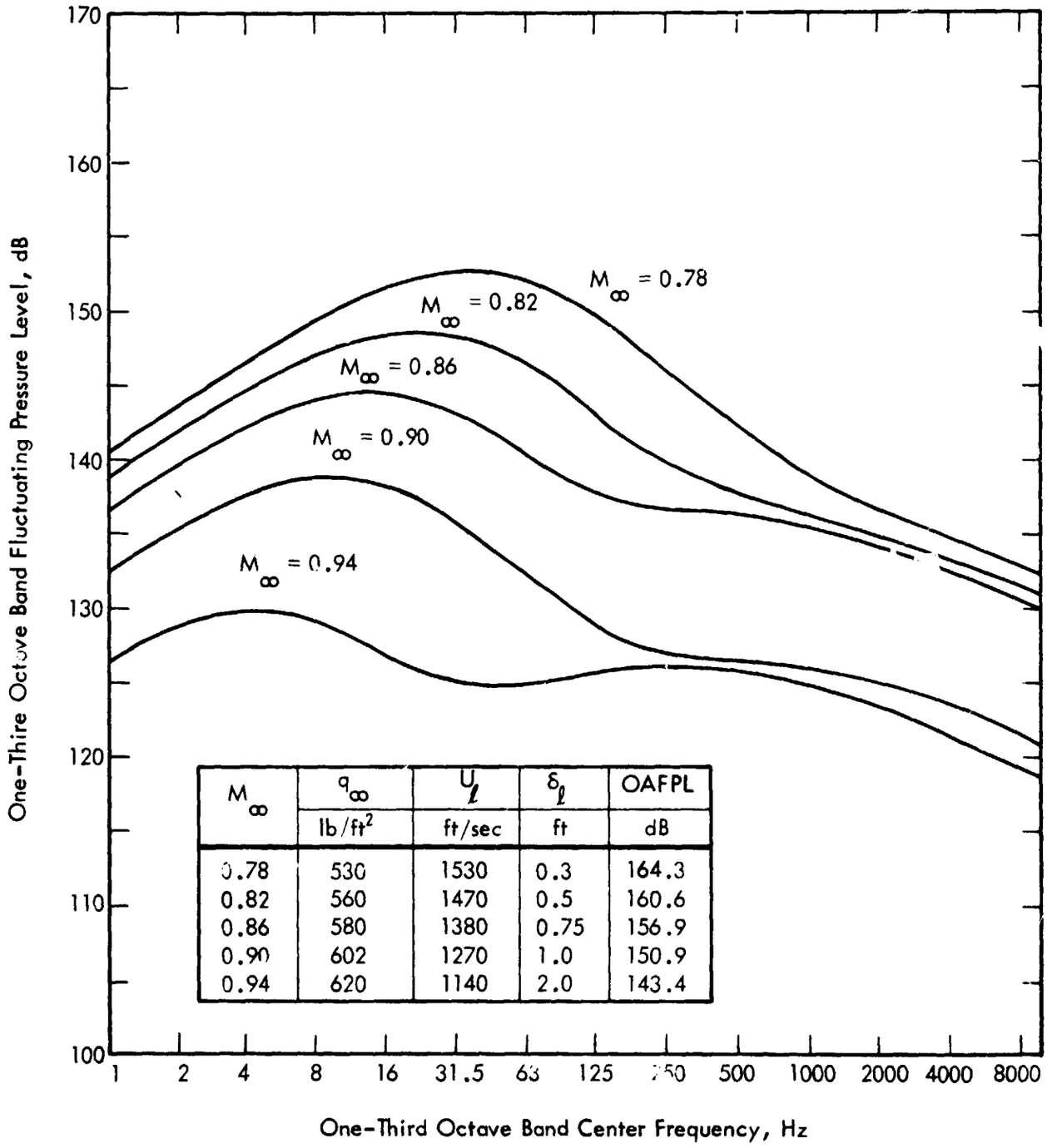

M_∞	q_∞	U_ℓ	δ_ℓ	OAFPL
	lb/ft^2	ft/sec	ft	dB
0.78	530	1530	0.3	164.3
0.82	560	1470	0.5	160.6
0.86	580	1380	0.75	156.9
0.90	602	1270	1.0	150.9
0.94	620	1140	2.0	143.4

Figure 23. One-Third Octave Band Spectra for Terminal Shock-Wave Oscillation on the SRB at Transonic Mach Numbers

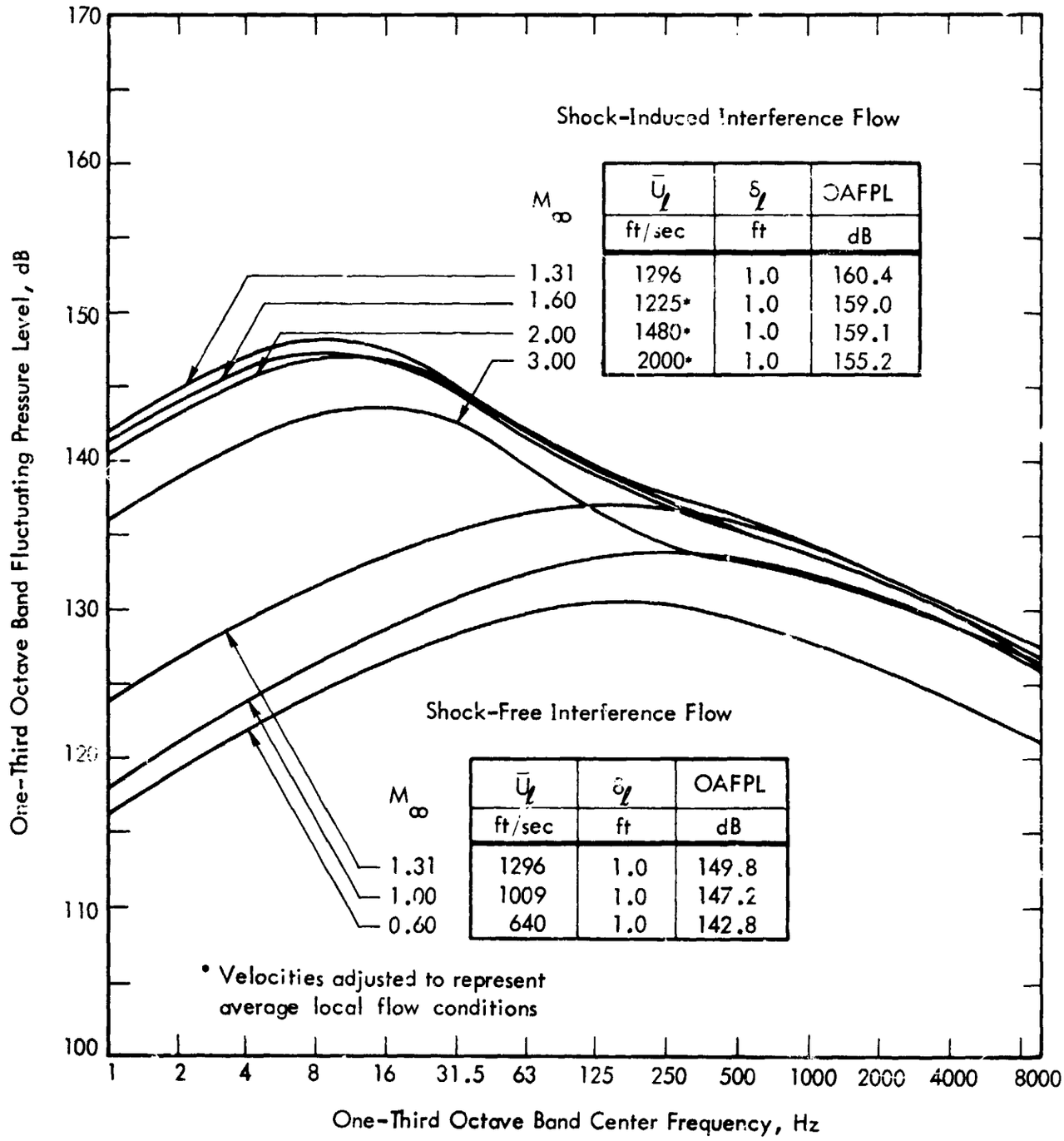

Figure 24. One-Third Octave Band Spectra for Critical Interference-Flow Environments

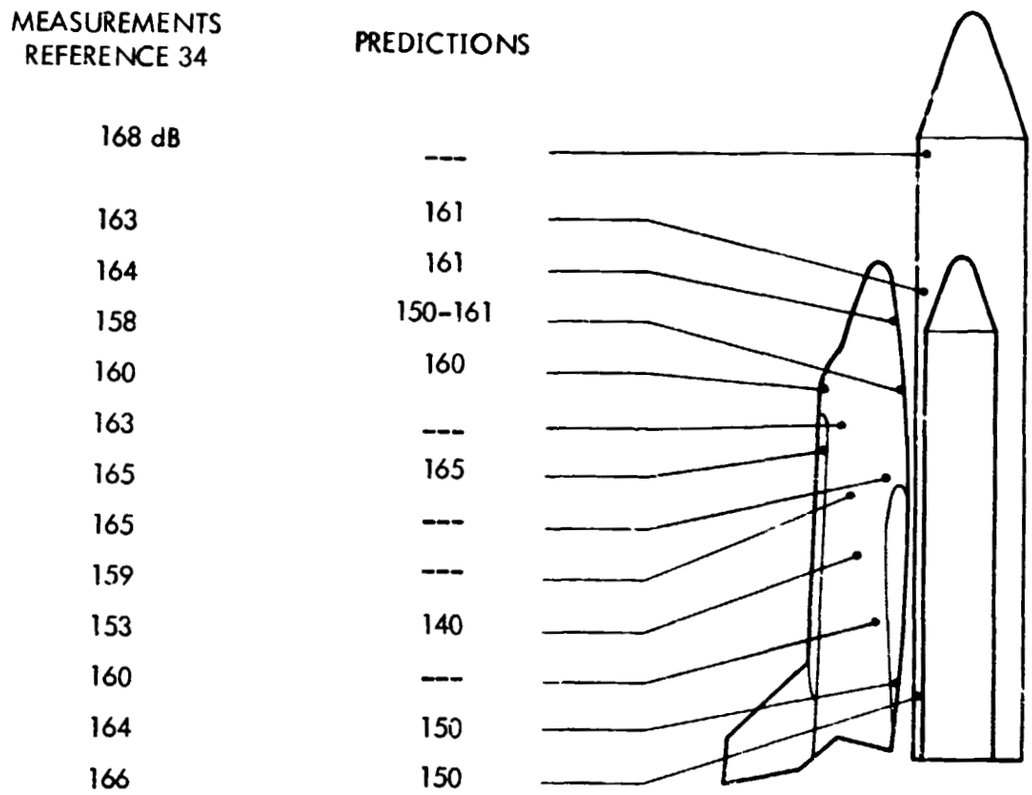

Figure 25. Comparison of Measured and Predicted Overall Fluctuating Pressure Levels for a Typical Parallel-Burn Space Shuttle Launch Configuration at Transonic Mach Number.

APPENDIX A

SUMMARY OF PREDICTION METHODS FOR IN-FLIGHT FLUCTUATING PRESSURE ENVIRONMENTS

APPENDIX A

SUMMARY OF PREDICTION METHODS FOR IN-FLIGHT FLUCTUATING PRESSURE ENVIRONMENTS

1.0 INTRODUCTION

When a vehicle moves through air there are two basic means by which it can produce noise: (1) by its propulsion mechanism (motor-jet, rocket, etc.,) and (2) by its interaction with its surroundings. At low speeds, for example, during and immediately after lift-off, the first of these is by far the dominant one while near or above the speed of sound, mechanism (2) becomes most important.

During any flight cycle for an aerospace vehicle, there are three important phases of the flight which should be investigated in order to assess the structural loading due to fluctuating pressures. These are listed in the chronological order in which they occur.

- Lift-off phase during which acoustic excitation results from the rocket exhaust noise.
- Launch flight to orbit phase, during which rocket exhaust noise diminishes and aerodynamic fluctuating pressures (pseudo-sound) starts to dominate. From an aerodynamic noise viewpoint, this phase becomes most critical at transonic Mach numbers $(0.60 \leq M \leq 1.6)$
- Re-entry phase during which only aerodynamic fluctuating pressures are present.

This Appendix is devoted to the specification of surface fluctuating pressures resulting from unsteady aerodynamic phenomena during the launch phase of flight. Aerodynamic fluctuating pressures (pseudo-sound) are zero at launch and increase to peak values as the vehicle passes through the transonic Mach number range. Previous wind tunnel and flight data show that fluctuating pressures are proportional to free-stream dynamic pressure q_∞ $(= \gamma P_\infty M_\infty^2/2$, where γ is the ratio of specific heats, P_∞ is the free-stream static pressure, and M_∞ is the free-stream Mach number) for a given unsteady flow phenomenon. However, peak fluctuating pressures do not necessarily occur at maximum q_∞ for certain regions of a vehicle due to the non-homogeneous nature of the flow field. For example, regions of the vehicle exposed to separated flow and the impingement of oscillating shock waves will experience fluctuating pressures at least an

order of magnitude greater than regions exposed to attached flow. Thus, if separated flow and oscillating shock waves are present, say at Mach numbers other than the range of maximum q_∞, then peak fluctuating pressures will also be encountered at conditions other than at maximum q_∞. Thus, it is easily seen that vehicle configuration is very important in the specification of fluctuating pressure levels since the source phenomena are highly configuration dependent in addition to varying with Mach number and angle of attack.

In light of the foregoing discussion, one general statement can be made in regard to aerodynamic fluctuating pressures. Regions exposed to the same unsteady phenomenon will experience fluctuating pressure levels which are proportional to free-stream dynamic pressure. Thus, it can be readily seen that a fundamental parameter in the specification of the surface excitation is free-stream dynamic pressure and its variation with Mach number. For a given configuration, Mach number and angle of attack define the phenomena, and dynamic pressure defines the fluctuating pressure levels associated with the phenomena.

Unsteady aerodynamic flow and the attendant fluctuating pressures experienced by aerospace vehicles naturally depend on the flight environments and the geometry of the vehicle. There are an infinite number of possible configurations and any discussion of their fluctuating pressure environment must be general. Practically all experimental data for unsteady aerodynamic flow have been [illegible]ed for bodies of revolution which are typical of missile configurations. As a result of these studies, it is well known that certain basic unsteady flow conditions will occur regardless of the detailed geometry of the vehicle. The occurrence of these basic fluctuating pressure phenomena and their statistical properties can be predicted quite accurately. It is convenient to discuss these basic flow conditions for bodies of revolution; however, this is certainly no restriction on either the feasibility or the practicality of predicting their occurrence on more complicated configurations. Thus, in the following paragraphs, general features of typical bodies of revolution are defined and the unsteady flow fields which they encounter are discussed. Furthermore, aerospace vehicles may have a number of protuberances projecting from their surfa[illegible] in which case the flow field is complicated

by the super-position of the protuberance flow field onto the flow field of the basic structure. Most protuberances are three-dimensional projections and general characteristics of these flows should be considered as separate and unique problems.

2.0 BASIC FLUCTUATING PRESSURE PHENOMENA

Examples of several bodies of revolution are shown in Figure 1. For the purpose of the present discussion, three basic configurations will be considered as specified below:

- Cone-cylinder shroud
- Cone-cylinder-flare shroud
- Cone-cylinder-boattail shroud

Virtually all axisymmetric vehicles fall into one of these categories although numerous modifications to the basic geometry have been employed in the past.

Several fluctuating pressure environments having different statistical properties may exist over a vehicle at any given instant in the flight trajectory. It is convenient to consider three separate Mach number ranges — subsonic, transonic, and supersonic — for each of the three basic shroud configurations. Further, the flow fields will depend on the angle of attack of the vehicle which causes nonsymmetrical loading (both statically and dynamically); however, for the purpose of this discussion, nonsymmetrical loading will not be discussed.

Schematics of subsonic, transonic and supersonic flow fields for the basic configurations are shown in Figure 1. At subsonic speeds, all three configurations experience regions of attached flow and separated flow. The cone-cylinder portion of each configuration induces separated flow immediately aft of the cone cylinder juncture for cones having half-angles greater than approximately 15 degrees. Re-attachment occurs within approximately one diameter aft of the shoulder (depending on cone angle) for the cone-cylinder and boattail configurations, whereas for the flare body, separation may continue over the flare. Both the flare and boattail induce separation for typical configurations. At high transonic speeds, the flow negotiates the shoulder of a cone-cylinder

body without separating, reaches supersonic speed immediately aft of the shoulder and produces a near-normal, terminal, shock wave a short distance aft of the shoulder. The boundary layer immediately aft of the shock may or may not separate depending on the strength of the shock wave. At transonic speeds, the boattail and flare region produce separated flow which may be accompanied by weak shock waves in the vicinity of the separation and reattachment points. At supersonic speeds, the cone-cylinder configurations produce regions of attached flow. For the flare configuration, the separated flow is bounded by shock waves at the separation and reattachment points, whereas for the boattail configuration, separation occurs at the shoulder of the boattail (expansion region) and is bounded at the reattachment point by a shock wave.

It is evident that even simple vehicle shapes, such as cone-cylinders, produce complex and highly nonhomogeneous flow fields at certain Mach numbers — particularly at subsonic and transonic speeds. The unsteady flow phenomena are of particular importance at transonic speeds, since in this range, fluctuating pressures reach maximum values due to their proportionality to dynamic pressure. In order to assess the fluctuating pressure environment of a vehicle of any arbitrary geometry, it is convenient to discuss the statistical properties of the fluctuating pressures for each of the basic types of unsteady flow condition. From Figure 1 it will be noted that the following flow conditions may occur for various regions of a vehicle.

- Attached flow
- Separated flow
- Shock-boundary layer interaction

Each of the above flow conditions exhibits different statistical characteristics. Attached flow pressure fluctuations result from the disturbances within turbulent boundary layers. Separated flow pressure fluctuations result from disturbances within the separated shear layer and instabilities associated with the separation and reattachment points. Pressure fluctuations for shock-boundary layer interaction result from the movement of the shock wave and the static pressure discontinuity associated with the shock wave. The statistical characteristics of each fluctuating pressure environment

that are important in the analysis of structural response may be classified under three parameters:

- The overall level
- The power spectrum
- The cross-power spectrum (or narrow band cross correlation)

Each unsteady flow condition with general statistical characteristics will be discussed separately in the following subsections.

2.1 Attached Turbulent Boundary Layers

The surface fluctuating pressures beneath attached turbulent boundary layers have been the subject of both theoretical and experimental study for a number of years. The turbulent boundary layer extends over a considerable portion of the surface of vehicles in flight and, thus, it is considered to be one of the principle sources of aero-acoustic excitation to the vehicle structure. Several years ago, workers such as Kraichman, Lilley, and Hodgson developed theoretical formulations for the fluctuating pressures under turbulent boundary layers and, more recently, several carefully planned experiments have provided additional information on the statistical characteristics of the pertubations. Lowson, Reference 1 , presents a good summary of the results of studies on this subject, with the exception of some recent measurements by NASA-Ames. In Lowson's report, the basic mechanism underlying the production of the surface pressure fluctuations beneath turbulent boundary layers is discussed, together with a presentation of empirical and semi-empirical prediction techniques. This section of the present discussion is a brief overview of Lowson's prediction formulae with the exception of the power spectra, which has been modified to be more consistent with the power spectra at low Strouhal numbers. The following discussion presents a review of the experimental results and prediction formulae in terms of the most important statistical parameters.

Overall Level

The correct method of presenting overall fluctuating pressure levels for surfaces beneath the convected turbulence in boundary layers is in terms of the root-mean-square fluctuating pressure level, $\sqrt{\overline{p^2}}$. Free-stream dynamic pressure, q_∞, local dynamic pressure, q_l, and wall shear stress, τ_ω, have been used to normalize $\sqrt{\overline{p^2}}$ so that meaningful data collapse can be realized throughout the Mach number range. The most generally accepted normalizing parameter is q_∞ and thus, will be used in the current expressions.

The effects of free-stream Mach number, M_∞, on the normalized RMS intensities of the fluctuating pressures in attached flows are shown in Figure 2. There is significant scatter in the data which may be attributed to several factors: 1) background noise and free-stream turbulence in the testing medium, 2) instrumentation quality and the precision of the experimental technique, 3) data acquisition and reduction techniques, etc. For the range of Mach numbers covered in the data of Figure 2, the normalized RMS value of the fluctuating pressure varies from $\sqrt{\overline{p^2}}/q_\infty \approx 0.006$ at subsonic Mach numbers to 0.002 at supersonic Mach numbers. Lowson, Reference 1, proposed the following semi-empirical prediction formula which appears to agree with the general trend in the data:

$$\sqrt{\overline{p^2}}/q_\infty = 0.006/(1 + 0.14 M_\infty^{\,2}) \qquad (1)$$

It is important to note that this formula has some theoretical basis and is not strictly an empirical approximation of measured results (see Reference 1). The use of this formula at high supersonic and hypersonic Mach numbers should be done so with the understanding that it has not been verified in this Mach number range and may lead to significant error. However, in the Mach number range up to, say $M_\infty = 3.0$, it is in good agreement with experimental results.

It should be noted that the results presented in Figure 2 , particularly the wind tunnel results, were obtained for both homogeneous and stationary flows at free-stream conditions and in the absence of external pressure gradients. Consideration should be given to local conditions which deviate from free-stream conditions.

Power Spectra

Power spectra represent the distributions of the mean square fluctuating pressure with frequency. Power spectra for attached turbulent boundary layers are found to scale on a Strouhal number basis; that is, the frequency is normalized by multiplying by a typical length and dividing by a typical velocity. The advantages of using normalized spectra are obvious since it enables similar, homogeneous, flows to be represented by a single spectrum regardless of the scale of the flow field or the free-stream velocity.

Numerous studies have been conducted to determine the proper parameters to be used to nondimensionalize the spectra for various aero-acoustic environments. Unfortunately, the choice of parameters which best collapses the data appear to be dependent on the nature of the fluctuating pressure environment. In general, free-stream velocity is used as the normalizing velocity parameter, although a typical eddy convection velocity (itself a function of frequency) has been used occasionally. The local convection velocity appears to correspond more closely with the physical situation for fluctuating pressures due to turbulent eddies. Selection of a typical length is more difficult. Boundary layer thickness (δ_b), displacement thickness (δ^*), wall shear stress (τ_ω) and momentum thickness (θ) have all been used by various investigators. The most generally used typical lengths are δ_b and δ^*.

Lowson, Reference 1 , proposed an empirical formula for the power spectrum for attached turbulent boundary layers based, primarily, on the experimental results of Speaker and Ailman. In comparing this formula with other data, and in particular, with recent measurements at supersonic speeds by NASA-Ames, the Lowson prediction appears to underestimate the spectral levels at low Strouhal numbers and also gives too large a roll-off at high Strouhal numbers. Therefore, a new formula is presented

which appears to be more representative of e cperimental findings throughout the Mach number range. In this formula, it will be noted that δ^* and U_∞ (the free-stream velocity) have been used as normalizing parameters. The power spectral density, $\Phi(\omega)$ is given by the relation:

$$\frac{\Phi(\omega)\, U_\infty}{q_\infty^2\, \delta^*} = \frac{\left(\overline{P^2}/q_\infty^2\right)}{\frac{\omega_0\, \delta^*}{U_\infty} \left\{ 1 + (\omega/\omega_0)^{0.9} \right\}^{2.0}} \tag{2}$$

where $\omega_0 = 0.5 \dfrac{U_\infty}{\delta^*}$

$$\overline{P^2}/q_\infty^2 = \frac{(0.006)^2}{(1 + 0.14 M_\infty^2)^2}$$

$$\delta^* = \delta_b/8 \quad \text{for } M < 1.0$$

$$\delta^* = \frac{(1.3 + 0.43 M_\infty^2)\, \delta_b}{10.4 + 0.5 M_\infty^2 \left[1 + 2.10^{-8}\, R_e\right]^{1/3}} \quad \text{for } M > 1.0$$

$$\delta_b = x \left[0.37\, R_e^{-0.2} \left\{ 1 + \left(\frac{R_e}{6.9 \cdot 10^7} \right)^2 \right\}^{0.1} \right]$$

x = Downstream distance from the leading edge

R_e = Reynolds number = $U_\infty\, x/\nu$

ν = Kinematic viscosity

A comparison of the predicted power spectrum with experimental spectra is presented in Figure 3.

Cross-Power Spectra

The final requirement in determining the characteristics of the fluctuating pressure field of the turbulent boundary layer is to define the narrow band, space correlation function or co-power spectral density. This parameter is the key function needed to describe an impinging pressure field on a structure in order to calculate the induced mean-square response of the structure (see, for example, Reference 17 for the structural response computational technique). The spatial correlation properties of a fluctuating pressure field can be obtained only from a careful and detailed examination of the field at a large number of points. Measurements by several investigators have shown that the co-power spectral density of turbulent boundary layer pressure fluctuations in the direction of the flow can be approximated by an exponentially damped cosine function, and the lateral co-spectral density can be approximated by an exponential function. The general form of the cross-power spectral density is:

$$S_{pp}(\zeta, \eta, \omega) = \Phi(\omega) A(\zeta, \eta, \omega) \cos\left(\frac{\omega \zeta}{U_c}\right) \tag{3}$$

where $A(\zeta, \eta, \omega)$ is the modulus of the cross-power spectral density, and $\Phi(\omega)$ is the power spectral density of the homogeneous field.

Here, it is assumed that the pressure field is homogeneous, in the sense that the cross-power spectral density is a function only of the separation distances (ζ in the longitudinal direction and η in the lateral direction) so that it is independent of the actual positions (say x and $x + \zeta$ longitudinally and y and $y + \eta$ laterally). Further, ω and U_c are the circular frequency and convection velocity, respectively. Assuming that $A(\zeta, \eta, \omega)$ is separable into its longitudinal and lateral components, and normalizing by the power spectral density of the homogenous field gives (Reference 1):

$$G_{pp}(\zeta, \eta, \omega) = G_{\zeta}(\zeta, \omega)\, G_{\eta}(\eta, \omega) = \left\{ A_{\zeta}(\zeta, \omega) \cdot \cos\left(\frac{\omega \zeta}{U_c}\right) \right\} \cdot A_{\eta}(\eta, \omega)$$

$$= C(\zeta, \omega) \cdot C(\eta, \omega) \tag{4}$$

where $C(\zeta, \omega)$ and $C(\eta, \omega)$ are the correlation coefficients in the longitudinal and lateral directions, respectively. The assumed separable form leads to the prediction that the magnitude of C is constant along straight lines on the surface, forming a diamond pattern surrounding the origin. This characteristic is somewhat physically unreasonable (see Reference 2); however, for purposes of calculating the induced structural response the assumption of separability greatly simplifies the mathematics and, hence, it is generally accepted. However, Lowson (Reference 1) notes that a more likely form for the lines of constant amplitude would be elliptic, suggesting that the usual separable solution underestimates the correlation area by $\pi/2$. Thus, integration of formula containing the cross-spectral density function should be multiplied by a factor of $\pi/2$ to allow for its probable underestimate of the correlation area at any frequency.

Measurements of the correlation coefficients have been made by Bull and others (see Reference 1) and the results are presented in Figures 4a and 4b. It is seen that the data in Figures 4a and 4b have been collapsed based on Strouhal numbers $\frac{\zeta\omega}{U_c}$ and $\frac{\eta\omega}{U_c}$. From these data, the following empirical expressions were derived for the correlation coefficients:

$$C(\zeta, \omega) = \exp\left(-0.10 \left|\zeta\right| \omega/U_c\right) \cdot \cos\left(\frac{\omega \zeta}{U_c}\right) \tag{5}$$

$$C(\eta, \omega) = \exp\left(-0.715 \left|\eta\right| \omega/U_c\right) \tag{6}$$

These correlation curves have been inserted in Figures 4a and 4b for comparison. Typical values of the convection velocity (itself a function of frequency) for subsonic flow are $U_c = 0.6\, U_\infty$ for the small scale eddies near the wall and $U_c = 0.9\, U_\infty$ for the large scale eddies near the outer edge of the boundary layer.

The accuracy of Equations (5) and (6) break down at small values of $\frac{\omega \zeta}{U_c}$; however, in Reference 3, Bull presents measured asymptotic values of the correlation coefficients for small values of $\frac{\omega \zeta}{U_c}$ and $\frac{\eta \zeta}{U_c}$. Based on these data, the Equations (5) and (6) may be corrected to include the lower frequencies, and the resulting expressions are:

$$C(\zeta, \omega) = \exp\left(-0.10\, |\zeta|\, \omega / U_c\right) \cdot \exp\left(-0.27\, |\zeta| / \delta_b\right) \cdot \cos\left(\frac{\omega \zeta}{U_c}\right) \tag{7}$$

$$C(\eta, \omega) = \exp\left(-0.72\, |\eta|\, \omega / U_c\right) \cdot \exp\left(-2.0\, |\eta| / \delta_b\right) \tag{8}$$

These expressions appear to be valid at both subsonic and supersonic speeds.

2.2 Separated Flow

Separated flows as induced by steps, wedges, flares and other, basically two-dimensional geometric changes have undergone considerable study only in recent years. Considerably less data is available on the fluctuating pressure environments within separated flow regions than is the case with attached turbulent boundary layers. Furthermore, there are various types of separated flows and little is known of the similarities and differences of their statistical properties. Example separated flow environments are listed below:

- Blunt body-induced separation (as occur at cone-cylinder and flare-cylinder expansion corners at subsonic Mach numbers)
- Flare-induced, step induced, and wedge-induced separation (as occur in compression corners)
- Shock-induced separation (as occur on cylinders, airfoils, etc., beneath terminal shock waves at transonic speeds and due to shock wave impingement at supersonic speeds)
- Boattail-induced and rearward facing-step-induced separation (such as occur in the base region of launch vehicles).

All of the foregoing environments differ to some degree in their aerodynamic structure. However, some basic comments can be made in regard to their fluctuating pressure characteristics. First, all of these environments may be regarded as two-dimensional type separated flows having mean separation and reattachment lines which are normal to the free-stream. Second, a general characteristic is that if the flow separates from an expansion corner, the separation line is quite stable in that oscillations which produce fluctuating pressures are not generated. However, if separation occurs, say, on the cylindrical portion of a payload fairing (flare induced separation), the separation point is unstable and may produce significant fluctuating pressures, particularly at supersonic speeds where the separation is accompanied by an oblique shock wave.

Third, the reattachment point of the separated flow field produces rather large fluctuating pressure levels for virtually all types of separated flow fields. The region within the separated flow field (between the separation and reattachment points) is a fairly homogeneous environment which is characterized by fluctuating pressure levels greater than those for attached flow but less than those encountered at the separation and reattachment points. Example data for various separated flow fields are presented in the following sections.

Overall Level

A typical example of the fluctuating pressures resulting from blunt-body separation is shown in Figure 5 (results taken from Reference 18). These data were obtained at high subsonic Mach numbers for a 25-degree cone-cylinder configuration. The axial distribution of $\sqrt{\overline{P^2}}/q_\infty$ shows a relatively nonhomogeneous environment with a peak level which moves aft with increasing Mach number. The peak in $\sqrt{\overline{P^2}}/q_\infty$ results from the reattachment of the separated flow from the shoulder. Thus, the extent of the separated region increases with increasing Mach number. Peak levels of rms fluctuating pressure reach 11 percent of free-stream dynamic pressure at a free-stream Mach number of 0.70, and results from the instability of the reattachment point. It will be noted that the fluctuating pressure levels near the shoulder ($X/D = 0$) are relatively low (same order of magnitude as generally found with the homogeneous region of two-dimensional separated flows and typical of the environment for separated shear layers) thus indicating that the separation point which occurs at the shoulder is relatively stable. Separated flow over the boattail region of a bulbous vehicle may be expected to exhibit fluctuating pressure characteristics very similar to the cone-cylinder; however, the blunt-body separation on a cone-cylinder body is limited to the subsonic speed range, whereas, the boattail configuration may induce separation at all Mach numbers.

Typical fluctuating pressure data for flare-induced separation are presented in Figure 6 (results taken from Reference 14). These data clearly show the region of homogeneous separated flow, bounded on the upstream by the oscillating shock wave (forward peak in $\sqrt{\overline{P^2}}/q_\infty$), and on the downstream by the reattachment perturbations (aft peak in $\sqrt{\overline{P^2}}/q_\infty$). Surface fluctuating pressures for the separated flow region range from 1.5 to 2.7 percent of the free stream dynamic pressure. Levels associated with the upstream shock wave generally range from 4 to 8 percent of the free-stream dynamic pressure (see Reference 14); whereas, levels in the region of reattachment may range from 6 to 12 percent of q_∞ and agree reasonably well with the reattachment levels for blunt body separation. Further discussion of shock-wave oscillation data is presented in a later section.

The variation of fluctuating pressure level, normalized by free-stream dynamic pressure, with local Mach number (M_ℓ) for various separated flow environments downstream of expansion corners is presented in Figure 7. The regions aft of cone-cylinder junctures and rearward-facing steps, and in the near wake of boattail configurations are represented by the data presented in Figure 7. These environments will be referred to as expansion induced separated flows and it will be noted that the attendant fluctuating pressures exhibit the same general trend with local Mach number. The largest levels occured at low Mach numbers and decreased as local Mach numbers increased. These data represent the region of plateau static pressure and the tolerance brackets on the data represent the variations due to non-homogeneous flow within the region of constant static pressure rather than scatter in the measurements. A good empirical approximation to these experimental measurements is:

Expansion Induced Separated Flow:

$$\sqrt{\overline{P^2}}/q_\infty = \frac{0.045}{1 + M_\ell^2} \tag{9}$$

This equation is similar in form to that previously proposed for attached turbulent boundary layers.

Fluctuating pressure measurements for the region of plateau static pressure upstream of compression corners are presented in Figure 8. The regions immediately upstream of forward-facing step, wedges, and flares are represented by the data presented in Figure 8. Also, the previous fluctuating pressure data for expansion induced separated flow, shown in Figure 7, are presented in this figure for comparison. In general, the compression corner data show an increase in fluctuating pressure level with increasing free-stream Mach number in the range, $1.0 \leq M_\infty \leq 2.0$ — reaching a constant level at Mach numbers above 2.0. Free-stream Mach number is used here because adequate data is not available for determining the local Mach number in the vicinity of the compression induced separated flow region. Derivation of an empirical prediction formula for the fluctuating pressure level within compression induced separated flows has not been attempted at this time.

Power Spectra

The most comprehensive available data for power spectra of the fluctuating pressure within separated flows was obtained for the homogeneous region of compression corners at supersonic Mach numbers (References 14, 19, 20 and 21). These data, presented in Figure 9, were obtained for forward facing steps, wedges and conical frustums. All data, represented by the cross-hatched band, showed a distinct similarity in spectral characteristics when compared using normalized spectral level and frequency expressed as functions of local velocity, free-stream dynamic pressure, and local boundary layer thickness. A number of velocity, length and pressure parameters were used to collapse the data; however, local velocity (U_ℓ), local boundary layer thickness (δ_ℓ) and free-stream dynamic pressure appeared to be adequately representative of the parameter dependence of the fluctuating pressures for the configurations studied. Power spectra of the fluctuating pressures within the homogeneous region of separated flows may be represented by the following empirical formula:

$$\frac{\Phi(f)\, U_\ell}{q_\infty^2\, \delta_\ell} = \frac{\overline{P^2}/q_\infty^2}{\frac{f_0\, \delta_\ell}{U_\ell} \left\{ 1 + \left(f/f_0 \right)^{0.83} \right\}^{2.15}} \tag{10}$$

where $f_0 = 0.17 \frac{U_\ell}{\delta_\ell}$

$\overline{P^2}/q_\infty^2 = \frac{0.045}{1+M_\ell^2}$, Figure 7, for expansion induced separated flows.

$\overline{P^2}/q_\infty^2$ = the results as determined in Figure 8 for compression induced separated flows.

and the subscripts ℓ and ∞ refer to local and free-stream conditions respectively.

It is anticipated that Equation 10 can be used with good accuracy to predict the power spectra for fluctuating pressures within the homogeneous region of expansion induced separated flows although it was derived based on data taken in compression corners.

Cross-Power Spectra

Typical cross-power spectra for the homogeneous region of two-dimensional separated flows are presented in Figure 10. Again, noting that the co-spectral density is the same as the narrow-band spatial correlation, it is seen that the separated flow exhibits spatial coherence very similar to that of attached turbulent boundary layers. The damping of the sinusoidal cross spectra for separated flow is exponential at high values of $\omega\zeta/U_c$ as is the case for attached flow. Thus as a first approximation, the normalized longitudinal co-spectra may be represented by:

$$C(\zeta, f) = e^{-a\omega\zeta/U_c} \cos \frac{\omega\zeta}{U_c} \tag{11}$$

The damping coefficient, α, is dependent on free-stream Mach number according to the results presented in Reference 14. The Chyu and Hanely results show damping coefficients ranging from approximately 0.13 at $M_\infty = 2.5$ to a value of 0.33 at $M_\infty = 1.6$. This suggests that the turbulence structure in separated flows decays somewhat more rapidly than for attached flow which has a coefficient of exponential decay of 0.10. It should be noted that the exponential decays represent the envelope of the cross-spectra for various spatial distances, ζ. For a given value of ζ, the cross spectra can be represented by the exponential envelope only at high frequencies, the lower limits of which increase with increasing distance between measurement points.

The loss of coherence at low frequencies precludes a general collapse of the data using a constant damping coefficient. This problem was overcome by Coe and Rechtien, Reference 20, by introducing an attenuation coefficient which is related to the normalized modulus of the cross-power spectral density by

$$\left| G\left(\zeta, \frac{f\,\delta_\ell}{U_\ell}\right) \right|_{norm} = e^{-\alpha \zeta} \tag{12}$$

The normalized modulii for available or selected transducer spacings, ζ, were curve-fitted by an exponential function using the method of least squares to obtain a non-dimensional attenuation-coefficient function $\alpha\left(\zeta, f\,\delta_\ell / U_\ell\right) \cdot h$ in References 19-21. The parameter h is the height of the protuberances used to generate the separated flow field. Empirical approximations of the attenuation coefficient, based on the experimental results of Coe and Rechtien, are:

$$\alpha\left(\zeta, \frac{f\,\delta_\ell}{U_\ell}\right) = 0.75/\text{ in.} \quad , \quad \frac{f\,\delta_\ell}{U_\ell} < 6 \times 10^{-3} \tag{13}$$

$$\alpha\left(\zeta, \frac{f\delta_\ell}{U_\ell}\right) = 0.75\left[\frac{f\delta_\ell/U_\ell}{\left(f\delta_\ell/U_\ell\right)_0}\right], \tag{14}$$

$$6 \times 10^{-3} \leq \frac{f\delta_\ell}{U_\ell} \leq 6 \times 10^{-2}$$

where $$\left(\frac{f\delta_\ell}{U_\ell}\right)_0 = 6 \times 10^{-3}$$

$$\alpha\left(\zeta, \frac{f\delta_\ell}{U_\ell}\right) = 1.5/\text{in.} \quad , \frac{f\delta_\ell}{U_\ell} > 6 \times 10^{-2} \tag{15}$$

Lateral Direction

$$\alpha\left(\eta, \frac{f\delta_\ell}{U_\ell}\right) = 0.75/\text{in.} \quad , \frac{f\delta_\ell}{U_\ell} < 6 \times 10^{-3} \tag{16}$$

$$\alpha\left(\eta, \frac{f\delta_\ell}{U_\ell}\right) = 0.75/\text{in.}\left[\frac{f\delta_\ell/U_\ell}{\left(f\delta_\ell/U_\ell\right)_0}\right]^{0.3} , \frac{f\delta_\ell}{U_\ell} \geq 6 \times 10^{-3} \tag{17}$$

where $$\left(\frac{f\delta_\ell}{U_\ell}\right)_0 = 6 \times 10^{-3}$$

It will be noted that the longitudinal and lateral attenuation coefficients are the same at Strouhal numbers, $f\delta_\ell/U_\ell < 6 \times 10^{-2}$ and that the lateral attenuation coefficient becomes larger than the longitudinal value at $f\delta_\ell/U_\ell \geq 6 \times 10^{-2}$. It was pointed out in Reference 19 that this spatial characteristic indicates that the predominant turbulence is nonconvective at the lower frequencies and that contours of equal

correlation would be circular; whereas, at $f\,\delta_\ell / U_\ell > 6 \times 10^{-2}$ the divergence of the longitudinal and lateral attenuation coefficients indicate a progressively extended correlation pattern in the direction of the free-stream with increasing frequency. This statement is not entirely true since the usual separable form of the cross-power spectral density leads to the prediction that the magnitude of the normalized modulus is constant along straight lines on the surface, forming a diamond pattern surrounding the origin rather than a circular or elliptic pattern. Under the assumption of separability of the longitudinal and lateral cross-power spectra, the following equations (which employ the attenuation coefficient) may be used as prediction formula for the normalized longitudinal and lateral co-spectra.

Longitudinal Co-Spectra

$$C\left(\zeta, \frac{f\,\delta_\ell}{U_\ell}\right) = e^{-\alpha_\zeta \zeta} \cos \frac{\omega \zeta}{U_c} \tag{18}$$

Lateral Co-Spectra

$$C\left(\eta, \frac{f\,\delta_\ell}{U_\ell}\right) = e^{-\alpha_\eta \eta} \tag{19}$$

where $\alpha_\zeta = \alpha\left(\zeta, \frac{f\delta_\ell}{U_\ell}\right)$ as defined in Equations 13, 14 and 15.

$\alpha_\eta = \alpha\left(\eta, \frac{f\,\delta_\ell}{U_\ell}\right)$ as defined in Equations 16 and 17.

2.3 Shock-Wave Oscillation

Generally, shock wave oscillation produces the most intense fluctuating pressure levels that are usually encountered by a vehicle. As for the case of separated flow, there are many types of shock-wave oscillation and little is known in regard to the similarities and differences of their statistical parameters. Typical shock waves encountered by vehicles are:

- Terminal shock waves for regions of transonic flow
- Displaced oblique shock waves as induced by the separated flow in compression corners at local supersonic speeds
- Reattachment shock waves in the vicinity of the reattachment point for separated flows generated by both compression and expansion corners.
- Impingement shock waves as caused by local bodies such as strap-on rockets.

All shock waves may be expected to produce similar fluctuating pressure environments since the movement of the shock wave results from the interaction with the separated flow at the foot of the shock wave (see Reference 19) and the fluctuating pressure is the result of the modulation of the pressure gradient through the shock wave. A special case of shock wave oscillation is referred to as an alternating flow condition, whereby, the flow at an expansion corner intermittently fluctuates between a separated and attached condition. This environment is illustrated schematically in Figure 11 for a 25 degree cone angle together with the more common terminal shock-wave oscillation case. Example data for various shock wave oscillation environments are presented in the following sections.

Overall Level

The axial distribution of rms fluctuating pressure resulting from terminal shock wave oscillation is shown in Figure 11 (from Reference 18). A special case of terminal shock wave oscillation results when the terminal shock wave moves forward to the expansion shoulder of a cone-cylinder. For this case, the flow intermittently fluctuates between the blunt-body separated flow condition and the attached flow condition at high subsonic (low transonic) Mach numbers. This condition represents an alternating unbalance between the large pressure rise through the shock wave that exceeds the values required to separate the flow and the small pressure rise that is too small to maintain fully separated conditions.

Extremely large fluctuating pressures result from this condition; however, it should be noted that this phenomenon occurs over a small Mach number range and generally is of very low frequency. Thus for large Mach number transients, this phenomenon may not occur. On the other hand, some experimental studies using aeroelastic wind tunnel models indicate that this phenomenon may become coupled with the vibrational response of vehicles such that flutter in the lower order bending modes would result for certain configurations — particularly for bulbous shaped payloads on rather slender launch vehicles.

As Mach number is increased above the range of alternating flow, the localized oscillation of the shock wave produces intense fluctuating pressures for the region in close proximity to the shock wave as shown in Figure 11. The shock wave moves aft with diminishing strength with increasing Mach number such that the rms fluctuating presssure levels also decreases. In addition to the results presented in Figure 11, the fluctuating pressures which occur at the separation and reattachment points for separated flow over compression corners (Figure 6) are fairly complete examples of shock-wave oscillation data.

Power Spectra

Only recently has comprehensive data been presented on the spectral characteristics of shock-wave oscillation. Much of the previous data were presented in linear—linear graphical form rather than using log—log scales. As a result, much resolution was lost at the high frequencies. Recent experimental data by Coe and Richtien (Reference 20) gives a clearly defined spectrum for shock wave oscillation at $M_\infty = 2.0$; however, data at other Mach numbers have not been published. Data obtained for three-dimensional protuberance flows do agree with the Coe and Richtien data and thus substantiates their limited published results. The normalized power spectra for shock-wave oscillation for both two- and three-dimensional protuberances (References 18 and 19) are presented in Figure 12. The power spectrum shows a relatively steep roll-off starting at a Strouhal frequency $(f\,\delta_0 / U_0)$ of 1×10^{-2}, where the subscript $_0$ denotes local velocity and boundary layer thickness upstream of the shock wave. The roll-off is 8 dB per octave for the range $1 \times 10^{-2} \leq f\,\delta_0 / U_0 \leq 2 \times 10^{-1}$ and above this range the roll-off changes suddenly to 4 dB per octave. These unique spectral characteristics of shock-wave induced fluctuating pressures are explained by the physical behavior of the shock-wave oscillation and the resulting pressure time history. The shock wave is basically a pressure discontinuity which becomes slightly distorted by the boundary layer such that a finite gradient through the shock wave is observed at the surface. Oscillation of the shock wave produces a wave form which approaches a random-rectangular wave as the displacement of the oscillation increases. Superimposed upon this signal is the low amplitude, high frequency disturbance associated with the attached boundary layer (for that portion of the signal when the shock wave is aft of the measurement point) and the moderate amplitude and frequency disturbances associated with separated flow (for that portion of the signal when the shock wave is forward of the measurement point). The roll-off rate of the power spectrum for a random-rectangular wave form is 6 dB per octave which is 2 dB lower than the experimentally observed value. Above $f\,\delta_0 / U_0 = 2 \times 10^{-1}$, the power spectral density

for the random modulation of the shock wave diminishes below the power spectral density for the turbulence portion of the signal. Thus, the roll-off rate changes to a value roughly equal to that for separated flow since this environment is the larger of the two turbulence generating mechanisms (the other being attached flow).

Noting that the power spectra for shock wave oscillation is composed of 1) low frequency spectral energy of the shock wave and 2) high frequency spectral energy of the separated flow and attached boundary layer, the resulting empirical formula for the power spectra may be written as a combination of power spectra of the contributing sources:

$$\left[\Phi(f)\right]_{SW}^{H} = \left[\Phi(f)\right]_{SW}^{I,\,H} + k_1 \left[\Phi(f)\right]_{S}^{H} + k_2 \left[\Phi(f)\right]_{A}^{H} \qquad (20)$$

where the subscripts and superscripts denote the following:

Subscripts:	SW	-	shock wave
	S	-	separated flow
	A	-	attached flow
Superscripts:	I	-	absence of viscosity (inviscid)
	H	-	homogeneous flow

The constants, k_1 and k_2 are weighting functions which account for that portion of the total energy resulting from the presence of viscous flow in the form of separated flow and attached flow respectively. It should be noted that the two secondary environments (separated flow and attached flow) are not simultaneously superimposed on the shock wave signal but rather are time shared. This, together with the fact that these environments may be correlated with the gross motion of the shock wave results in values of k_1 and k_2 less than 1.0. Finally, for peak overall levels of shock wave oscillation (corresponding to a point located at the mean position of the shock wave) the contribution of attached flow is negligible in comparison to that for separated flow. Thus, Equation 20 may be simplified to

$$\left[\Phi(f)\right]_{SW}^{H} = \left[\Phi(f)\right]_{SW}^{I,H} + k_1 \left[\Phi(f)\right]_{S}^{H} \tag{21}$$

Based on the experimental data of Reference 19, the power spectra $\left[\Phi(f)\right]_{SW}^{I,H}$ for shock wave oscillation in the absence of viscous flow normalized by local inflowing boundary layer thickness and velocity and free-stream dynamic pressure is given by:

$$\left[\frac{\Phi(f)\, U_0}{q_\infty^2\, \delta_0}\right]_{SW}^{I,H} = \frac{\left(\overline{P^2}/q_\infty^2\right)_{SW}^{I,H}}{\left(\frac{f_0\, \delta_0}{U_0}\right)_{SW} \left\{1 + \left(f/f_0\right)^{1.55}\right\}^{1.7}} \tag{22}$$

where:

$$\left[\overline{P^2}/q_\infty^2\right]_{SW}^{I,H} = \left[\overline{P^2}/q_\infty^2\right]_{SW}^{H} - k_1 \left[\overline{P^2}/q_\infty^2\right]_{S}^{H}$$

$\left[\overline{P^2}/q_\infty^2\right]_{SW}^{H}$ - overall level of shock oscillation peak corresponding to the mean location of the shock wave.

$\left[\overline{P^2}/q_\infty^2\right]_{S}^{H}$ - overall level of homogeneous separated flow as defined from Figures 7 and 8.

The subscript 0 denotes local velocity and boundary layer thickness upstream of the shock wave.

$$\left.\begin{aligned} \left(\frac{f_0 \delta_0}{U_0}\right)_{SW} &= 1 \times 10^{-2} \\ k_1 &= 0.25 \end{aligned}\right\} \quad \text{determined empirically from experimental data of Reference 19}$$

Substitution of Equations 10 and 22 into Equation 21 gives the final expression for the power spectra for shock wave oscillation.

$$\left[\frac{\phi(f)\, U_0}{q_\infty^2\, \delta_0}\right]_{SW}^{H} = \frac{\left(\overline{P^2}/q_\infty^2\right)_{SW}^{I,H}}{\left(\frac{f_0 \delta_0}{U_0}\right)_{SW}\left\{1 + \left(f/f_0\right)^{1.55}\right\}^{1.7}} + 0.25\, \frac{\left(\overline{P^2}/q_\infty^2\right)_{S}^{H}}{\left(\frac{f_0 \delta_0}{U_0}\right)_{S}\left\{1 + \left(f/f_0\right)^{0.83}\right\}^{2.15}} \qquad (23)$$

where $(f_0 \delta_0/U_0)_S$ is now defined for conditions upstream of the shock wave.

A comparison of the predicted power spectra for shock-wave oscillation with experimental measurements is presented in Figure 13. Also shown in the upper right hand corner of this figure is the variation in $\sqrt{\overline{P^2}}/q_\infty$ with distance upstream from the 45 degree wedge. It should be noted that this prediction formula holds true only at a point corresponding to the mean location of the shock wave. On either side of the shock wave, the influence of the shock diminishes rapidly due to its small displacement such that the environment is basically either attached or separated flow with some low frequency intermittency due to the shock wave. It is convenient to refer to these regions as non-homogeneous attached and separated flows and they will be discussed later in Section 2.4.

Cross-Power Spectra

Very little data has been published in the form of cross-power spectra of fluctuating pressures beneath oscillating shock waves. Because oscillating shock waves at a given flight condition are confined to relatively small areas of the vehicle surface, it is extremely difficult to define the spatial characteristics of the attendant fluctuating pressures. Fluctuating pressures in the vicinity of the shock wave are highly non-homogeneous; although they do appear to be related in both spectral shape and spatial coherence. The only significant results on the spatial coherence of fluctuating pressures in the vicinity of shock-waves are those by Coe and Rechtien (Reference 20) Their data indicate that the fluctuating pressures generated by the shock wave are related only at frequencies below $f\delta_0/U_0 = 0.08$ for the region immediately downstream of the mean location of the shock wave (Figure 14). For the region immediately upstream of the shock-wave, a small degree of coherence is also evident in this frequency range as well as at $f\delta_0/U_0 \geq 0.2$. A comparison of the power spectra and coherence function shows some very interesting characteristics of shock-induced fluctuating pressures. First, the power spectra of fluctuating pressures on each side of the peak level point show large low frequence energy which can be identified as having the same basic characteristics as the shock wave spectrum for $f\delta_0/U_0 \leq 0.08$. This is confirmed by the coherence of the data over the same frequency range $\left(f\delta_0/U_0 \leq 0.08\right)$. For $f\delta_0/U_0 > 0.08$, power spectra immediately upstream and downstream of the shock wave show spectral characteristics identical to attached turbulent boundary layer and separated flow, respectively. Thus, for $f\delta_0/U_0 > 0.8$, the spatial correlation of fluctuating pressure immediately upstream of the peak should be characteristic of attached flow; whereas, immediately downstream of the peak they should be characteristic of separated flow. However, when the spatial correlation is normalized by the power spectral densities to obtain the coherence function, this coherence appears to be minimized due to the large spectrum level for the point of peak fluctuating pressure. Further discussion on th

characteristic will be given later in the section on non-homogeneous attached and separated flows.

The spatial decay of the low frequency, shock induced fluctuating pressure in the longitudinal direction as shown in Figure 14 may be represented by an exponential coherence function as follows:

$$\gamma\left(\zeta, \frac{f\delta_0}{U_0}\right) = e^{-80\ f\delta_0/U_0} \tag{24}$$

A comparison of this empirical prediction with experimental data is presented in Figure 14. It should be noted that, as separation distance is increased, the above formula fails to account for the low coherence at low frequencies. However, because the large non-homogeneous effects associated with the flow in close proximity of the shock wave, the application of classical statistical methods to define the spatial characteristics for large separation distances may be questionable. Thus, for regions under the peak, Equation 24 is felt to be an accurate representation of the spatial characteristics of the fluctuating pressures in the longitudinal direction.

The longitudinal co-spectra may be written:

$$C(\zeta, f) = e^{-40\ f\delta_0/U_0} \cos 2\pi \frac{f\delta_0}{U_0} \tag{25}$$

Published data is not available on the transverse spatial characteristics of shock-induced fluctuating pressures. However, it is anticipated that these disturbances will be reasonably correlated over much larger distances in the transverse direction than in the longitudinal direction because of the continuity of the shock wave in the plane normal to the flow.

C-2

2.4 Non-Homogeneous Attached and Separated Flows

Non-homogeneous attached and separated flows are defined as environments which are basically attached or separated; however, the statistical properties of their attendant fluctuating pressures vary with spatial location. Examples to be considered herein are attached and separated flows immediately upstream and downstream of oscillating shock waves, respectively. The non-homogeneity may result from intermittency of the shock wave oscillation or from a more basic modification to the turbulence structure of attached and separated flow due to the motion of the shock wave. The variations in both the overall level and power spectra with position relative to the shock wave are evident in Figure 13. These data are shown in comparison with homogeneous attached and separated flow data to illustrate the presence of low frequency energy due to the shock wave. Again, basic characteristics of the overall levels, power spectra, and cross-power spectra will be discussed for the purpose of defining empirical prediction techniques for the non-homogeneous attached and separated flows.

Overall Level

The overall fluctuating pressure levels for attached and separated flow in close proximity to an oscillating shock wave are bounded on the low side by the levels of fluctuating pressures corresponding to homogeneous environments and are bounded on the high side by the peak fluctuating pressures corresponding to shock wave oscillation. In essence, this means that the differences between the homogeneous and non-homogeneous fluctuating pressure levels may be attributed directly to fluctuating pressures induced by the oscillating shock wave for the case considered here. Thus, normalized fluctuating pressure levels for non-homogeneous flows may be defined as:

$$\left(\frac{\sqrt{\overline{p^2}}}{q_\infty}\right)_A^H \leq \left(\frac{\sqrt{\overline{p^2}}}{q_\infty}\right)_A^{NH} \leq \left(\frac{\sqrt{\overline{p^2}}}{q_\infty}\right)_{SW}^H \tag{26}$$

$$\left(\frac{\sqrt{\overline{p^2}}}{q_\infty}\right)_S^H \leq \left(\frac{\sqrt{\overline{p^2}}}{q_\infty}\right)_S^{NH} \leq \left(\frac{\sqrt{\overline{p^2}}}{q_\infty}\right)_{SW}^H \tag{27}$$

where the subscripts and superscripts are defined as follows:

Subscripts	A	-	attached flow
	S	-	separated flow
	SW	-	shock wave
Superscripts	H	-	homogeneous condition
	NH	-	non-homogeneous condition

Under the assumption of statistical independence between the various sources, i.e., attached flow, separated flow and shock wave oscillation, the fluctuating pressure levels may be expressed as:

$$\left(\frac{\sqrt{\overline{p^2}}}{q_\infty}\right)_A^{NA} = \sqrt{\left[\left(\frac{\sqrt{\overline{p^2}}}{q_\infty}\right)_A^H\right]^2 + c_1\left[\left(\frac{\sqrt{\overline{p^2}}}{q_\infty}\right)_{SW}^H\right]^2} \tag{28}$$

$$\left(\frac{\sqrt{\overline{p^2}}}{q_\infty}\right)_S^{NH} = \sqrt{\left[\left(\frac{\sqrt{\overline{p^2}}}{q_\infty}\right)_S^H\right]^2 + c_2\left[\left(\frac{\sqrt{\overline{p^2}}}{q_\infty}\right)_{SW}^H\right]^2} \tag{29}$$

where c_1 and c_2 are weighting functions less than 1.0, which represent the contribution of the shock wave to the overall fluctuating pressure level. The values of c_1 and c_2 vary with spatial location relative to the shock wave and therefore, are difficult to predict. However, the above method of representation is useful in the prediction of power spectra for non-homogeneous flows as will be shown in the next section.

Power-Spectra

To predict the power spectra for non-homogeneous flows, a prior knowledge of the overall fluctuating pressure levels is required. Under the assumption of statistical independence between the various contributing sources, the power spectra for non-homogeneous environments may be written as the summation of power spectra of the contributing sources. Using the same symbolic representation as for the overall level, the power spectra for non-homogeneous environments may be written as:

$$\left[\phi(f)\right]_A^{NH} = \left[\phi(f)\right]_A^{H} + c_1 \left[\phi(f)\right]_{SW}^{I,H} \tag{30}$$

$$\left[\phi(f)\right]_S^{NH} = \left[\phi(f)\right]_S^{H} + c_2 \left[\phi(f)\right]_{SW}^{I,H} \tag{31}$$

From Equations 30 and 31 , c_1 and c_2 are given as

$$c_1 = \frac{\left(\dfrac{\overline{p^2}}{q_\infty^2}\right)_A^{NH} - \left(\dfrac{\overline{p^2}}{q_\infty^2}\right)_A^{H}}{\left(\dfrac{\overline{p^2}}{q_\infty^2}\right)_{SW}^{I,H}} \tag{32}$$

$$c_2 = \frac{\left(\frac{\overline{p^2}}{q_\infty^2}\right)_S^{NH} - \left(\frac{\overline{p^2}}{q_\infty^2}\right)_S^{H}}{\left(\frac{\overline{p^2}}{q_\infty^2}\right)_{SW}^{I,H}} \tag{33}$$

To determine the power spectra for non-homogeneous attached flow as caused by shock wave oscillation in the vicinity of the attached flow region, Equations 2, 22, and 32 are substituted into Equation 30, which gives a form normalized by local conditions upstream of the shock wave:

$$\left[\frac{\phi(f)\ U_0}{q_\infty^2\ \delta_0}\right]_A^{NH} = \frac{\left(\frac{\overline{p^2}}{q_\infty^2}\right)_A^{H}}{\left(\frac{f_0\ \delta_0}{U_0}\right)_A \left\{1 + \left(f/f_0\right)^{0.9}\right\}^2} +$$

$$\frac{\left(\frac{\overline{p^2}}{q_\infty^2}\right)_A^{NH} - \left(\frac{\overline{p^2}}{q_\infty^2}\right)_A^{H}}{\left(\frac{f_0\ \delta_0}{U_0}\right)_{SW} \left\{1 + \left(f/f_0\right)^{1.55}\right\}^{1.7}} \tag{34}$$

Similarly, substitution of Equations 10, 22, and 33 into Equation 31, leads to the following expression for non-homogeneous separated flow:

$$\left[\frac{\phi(f)\ U_0}{q_\infty^2\ \delta_0}\right]_S^{NH} = \frac{\left(\dfrac{\overline{p^2}}{q_\infty^2}\right)_S^H}{\left(\dfrac{f_0\ \delta_0}{U_0}\right)_S \left\{1 + \left(f/f_0\right)^{0.83}\right\}^{2.15}} + \frac{\left(\dfrac{\overline{p^2}}{q_\infty^2}\right)_S^{NH} - \left(\dfrac{\overline{p^2}}{q_\infty^2}\right)_S^H}{\left(\dfrac{f_0\ \delta_0}{U_0}\right)_{SW} \left\{1 + \left(f/f_0\right)^{1.55}\right\}^{1.7}} \qquad (35)$$

Comparison of these predictions with experimental measurements are shown in Figure 13.

APPENDIX – REFERENCES

1. Lowson, M. V., "Prediction of Boundary Layer Pressure Fluctuations," Wyle Laboratories Research Staff Report WR 67-15, October 1967.

2. Speaker, W. V. and Ailman, C. M., "Spectra and Space-Time Correlations of the Fluctuating Pressures at a Wall Beneath a Supersonic Turbulent Boundary Layer Perturbed by Steps and Shock Waves," NASA CR-486, May 1966.

3. Bull, M. K., "Properties of the Fluctuating Wall Pressure Field of a Turbulent Boundary Layer," AGARD Report 455, April 1963.

4. Bull, M. K., et al., "Wall Pressure Fluctuations in Boundary Layer Flow and Response of Simple Structure to Random Pressure Fields," University of Southampton, AASU Report 243, 1963.

5. Kistler, A. L. and Chen, W. S., "The Fluctuating Pressure Field in a Supersonic Turbulent Boundary Layer," Jet Propulsion Laboratory Technical Report No. 32-277, August 1962.

6. Belcher, P. M., "Predictions of Boundary Layer Turbulence Spectra and Correlations for Supersonic Flight," Presented at the 5th International Acoustic Congress, Liege, Belgium, September 1965.

7. Serafini, J. S., "Wall Pressure Fluctuations and Pressure Velocity Correlations in a Turbulent Boundary Layer," NASA TR R-165, December 1963.

8. Bakewell, H. P. Jr., et al., "Wall Pressure Correlation in Turbulent Pipe Flow," U. S. Navy Sound Laboratory Report No. 559, August 1962.

9. Shattuck, R. D., "Sound Pressures and Correlations of Noise on the Fuselage of a Jet Aircraft in Flight," NASA TN-D-1086, August 1961.

10. Willmarth, W. W. and Roos, F. W., "Resolution and Structure of the Wall Pressure Field Beneath a Turbulent Boundary Layer," J. Fluid Mech., Vol. 22, Part 1, pp. 81-94, 1965.

11. Maestrello, L., "Measurement of Noise Radiated by Boundary Layer Excited Panels," J. Sound Vib., 2 (2), 1965.

12. Hilton, D. A., "In-Flight Aerodynamic Noise Measurements on a Scout Launch Vehicle," NASA TN D-1818, July 1963.

13. Williams, D. J. M., "Measurements of the Surface Pressure Fluctuations in a Turbulent Boundary Layer in Air at Supersonic Speeds," University of Southampton, AASU Report No. 162, Department of Aeronautics and Astronautics, December 1960.

14. Chyu, W. J. and Hanly, R. D., "Power and Cross-Spectra and Space Time Correlation of Surface Fluctuating Pressures at Mach Numbers Between 1.6 and 2.5," AIAA Preprint No. 68-77, January 1968.

15. Maestrello, L., "Measurement and Analysis of the Response Field of Turbulent Boundary Layer Excited Panels," J. Sound and Vib., 2, No. 3, July 1965.

16. Willmarth, W. W. and Woolridge, C. E., "Measurements of the Fluctuation Pressure at the Wall Beneath a Thick Turbulent Boundary Layer," J. Fluid Mech., Vol. 14, pp. 187-210, 1962.

17. Bozich, D. J. and White, R. W., "Study of the Vibration Responses of Shells and Plates to Fluctuating Pressure Environments," Wyle Laboratories Research Staff Report WR 69-19, September 1969.

18. Robertson, J.E., "Wind Tunnel Investigation of the Effects of Reynolds Number and Model Size on the Steady and Fluctuating Pressures Experienced by Cone Cylinder Missile Configurations at Transonic Speeds," AEDC-TR-66-266, March 1967.

19. Coe, Charles F., "Surface Pressure Fluctuations Associated with Aerodynamic Noise," Basic Aerodynamic Noise Research Conference Proceedings, NASA SP-207.

20. Coe, Charles F., and Rechtien, R. D., "Scaling and Spatial Correlation of Surface Pressure Fluctuations in Separated Flow at Supersonic Mach Numbers," Paper presented at the AIAA Structural Dynamics and Aeroelasticity Specialist Conference, New Orleans, La., April 16-17, 1969.

21. Rechtien, Richard D., "A Study of the Fluctuating Pressure Field in Regions of Induced Flow Separation at Supersonic Speeds," University of Missouri - Rolla UMR Research Report, May 1970.

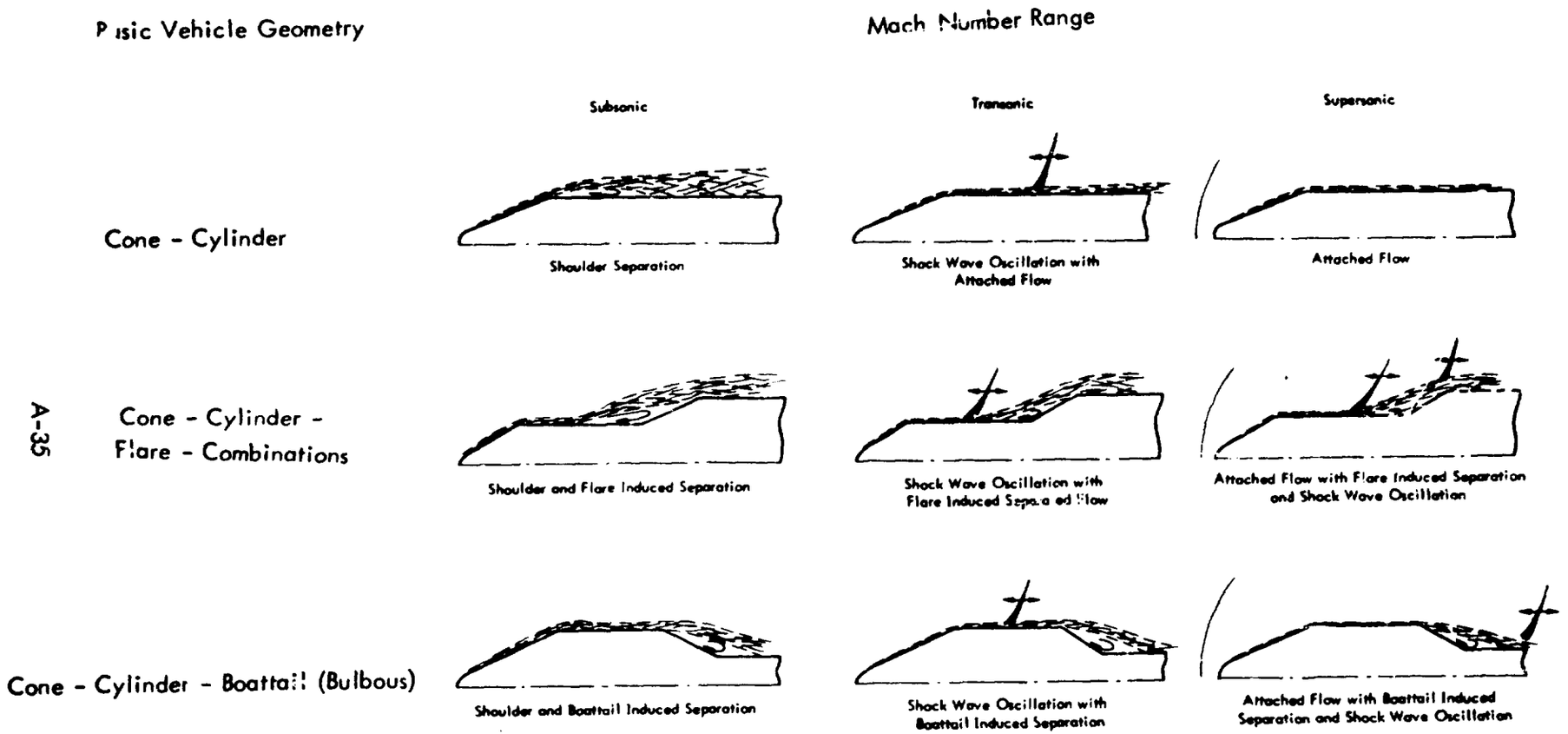

Figure 1. Subsonic, Transonic, and Supersonic Flow Fields for Basic Vehicle Configurations

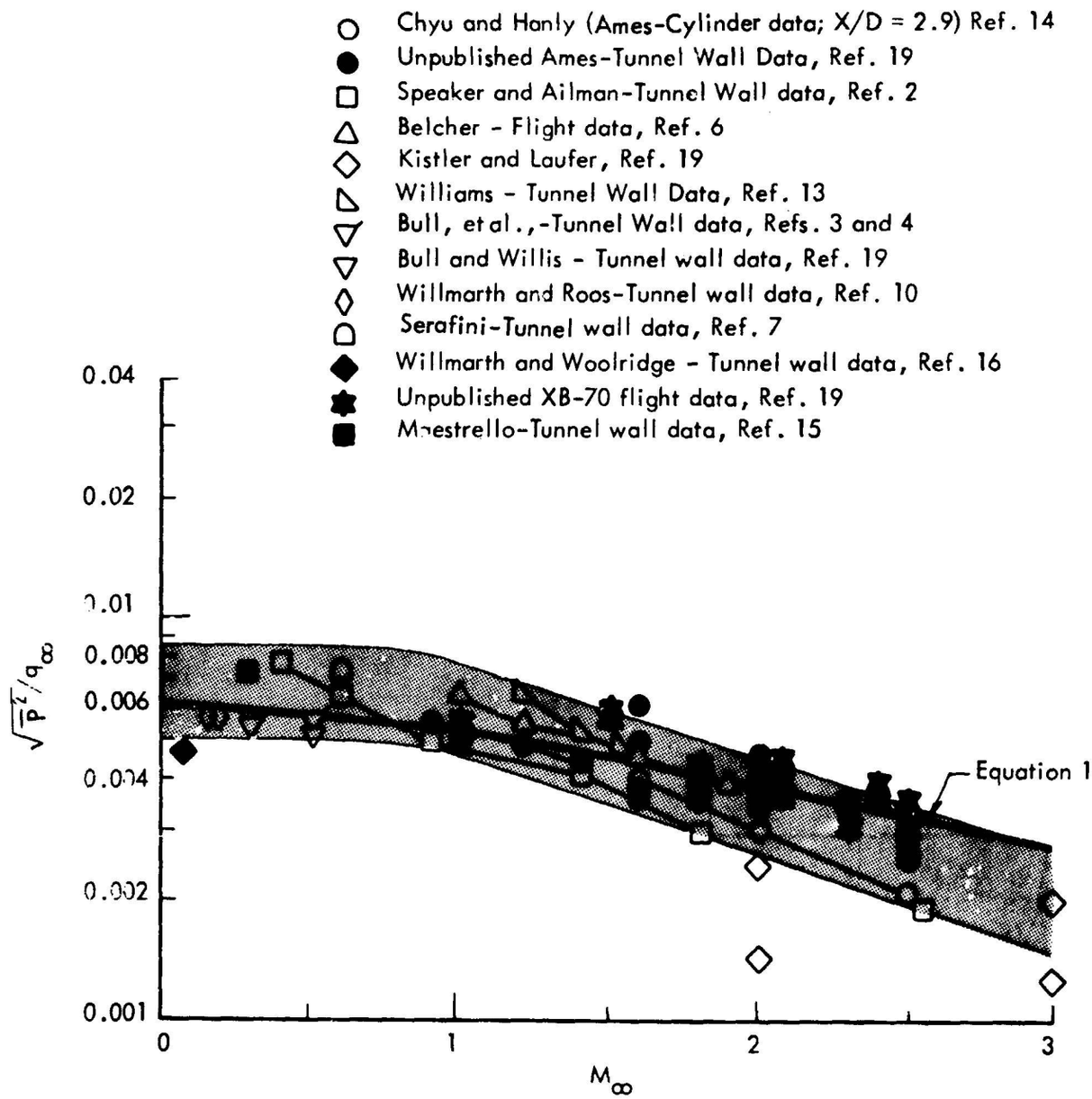

Figure 2. Comparison of Pressure Fluctuation Measurements beneath Attached Flows by Various Investigators

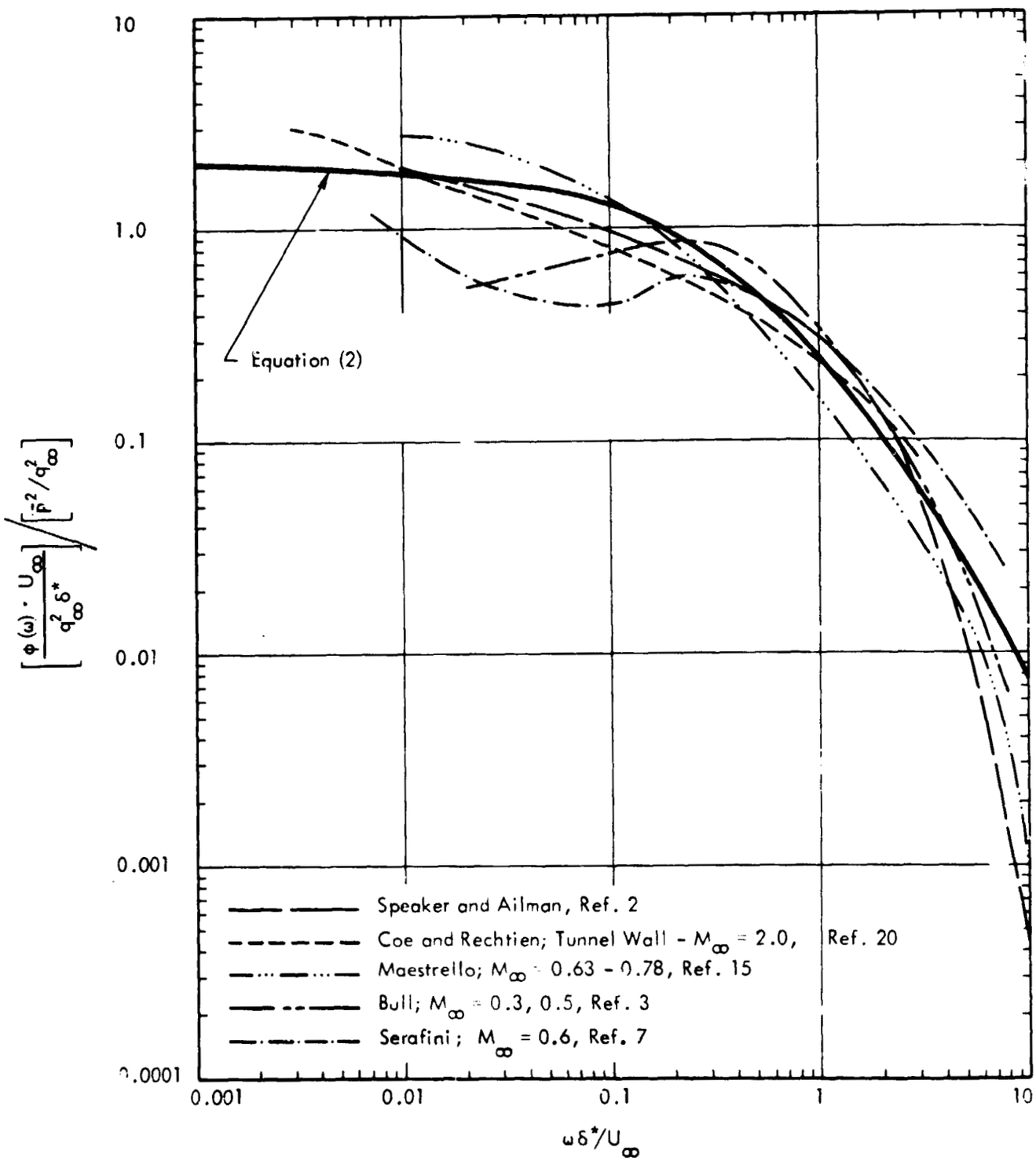

Figure 3. Power Spectra for Turbulent Boundary Layer Fluctuating Pressures

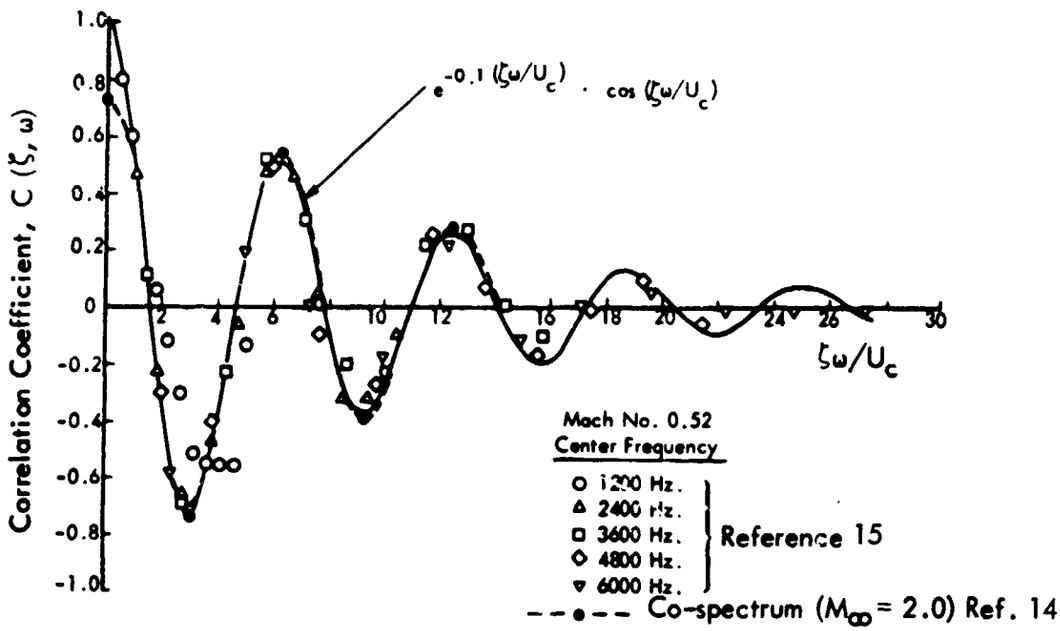

Figure 4a. Narrow Band Longitudinal Space Correlation Coefficient for Boundary Layer Fluctuating Pressures

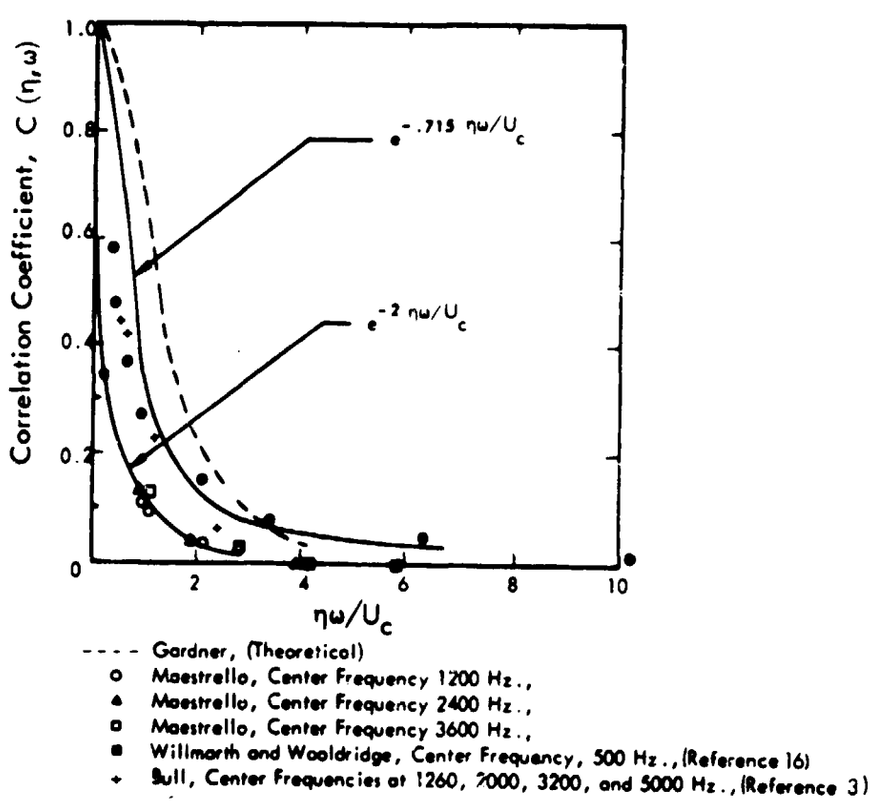

Figure 4b. Narrow Band Lateral Space Correlation Coefficient for Boundary Layer Fluctuating Pressures

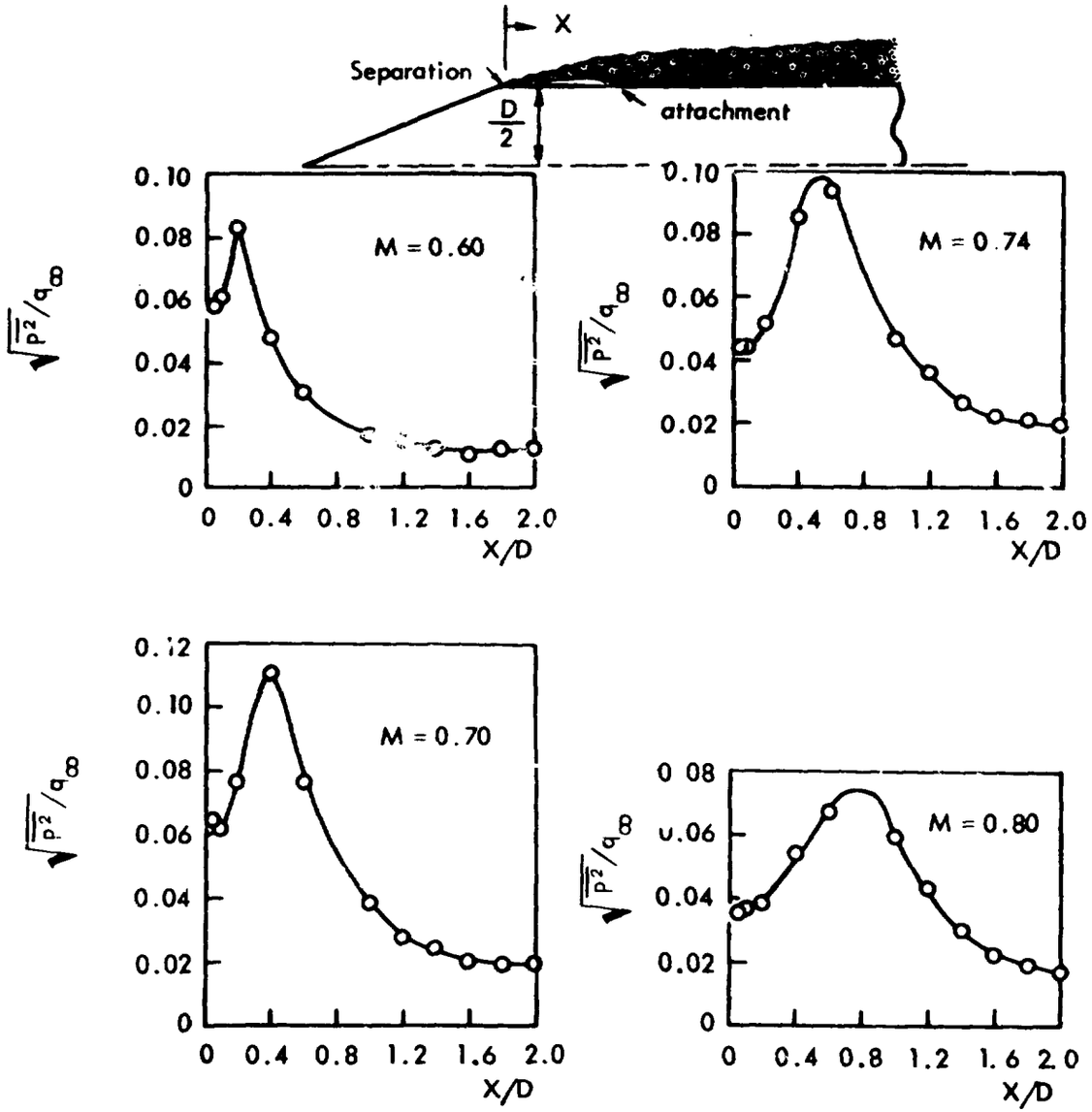

Figure 5. Axial Distributions of Fluctuating Pressures for Blunt Body Separated Flow; 25 Degree Cone-Cylinder (Reference 18)

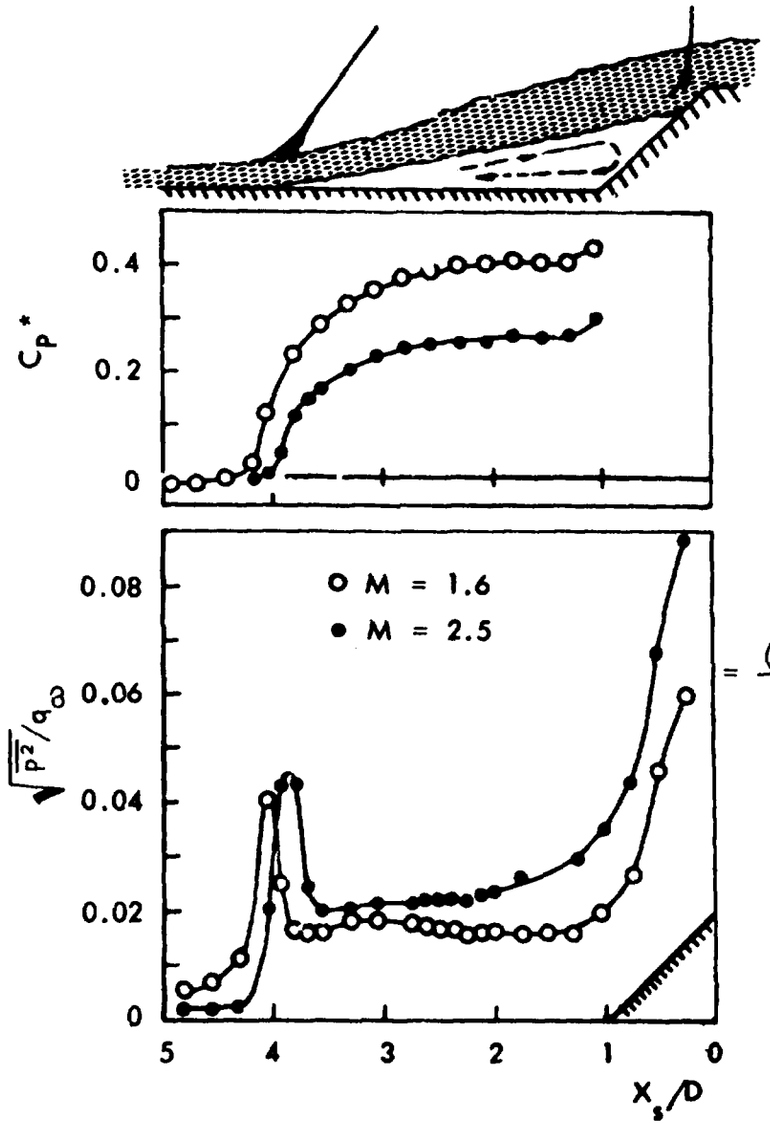

$$* \text{ NOTE: } C_p = \frac{P_{\ell s} - P_\infty}{q_\infty} = \frac{\text{(local static pressure)} - \text{(free-stream static pressure)}}{\text{free-stream dynamic pressure}}$$

Figure 6. Axial Distributions of Static and Fluctuating Pressures for 45 Degree Flare Induced Separation (Ref. 14)

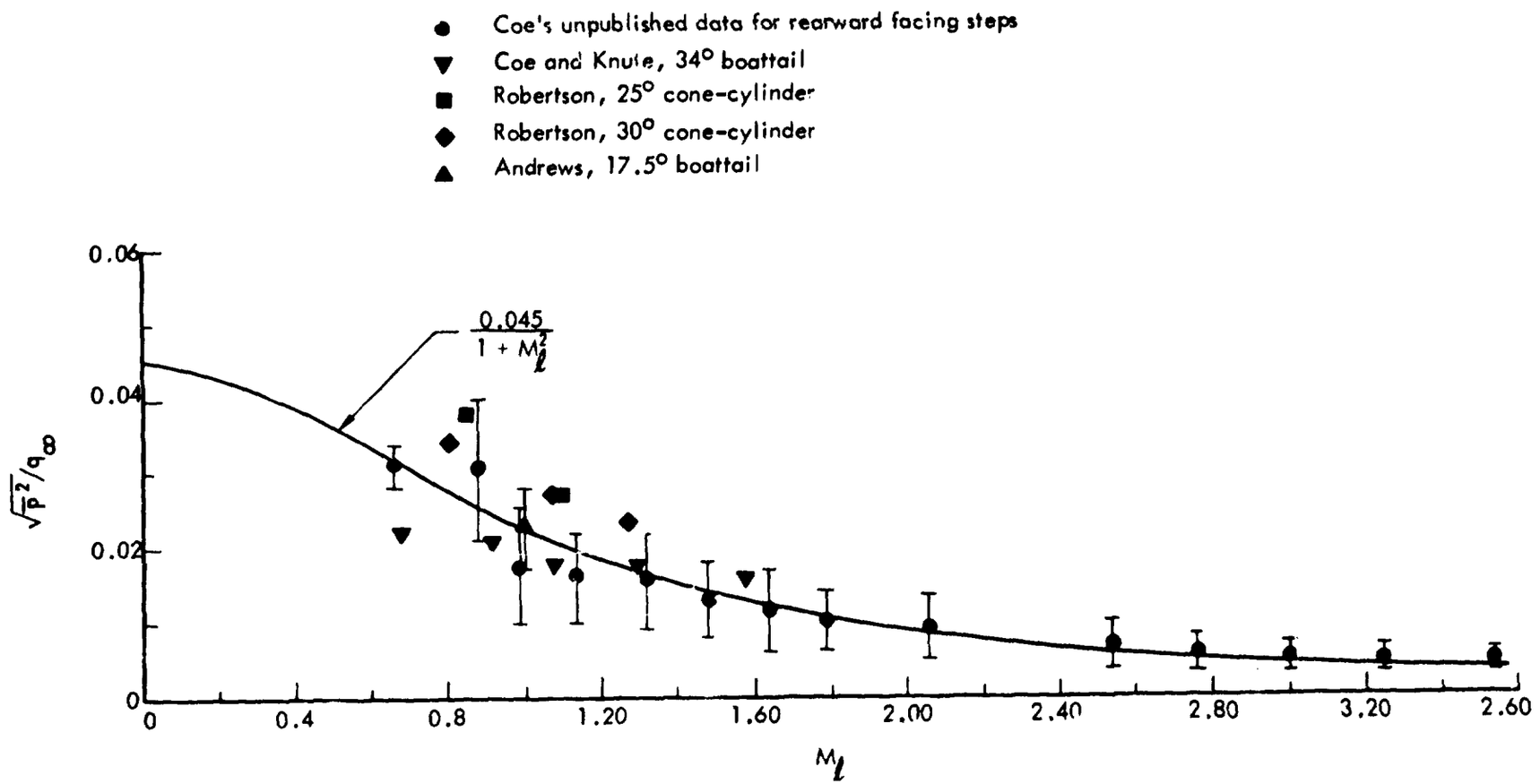

Figure 7. Variation of Normalized RMS Fluctuating Pressure Level with Local Mach Number for Expansion Induced Separated Flow

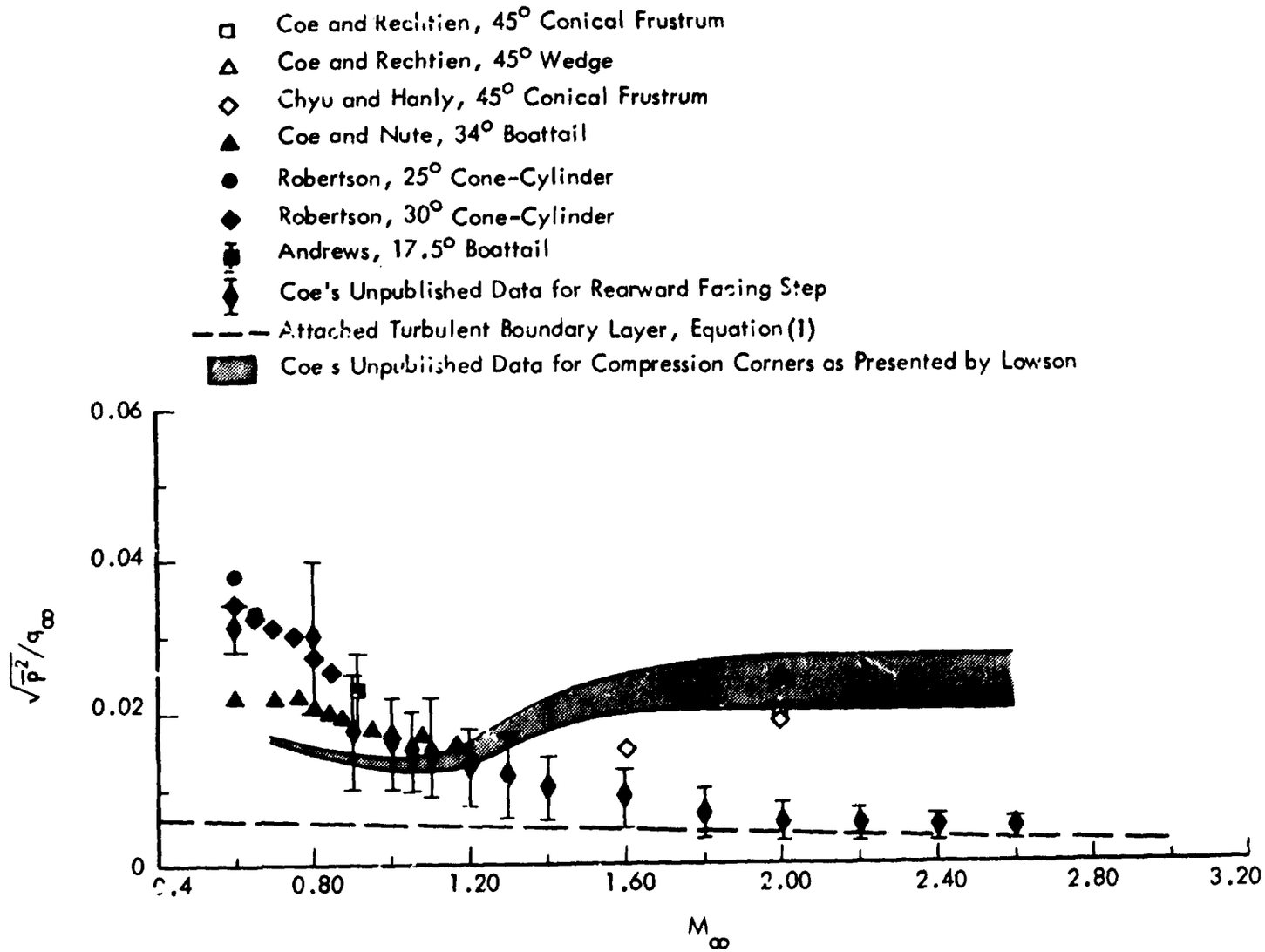

Figure 8. Variation of Normalized RMS Fluctuating Pressure Level with Free-Stream Mach Number for Expansion Induced and Compression Induced Separated Flows

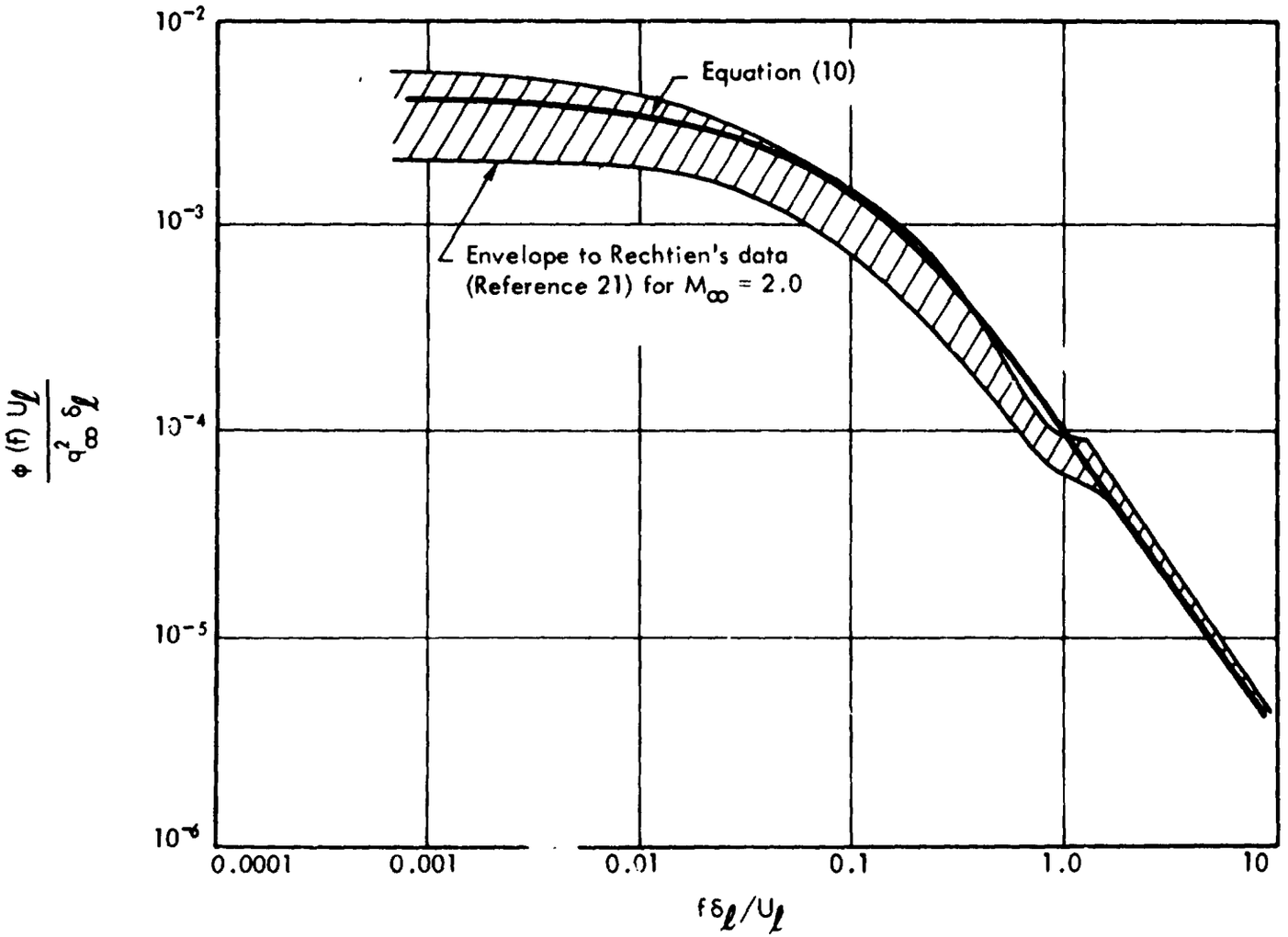

Figure 9. Power Spectrum of Fluctuating Pressures within Separated Flow Regions

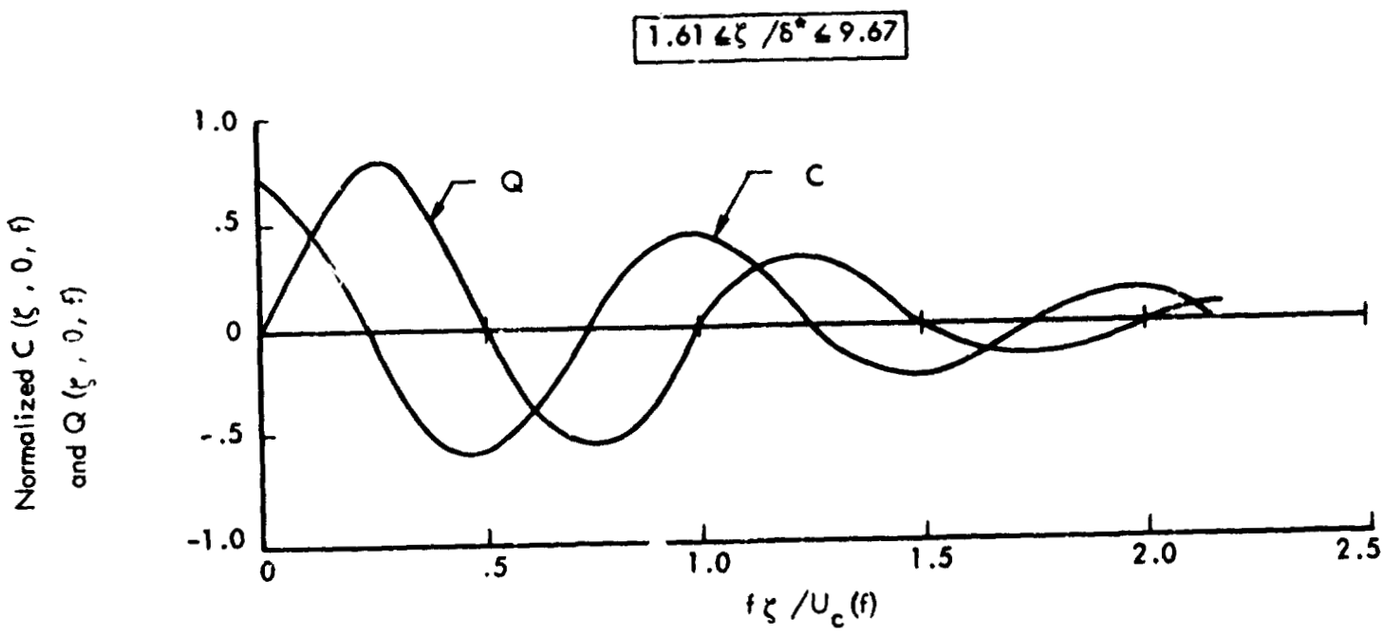

Figure 10. Typical Longitudinal Cross-Spectra of Pressure Fluctuations for Separated Flow (Ref. 14)

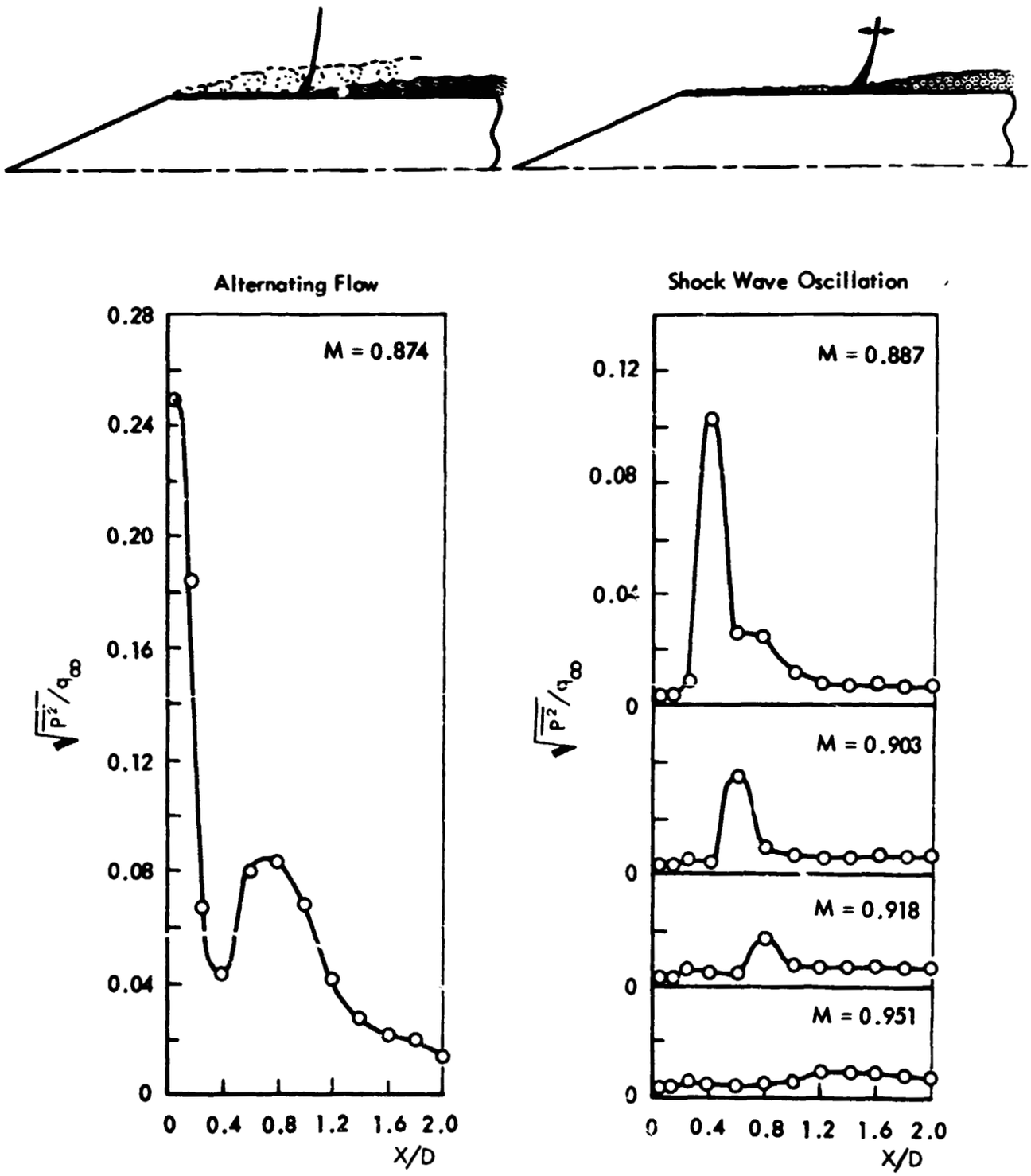

Figure 11. Axial Distribution of Fluctuating Pressures; 25 Degree Cone-Cylinder

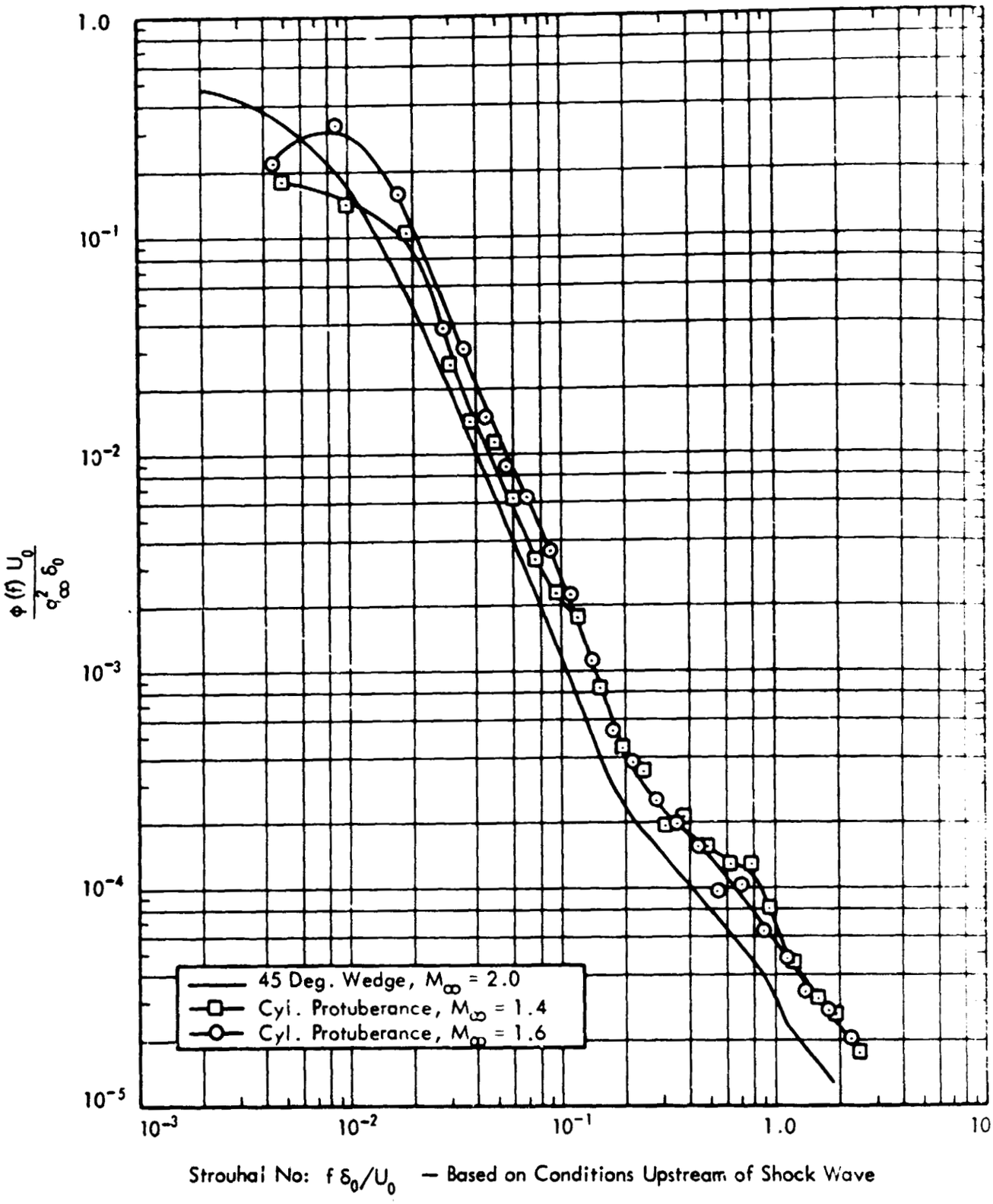

Figure 12. Comparison of Power Spectra for Shock-Wave Oscillation Induced by Two- and Three-Dimensional Protuberances

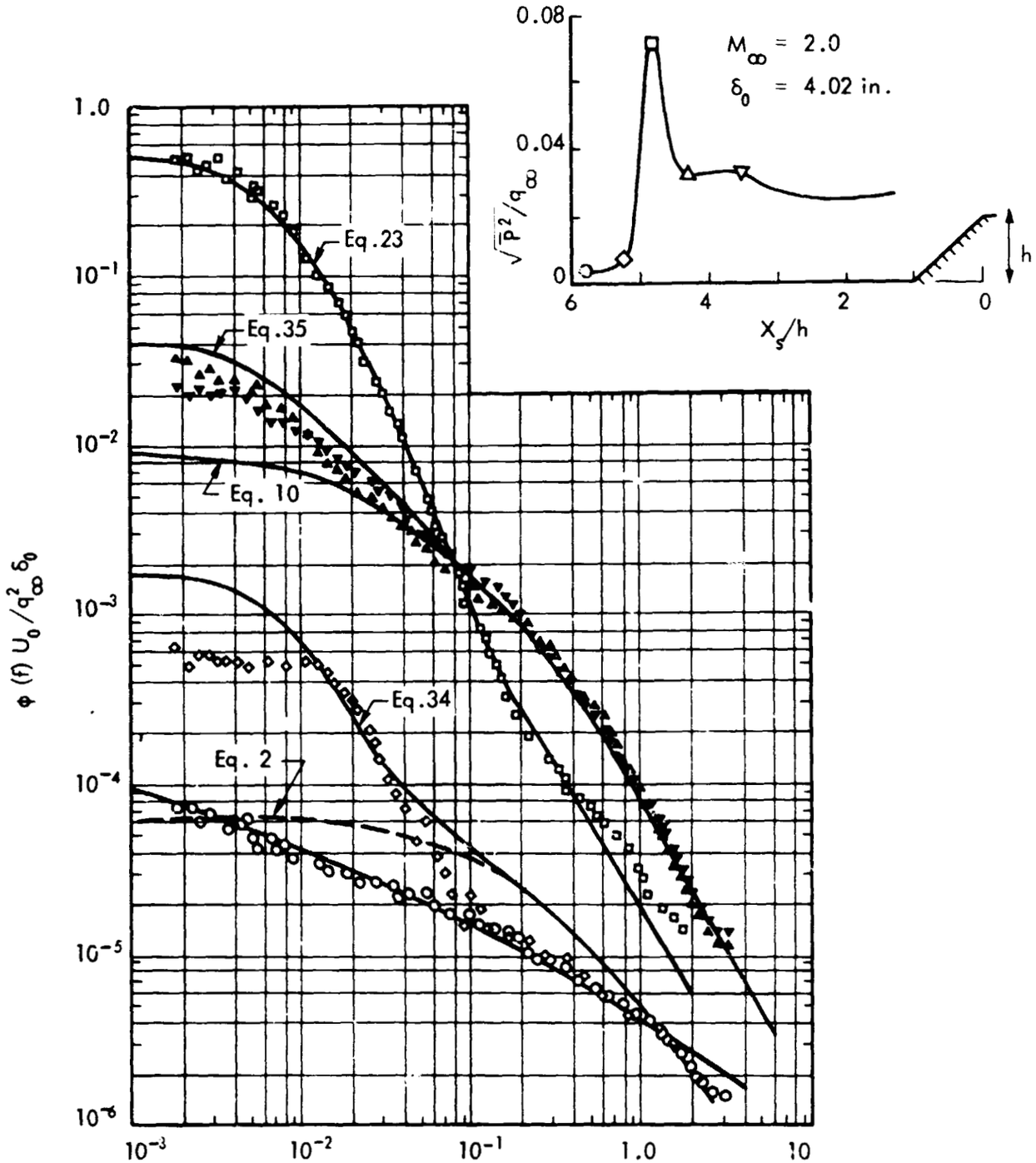

Strouhal No: $f\,\delta_0/U_0$ — Based on Conditions Upstream of Shock Wave

- ○ Attached turbulent boundary layer
- ◇ Non-homogeneous attached turbulent boundary layer
- ▽ △ Non-homogeneous separated flow
- □ Shock wave oscillation

Figure 13. Longitudinal Distribution of Pressure Fluctuations and Typical Power Spectra in Vicinity of Supersonic Flow Separation Ahead of a 45° Wedge

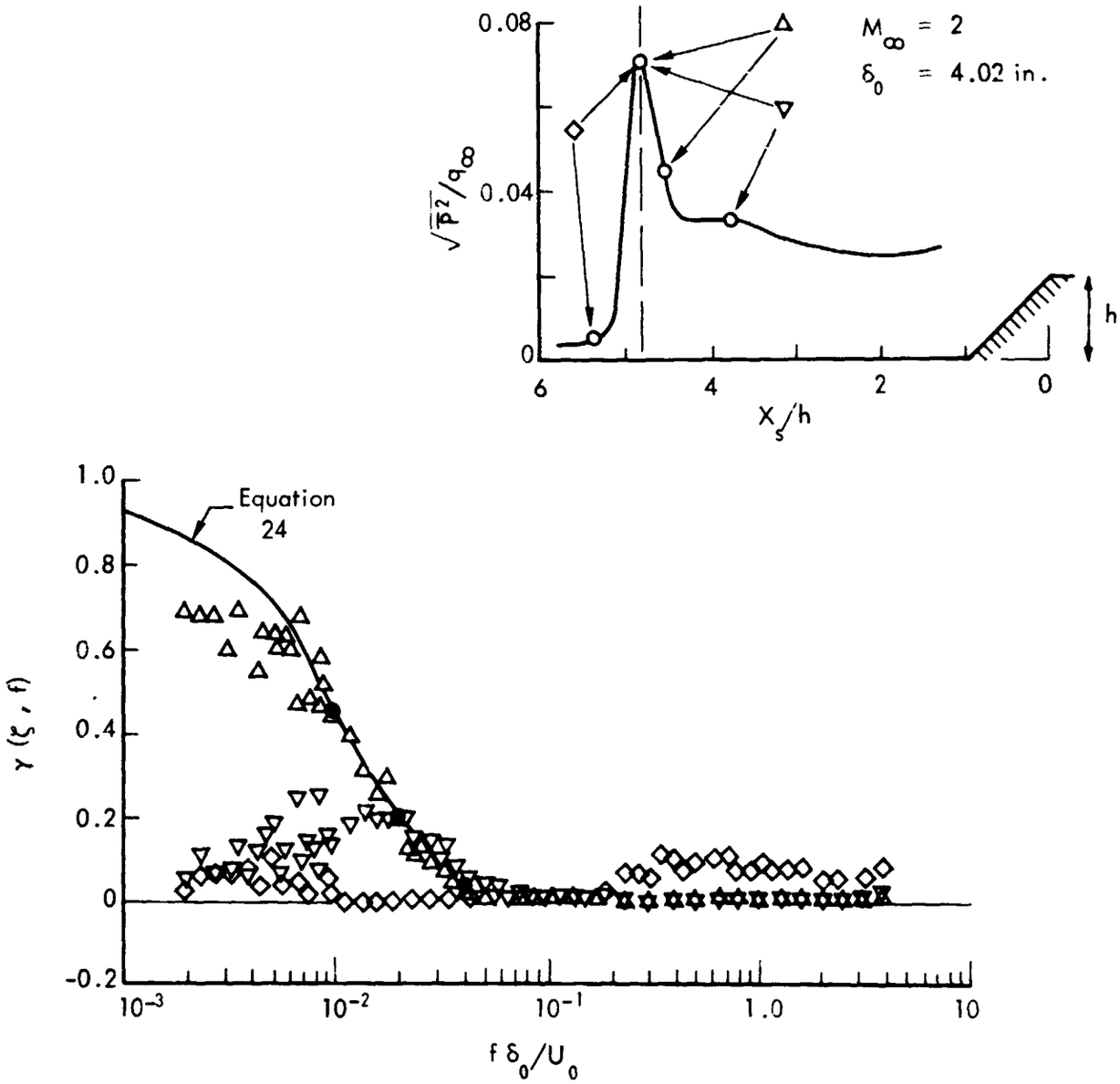

Figure 14. Correlation of Pressure Fluctuations Between Shock Wave and Adjacent Attached and Separated Flows (Reference 20)

APPENDIX B

SHOCK WAVE OSCILLATION DRIVEN BY TURBULENT BOUNDARY LAYER FLUCTUATIONS

APPENDIX B

SHOCK WAVE OSCILLATION DRIVEN BY TURBULENT BOUNDARY LAYER FLUCTUATIONS

High speed aerodynamic vehicles are subject to significant fluctuating pressure environments from various turbulent and compressible effects. One of the more severe environments encountered in transonic and supersonic flow is the oscillation of shock waves, where root mean square pressure fluctuations are on the order of 1/10 dynamic pressure. Oscillating shock waves are often associated with more complex fluctuating flow fields, such as separation in a compression corner. Although a considerable body of experimental data enables empirical predictions of some fluctuating flow environments to be made with confidence, a better understanding of the basic mechanisms is needed to extend available data to more general cases. Perhaps the most important feature of oscillating shock waves which must be determined is the driving mechanism of the oscillations — whether shock motion is caused by the incoming turbulent boundary layer, or by flowfield fluctuatings behind it. To answer this question, a simple model is proposed in which the incoming turbulent boundary layer drives shock motion. Analysis of this model shows excellent agreement with overall fluctuating pressure levels and spectra for shock waves in separated flow ahead of a compression corner. This analysis, performed under the present contract, is presented in Reference B-1 and is summarized in this Appendix.

Earlier treatments of the shock oscillation follow the approach of Trilling (Reference B-2) for interaction of a shock with a laminar boundary layer. In Trilling's analysis, frequencies were found for which oscillations would be self-sustaining. This would suggest that shock spectra would contain discrete frequencies. However, observed spectra are generally broadband, with no frequency peaks. The basic source of broadband fluctuations is the incoming turbulent boundary layer; it is therefore reasonable to look for a connection between this turbulence and shock motion.

Any oscillating motion is a combination of a forcing function and a restoring mechanism. Since a turbulent boundary layer contains velocity fluctuations, the shock wave within the boundary layer will be convected upstream or downstream. A one-dimensional model of this convection is adopted as the forcing function, so that speed of the shock wave (relative to its mean location) is given by the instantaneous streamwise velocity fluctuation within the boundary layer. This velocity fluctuation is represented as $a_\infty \epsilon \mu(t)$, where $\mu(t)$ is a stationary random function with zero mean and $\langle \mu^2 \rangle = 1$, and ϵ is the rms turbulent Mach number.

The restoring mechanism is dependent on the particular flowfield geometry. Attention is therefore directed to a specific geometry, separated flow in a compression corner, Figure B-1. The mean location of the separation point and shock wave is governed by viscous interaction and corner geometry. The mean location must be stable; otherwise the separation point would not be there. If the separation point is displaced a distance x, it will return. If x is small compared to separation length, it is reasonable to expect the rate of return to be proportional to x, so that the shock wave returns with speed $-\beta x$, where the constant β is a function of mean flow parameters and corner geometry.

Combining the random boundary layer convection with the linear restoring mechanism, the equation of motion for the foot of the shock wave is:

$$u = a_\infty \epsilon \mu(t) - \beta x \tag{B-1}$$

Equation (B-1) may be integrated to give the displacement:

$$x = e^{-\beta t} \epsilon a_\infty \int_0^t \mu(\xi)\, e^{\beta \xi}\, d\xi \tag{B-2}$$

Analysis of this equation of motion leads to the following statistical properties at large time:

- Root mean square displacement:

$$\langle x^2 \rangle^{\frac{1}{2}} = \epsilon a_\infty \left(\tau_\mu / \beta \right)^{\frac{1}{2}} \tag{B-3}$$

  where τ_μ = integral scale of boundary layer fluctuations.

  The analysis leading to Equations (B-2) and (B-3) for the displacement follows almost exactly that for the velocity of a particle in Brownian motion with damping (Reference B-3).

- Autocorrelation function:

$$R_x(\tau) \equiv \frac{\langle x(t)\, x(t+\tau) \rangle}{\langle x^2 \rangle} = e^{-\beta \tau} \tag{B-4}$$

  so that the integral scale of shock motion is $\tau_x = 1/\beta$. This result was obtained by using Equation (B-2) in the definition of $R_x(\tau)$. The manipulations, contained in Reference B-1, are somewhat lengthy but straightforward.

For a shock wave whose mean profile is $P(x)$ and thickness is greater than $\langle x^2 \rangle^{\frac{1}{2}}$, the fluctuating pressure intensity and spectrum are found to be:

$$\langle p^2 \rangle^{\frac{1}{2}} = \frac{dP}{dx} \langle x^2 \rangle^{\frac{1}{2}} \tag{B-5}$$

$$\phi(f) = \frac{4 \langle p^2 \rangle}{\beta \left[1 + \left(\frac{2\pi f}{\beta} \right)^2 \right]} \qquad \text{(B-6)}$$

Equation (B-5) assumes a constant gradient over the displacement distance; Equation (B-6) is the Fourier transform of Equation (B-4).

The fluctuating pressure level and spectrum given by this theory were compared with experimental data obtained by Coe and Rechtien (Reference B-4). Static and fluctuating data are shown in Figure B-2. For the $D = \infty$, $h = 8$ inches case of Figure B-2 present theory predicts $\langle p^2 \rangle^{\frac{1}{2}} / q_\infty = 0.068$. This is in excellent agreement with ata. The predicted spectrum is shown in Figure B-3, along with the measured spectrum from Reference B-4. Also shown in Figure B-3 are two spectra obtained by Robertson (Reference B-5) for cylindrical protuberances.

The straightforward physical model proposed and the excellent agreement with experimental data lead to the conclusion that shock wave oscillation is primarily due to velocity fluctuations in the incoming turbulent boundary layer. The agreement of the present theory with shock spectra from both a two-dimensional compression corner and three-dimensional protuberances, where the incoming boundary layer and separated shock are similar but the separated flow regions differ considerably, further substantiates this conclusion.

REFERENCES

B-1 Plotkin, Kenneth J., "Shock Wave Oscillation Driven by Turbulent Boundary Layer Fluctuations," Wyle Laboratories Research Staff Report WR 72-12, September 1972.

B-2 Trilling, Leon, "Oscillating Shock-Boundary Layer Interaction," J. Aero. Sci., 25, No. 5, 1958.

B-3 Uhlenbeck, G.E., and Ornstein, L.S., "On the Theory of Brownian Motion," Phys. Rev., 36, No. 3, September 1930. Reprinted in Selected Papers on Noise and Stochastic Processes, edited by Nelson Wax, Dover, New York, 1954.

B-4 Coe, C.F., and Rechtien, R.D., "Scaling and Spatial Correlation of Surface Pressure Fluctuations in Separated Flow at Supersonic Mach Numbers," Paper presented at AIAA Structural Dynamics and Aeroelasticity Specialist Conference, New Orleans, Louisiana, April 16-17, 1969.

B-5 Robertson, J.E., "Prediction of In-Flight Fluctuating Pressure Environments Including Protuberances Induced Flow," Wyle Laboratories Research Staff Report WR 71-10, March 1971.

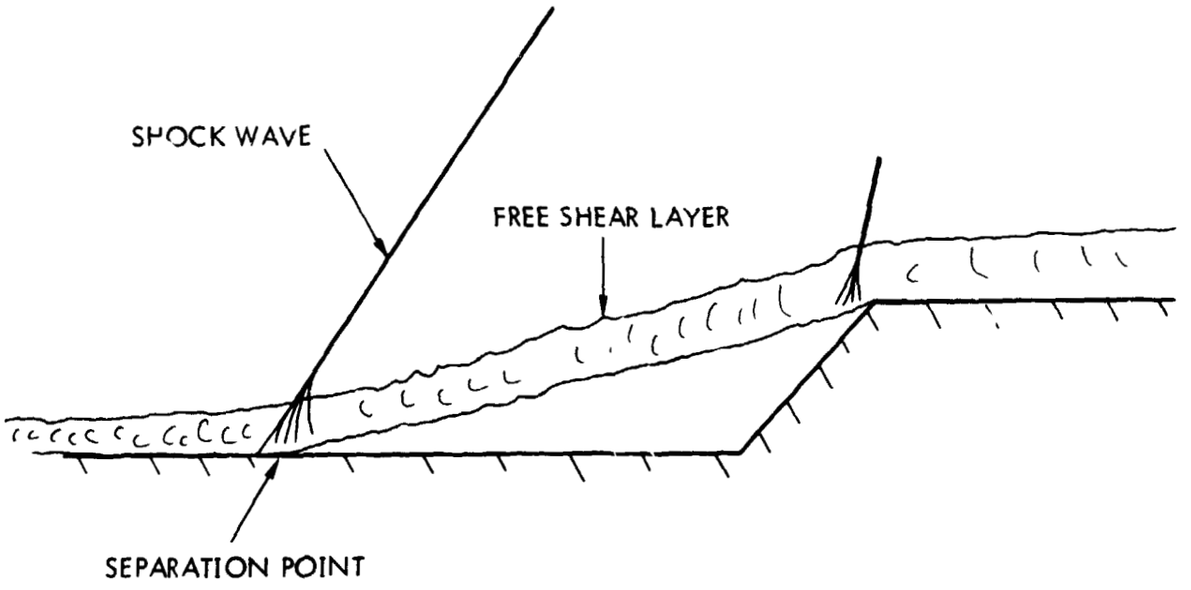

Figure B-1. Separation in a Compression Corner

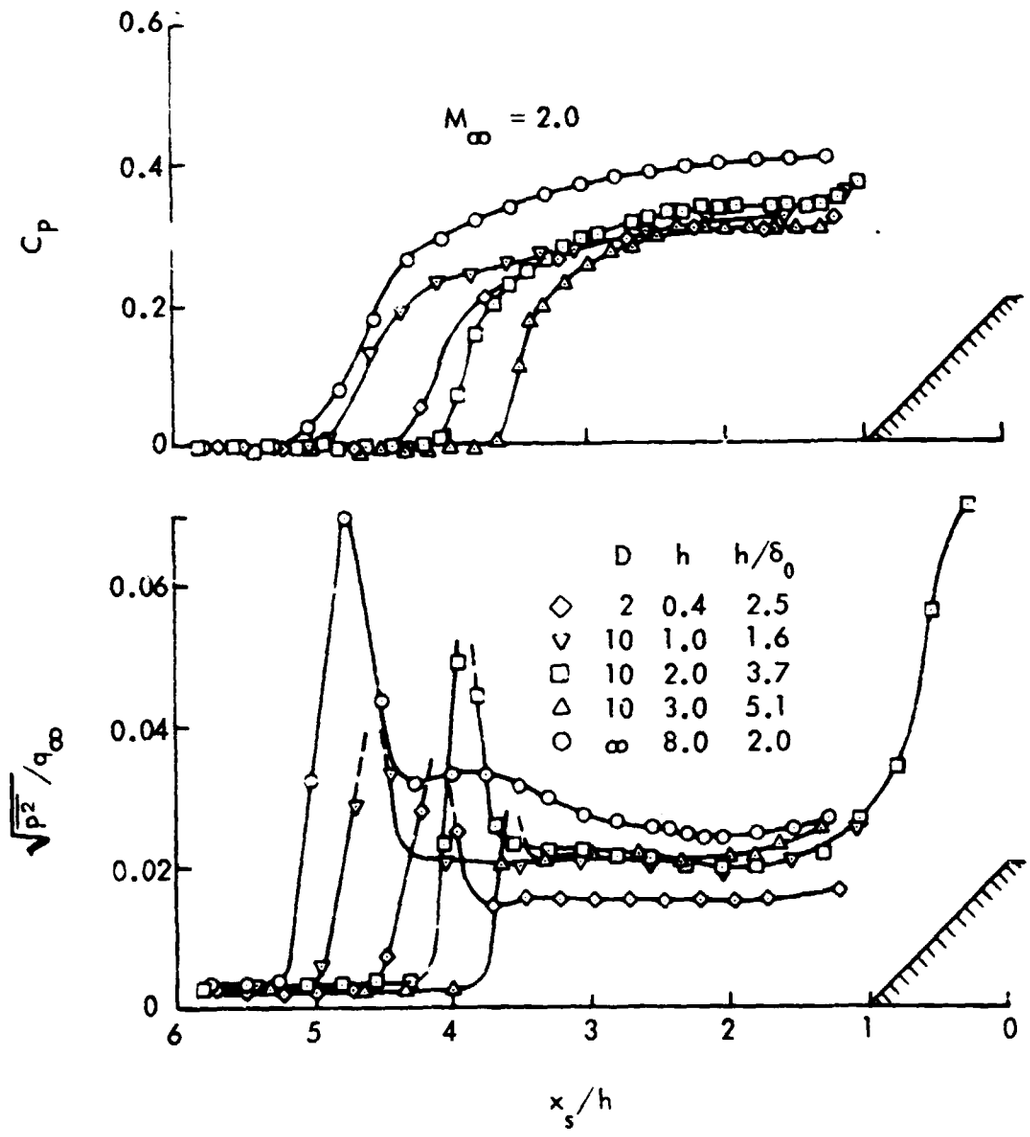

Figure B-2. Longitudinal Distributions of Steady and Fluctuating Pressures, from Reference 2

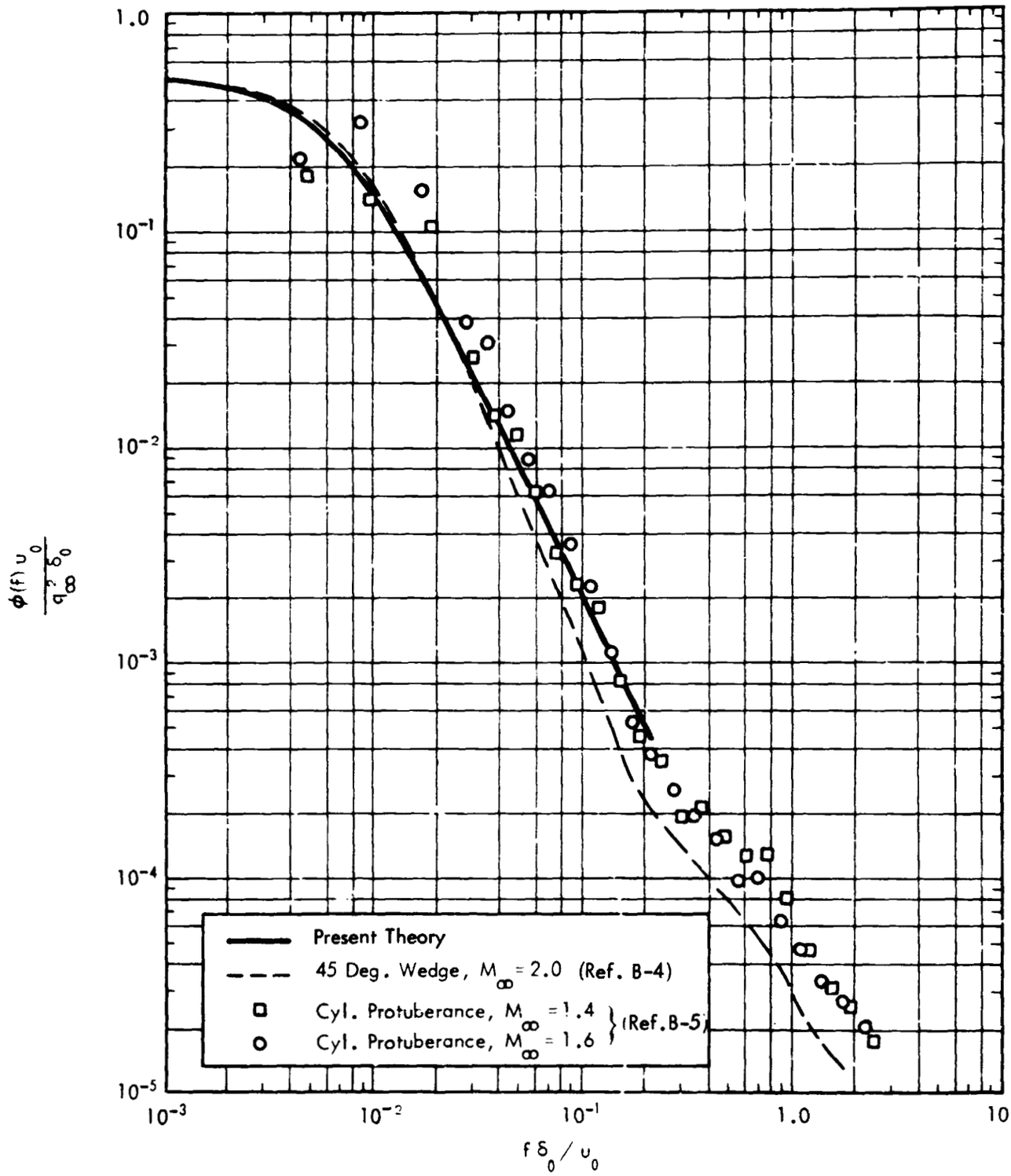

Figure B-3. Comparison of Predicted Spectrum with Measured Spectra

APPENDIX C

MATHEMATICAL PROPERTIES OF THE EMPIRICAL SPECTRA

APPENDIX C

MATHEMATICAL PROPERTIES OF THE EMPIRICAL SPECTRA

Spectral data for various fluctuating pressure environments have been analytically represented in the form:

$$\frac{\Phi(f)\,U}{q_\infty^2\,L} = \frac{\overline{p^2}/q_\infty^2}{\frac{f_0 L}{U}\left\{1 + (f/f_0)^n\right\}^k} \qquad \text{(C-1)}$$

where:

U	=	Characteristic velocity
L	=	Characteristic length
f_0	=	Characteristic frequency
n, k	=	Spectrum shape factors

The parameters f_0, n and k are empirically determined. Characteristic velocity and length are chosen as those which give the most general value of $f_0\,L/U$ over a range of flow conditions; U is either free stream or local velocity, while L may be δ, δ^*, or a body characteristic length.

Equation (C-1) may be re-arranged to represent the normalized spectrum:

$$\varphi(f) = \frac{\Phi(f)}{p^2} = \frac{1/f_0}{\left\{1 + (f/f_0)^n\right\}^k} \qquad \text{(C-2)}$$

The integrated spectral density must equal the overall level, $\int_0^\infty \Phi(f)\,df = \overline{p^2}$, so that

$$\int_0^\infty \varphi(f)\,df = \int_0^\infty \frac{d\,(f/f_0)}{\left\{1 + (f/f_0)^n\right\}^k} = 1 \qquad \text{(C-3)}$$

Introduce the transformation:

$$t = \frac{1}{1 + (f/f_0)^n}$$

for which $d(f/f_0) = \frac{1}{n}\left(\frac{1}{t} - 1\right)^{\frac{1}{n}-1} \frac{1}{t^2}$, $(f/f_0)\Big|_0^{\infty} = t\Big|_0^1$

After slight manipulation, Equation (C-3) becomes

$$\int_0^{\infty} \varphi(f)\, df = \frac{1}{n}\int_0^1 (1-t)^{\frac{1}{n}-1}\, t^{k-\frac{1}{n}-1}\, dt = 1 \qquad \text{(C-4)}$$

The definition of the Beta function is (Equation 6.370 of Reference C-1):

$$B(x,y) = \int_0^1 t^{x-1}\,(1-t)^{y-1}\, dt\,, \qquad \begin{array}{l} \mathrm{Re}\,(x) > 0 \\ \mathrm{Re}\,(y) > 0 \end{array} \qquad \text{(C-5)}$$

so that Equation (C-4) is:

$$\frac{1}{n}\, B\left(k - \frac{1}{n}, \frac{1}{n}\right) = 1 \qquad \text{(C-6)}$$

The Beta function may be represented in terms of the Gamma function (Equation 6.381 of Reference C-1):

$$B(x,y) = \frac{\Gamma(x)\,\Gamma(y)}{\Gamma(x+y)} \qquad \text{(C-7)}$$

so that the present condition is:

$$\frac{1}{n}\,\frac{\Gamma\left(k - \frac{1}{n}\right)\Gamma\left(\frac{1}{n}\right)}{\Gamma(k)} = 1 \qquad \text{(C-8)}$$

Noting the well known properties of the Gamma function:

$$\Gamma(1) = 1 \qquad \text{(C-9c)}$$

$$\Gamma(x+1) = x\,\Gamma(x) \qquad \text{(C-9b)}$$

Equation (C-8) is satisfied by:

$$k = 1 + \frac{1}{n} \tag{C-10}$$

It is obvious from Equation (C-3) that for each value of n there is a unique correct value of k. Noting that Equation (C-10) and its inverse are single valued, Equation (C-10) is therefore the unique solution to Equation (C-3).

With Equation (C-10), the three free parameters f_0, n and k are reduced to two: f_0 and either n or k. The prediction formulae presented in the body of this report and in Appendix A did not make use of this relation, but rather fitted all three parameters independently, using three points in each measured spectrum. The values of n and k obtained are listed in Table C-1.

TABLE C-1

VALUES OF n AND k USED IN EMPIRICAL SPECTRA

Environment	n	k
Attached Flow	0.9	2.0
Separated Flow	0.83	2.15
Shock Oscillation	1.55	1.7

Figure C-1 shows these values of n and k as compared to Equation (C-10). The agreement is quite good. Although it should be understood that the present point is strictly a mathematical manipulation, the agreement shown in Figure C-1 provides additional justification for the use of the form of Equation (C-1).

The values of n and k shown in Table C-1 are sufficiently close to agreement with Equation (C-10) that they are retained unchanged in the prediction formulae. If at some future time it is desired to revise n and k, this can be easily done. It should be noted that the most natural way of fitting the two independent parameters, f_0 and n or k, is to utilize data at low frequencies ($f \ll f_0$) to obtain f_0, and high frequency data ($f \gg f_0$) to obtain n and k. At $f \gg f_0$, the slope of the spectrum on a log-log plot is $-nk$.

REFERENCES

C-1. Ryshik, I.M., and Gradstein, I.S., Tables of Series, Products and Integrals, VEB Deutscher Verlag der Wissenschaften, Berlin, 1963.

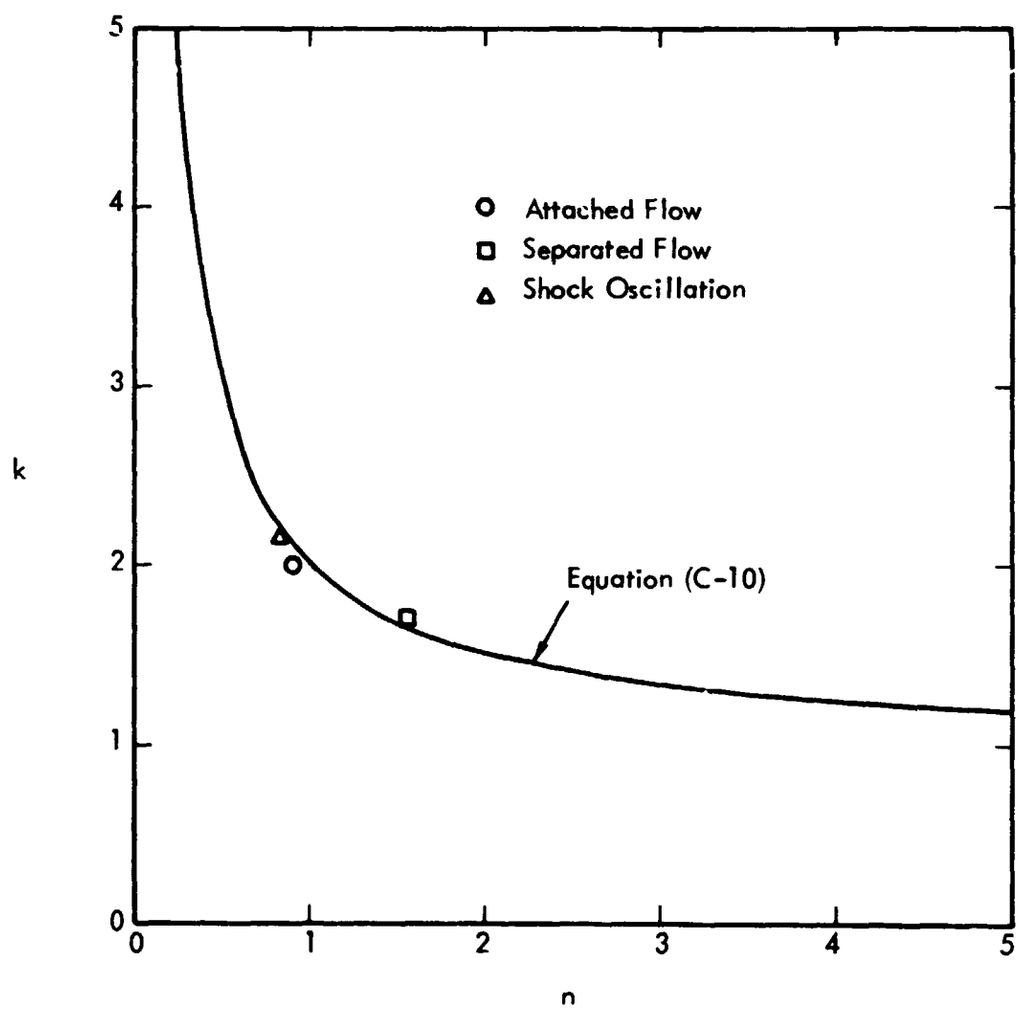

Figure C-1. Comparison of Fitted Values of n and k with Equation (C-10)

APPENDIX D

COMPUTER PROGRAM DESCRIPTIONS

WYLE LABORATORIES

COMPUTER PROGRAM DESCRIPTION

Program Number:	71/004S-1A
Authors:	D.Lister, K.Plotkin
Date:	May 1973
Source Language:	Fortran IV-H
Computer:	XDS Sigma 5

1.0 PROGRAM TITLE

Power Spectral Density

2.0 PURPOSE

Identical to Program 71/004S-1, written by D. Lister, except that the present version is a subroutine and does not provide plots.

3.0 METHOD

Same as Program 71/004S-1.

4.0 COMPUTER CONFIGURATION

The required hardware is: XDS Sigma 5 Computer with 16 K core, card reader and line printer.

5.0 CALL SEQUENCE

The program is entered by the call:

```
CALL PSDIN (FB, FE, ANN, TIT, IABCD, QS, DB, UL, PSQUAR,
      FZERO)
```

All input variables correspond to those described for 71/004S-1, with the following additional notations:

- IABCD is a 4 element array, such that

  IABCD (1) = IA
  IABCD (2) = IB
  IABCD (3) = IC
  IABCD (4) = ID

- PSQUAR is a 3 element array, such that

  PSQUAR (1) = PQSA
  PSQUAR (2) = PQSB
  PSQUAR (3) = PQST

- FZERO is a 3 element array, such that

  FZERO (1) = FDUA
  FZERO (2) = FDUB
  FZERO (3) = FDUT

After a call to PSDIN has been made, subsequent entries for identical values of FB, FE and ANN may be made by the statement

```
CALL PSD (TIT, IABCD, QS, DB, UL, PSQUAR, FZERO)
```

6.0 OUTPUT

The output is identical to 71/004S-1.

WYLE LABORATORIES

COMPUTER PROGRAM DESCRIPTION

Program Number:	73/004P - 1
Author:	K. J. Plotkin
Date:	April 1973
Source Language:	Fortran IV - H

1.0 PROGRAM TITLE

Correlation Function

2.0 PURPOSE

Given the local velocity and boundary layer thickness, the program computes and prints narrow band cross correlation functions for attached turbulent boundary layer flow, separated flow, and protuberance induced separated flow.

3.0 METHOD

The prediction method of Reference 1 is used. The formulae, presented in Reference 1, for longitudinal and lateral correlation functions may be written

Longitudinal: $$A_\xi(\xi, f) = \exp(-|\xi|/L_\xi) \cos 2\pi \frac{f\xi}{u_c}$$

Lateral: $$A_\eta = \exp(-|\eta|/L_\xi)$$

where ξ and η are streamwise and transverse coordinates, f is frequency and u_c is narrow band convection velocity. The present notation differs slightly from that of Reference 1 in that A_ξ here includes the cosine term. The notation L_ξ and L_η is introduced here, with these two quantities representing the exponential decay length scales of the correlation functions.

The quantities L_ξ, L_η and u_c are functions of frequency.

The program computes L_ξ, L_η, A_ξ and A_η for attached turbulent boundary layers and flare induced separated flows. Longitudinal quantities, L_ξ and A_ξ, are computed for protuberence induced separated flow.

4.0 COMPUTER CONFIGURATION

The required hardware is: XDS Sigma 5 Computer with 16K core, card reader, and line printer.

5.0 CALL SEQUENCES

This program is written as a subroutine, with four entry points. The entry names and call sequences are as follows:

Initial Entry: Initializes frequency range and computes decay length scales.

CALL CLENFR (FB, FE, ANN, DB, UL, IATT, ISEP, IPROT, IGNORE)

where

FB	=	Lower limit of frequency range of interest
FE	=	Upper limit of frequency range of interest
ANN	=	Number of frequency points per decade
DB	=	Local boundary layer thickness, feet
UL	=	Local velocity, feet second
IATT	=	$\begin{cases} 1 & \text{if computation desired for attached flow} \\ 0 & \text{if not desired} \end{cases}$
ISEP	=	$\begin{cases} 1 & \text{if computation desired for separated flow} \\ 0 & \text{if not desired} \end{cases}$
IPROT	=	$\begin{cases} 1 & \text{if computation desired for protuberance flow} \\ 0 & \text{if not desired} \end{cases}$
IGNORE	=	-1

An entry to CLENFR compures L_ξ and L_η for the desired frequency range and saves these for later printout. Storage is in a COMMON block described in Section 6.0. Any or all of the environments may be selected for computation. The first call to the routine, and any call with a change in FB, FE or ANN, must be to CLENFR. Each time CLENFR is called, the frequency range is printed out.

Subsequent Computation of L_ξ and L_η:

If it is desired to compute L_ξ and L_η for different flow conditions over the same

frequency range as before, this is accomplished by:

CALL CORLEN (DB, UL, IATT, ISEP, IPROT)

Computation of A_ξ and A_η :

A_ξ and A_η are computed as functions of distance for a specified frequency. The call is

CALL CORFUN (DB, UL, IATT, ISEP, IPROT, IGNORE,
IFREQ, XB, XE, DEL)

where

IGNORE	=	1 if previously computed values of L_ξ and L_η are to be used 0 if L_ξ and L_η are to be re-computed for the specified values of DB and UL
IFREQ	=	Index of the frequency for which A_ξ and A_η are to be computed
XB	=	Lower limit of separation distance range of interest
XE	=	Upper limit of separation distance range of interest
DEL	=	Increment between distance points to be computed

Longitudinal and lateral correlation function are computed for the specified separation distance range and the frequency corresponding to IFREQ. These values are saved for later printout.

Printout of Computed Values:

CALL CORPRT (TIT, ILEN, ICOR)

where

TIT	=	Name of a 20 element alphameric array containing a title to be printed out

$$\text{ILEN} = \begin{cases} 1 & \text{if } L_\xi \text{ and } L_\eta \text{ are to be printed} \\ 0 & \text{if not} \end{cases}$$

$$\text{ICOR} = \begin{cases} 1 & \text{if } A_\xi \text{ and } A_\eta \text{ are to be printed} \\ 0 & \text{if not} \end{cases}$$

A call to CORPRT with ILEN = 1 results in a printout of the last computed values of L_ξ and L_η for all three environments as a function of frequency. Strouhal number, $f\delta/u_\ell$, is also printed.

A call to CORPRT with ICOR = 1 results in a printout of the last computed values of A_ξ and A_η for all three environments.

The title TIT is printed above each table. Also printed are parameters of the frequency range.

A sample output is attached. The printout is sufficiently annotated so as to be self-explanatory.

6.0 STORAGE AND RETRIEVAL OF COMPUTED RESULTS

In the event that access is required to values computed by this subroutine, computed values are stored in a COMMON block designated COLD. To gain access, the following statement must be inserted into the main program or other subroutine:

```
COMMON /COLD/ F, ST, ATTLX, ATTLY, SEPLX, SEPLY, PROTLX,
UCATT, UCSEP, X, CORFAX, CORFAY, CORFSX, SORFSY, CORFPX
```

where each name is that of a 100 element one dimensional array. Each array contains the following:

F	=	Frequency
ST	=	Strouhal number, $f\delta/u_\ell$
ATTLX	=	L_ξ for attached flow
ATTLY	=	L_η for attached flow
SEPLX	=	L_ξ for separated flow
SEPLY	=	L_η for separated flow
PROTLX	=	L_x for protuberance flow
UCATT	=	Narrow band convection velocity for attached flow

UCSEP	=	Narrow band convection velocity for separated and protuberance flow
X	=	Distance coordinate for correlation function
CORFAX	=	A_ξ for attached flow
CORFAY	=	A_η for attached flow
CORFSX	=	A_ξ for separated flow
CORFSY	=	A_η for separated flow
CORFPX	=	A_ξ for protuberance flow

Different names may be used in the COMMON statement; however, the order must be preserved exactly and each array must be dimensioned exactly 100. The name COLD may not be used for any other purpose in the program.

Because of the dimension of 100, the frequency and distance parameters must be such that no more than 100 points are computed for each. If the frequency parameter (FB, FE, ANN) do not satisfy this restriction, CLENFR will substitute an acceptable value of ANN and proceed. If the distance parameters (XB, XE, DEL) do not satisfy this restriction, a message will be printed and the job terminated.

7.0 REFERENCES

1. Robertson, J. E., "Prediction of In-Flight Fluctuating Pressure Environments Including Protuberance Induced Flow," Wyle Laboratories Research Staff Report WR 71-10, March 1971.

```
INITIAL FREQUENCY =     0.10000E+01
  FINAL FREQUENCY =     0.10000E+05
POINTS PER DECADE =     0.10000E+02
```

PSC-049 SHUTTLE LAUNCH, DOF FAST, MAX Q, MACH NO. 1.33, NOMINAL DI = DINF

EXPONENTIAL DECAY SCALES OF CORRELATION FUNCTIONS

FREQUENCY	ATT BL, LONG.	ATT BL, LAT.	SEP FLOW LONG.	SEP FLOW LAT.	PROT FLOW LONG.	STROUHAL NO.
0.100000000E+01	0.369254780E+01	0.499020100E+00	0.111111104E+00	0.111111104E+00	0.872928619E+02	0.781372190E-03
0.125892448E+01	0.369061947E+01	0.498766601E+00	0.111111104E+00	0.111111104E+00	0.693392639E+02	0.983688515E-03
0.158489227E+01	0.368819904E+01	0.498448431E+00	0.111111104E+00	0.111111104E+00	0.550782125E+02	0.123839057E-02
0.199526119E+01	0.368515396E+01	0.498047829E+00	0.111111104E+00	0.111111104E+00	0.437501068E+02	0.155904144E-02
0.251188374E+01	0.368132591E+01	0.497544467E+00	0.111111104E+00	0.111111104E+00	0.347519531E+02	0.196271599E-02
0.316227341E+01	0.367651844E+01	0.496912062E+00	0.111111104E+00	0.111111104E+00	0.276044617E+02	0.247091241E-02
0.398106480E+01	0.367047977E+01	0.496117890E+00	0.111111104E+00	0.111111104E+00	0.219270020E+02	0.311069330E-02
0.501186562E+01	0.366290474E+01	0.495121360E+00	0.111111104E+00	0.111111104E+00	0.174172514E+02	0.391612947E-02
0.630956078E+01	0.365340519E+01	0.493871391E+00	0.111111104E+00	0.111111104E+00	0.138350220E+02	0.493011251E-02
0.794326782E+01	0.364150715E+01	0.492306292E+00	0.109988093E+00	0.109988093E+00	0.109895439E+02	0.620664656E-02
0.999998760E+01	0.362662792E+01	0.490347564E+00	0.102646828E+00	0.102646828E+00	0.872929859E+01	0.781371072E-02
0.125892162E+02	0.360804844E+01	0.487901747E+00	0.957956314E-01	0.957956314E-01	0.693394184E+01	0.983686000E-02
0.158488903E+02	0.358489132E+01	0.484852493E+00	0.894017220E-01	0.894017220E-01	0.550782204E+01	0.123838820E-01
0.199525299E+02	0.355611038E+01	0.481060803E+00	0.834345222E-01	0.834345222E-01	0.437502764E+01	0.155903511E-01
0.251187897E+02	0.352044773E+01	0.476361275E+00	0.778656602E-01	0.778656602E-01	0.347520256E+01	0.196271241E-01
0.316227112E+02	0.347643948E+01	0.470557809E+00	0.726683736E-01	0.726683736E-01	0.276044941E+01	0.247091055E-01
0.398105621E+02	0.342239571E+01	0.463425398E+00	0.678181052E-01	0.678181052E-01	0.219270704E+01	0.311068632E-01
0.501185913E+02	0.335642052E+01	0.454711616E+00	0.632915497E-01	0.632915497E-01	0.174172592E+01	0.391612723E-01
0.630954590E+02	0.327648067E+01	0.444142103E+00	0.590671636E-01	0.590671636E-01	0.138350391E+01	0.493010357E-01
0.794325256E+02	0.318048000E+01	0.431432128E+00	0.555555522E-01	0.551247299E-01	0.109895611E+01	0.620663650E-
0.999997253E+02	0.306642818E+01	0.416309059E+00	0.555555522E-01	0.514453799E-01	0.872931302E+00	0.781369805E-0
0.125892075E+03	0.293267155E+01	0.398540795E+00	0.555555522E-01	0.480116159E-01	0.693394721E+00	0.983685255E-01
0.158488800E+03	0.277816772E+01	0.377973080E+00	0.555555522E-01	0.448070392E-01	0.636021972E+00	0.123838723E+00
0.199525238E+03	0.260284328E+01	0.354577303E+00	0.555555522E-01	0.418163873E-01	0.578127801E+00	0.155903459E+00
0.251187683E+03	0.240789890E+01	0.328492165E+00	0.555555522E-01	0.390252955E-01	0.517142951E+00	0.196271062E+00
0.316226563E+03	0.219607735E+01	0.300063610E+00	0.555555522E-01	0.364205651E-01	0.456788778E+00	0.247090634E+00
0.398104980E+03	0.197172546E+01	0.269856215E+00	0.555555522E-01	0.339896455E-01	0.399386048E+00	0.311068118E+00
0.501185547E+03	0.174062729E+01	0.238635421E+00	0.555555522E-01	0.317209587E-01	0.346271694E+00	0.391612411E+00
0.630954102E+03	0.150958729E+01	0.207315385E+00	0.555555522E-01	0.296037570E-01	0.298112273E+00	0.493009984E+00
0.794324707E+03	0.128573227E+01	0.176866770E+00	0.555555522E-01	0.276278295E-01	0.255114734E+00	0.620663226E+00
0.999996338E+03	0.107576275E+01	0.148214459E+00	0.555555522E-01	0.257837461E-01	0.217193604E+00	0.781369328E+00
0.125891895E+04	0.885196626E+00	0.122132301E+00	0.555555522E-01	0.240628421E-01	0.184079766E+00	0.983684242E+00
0.158488574E+04	0.717811465E+00	0.991616249E-01	0.555555522E-01	0.224567503E-01	0.146875620E+00	0.123838520E+01
0.199524976E+04	0.575373590E+00	0.795692801E-01	0.555555522E-01	0.209578574E-01	0.116667569E+00	0.155903244E+01
0.251187524E+04	0.457652748E+00	0.633451939E-01	0.555555522E-01	0.195589960E-01	0.926721692E-01	0.196270943E+01
0.316226270E+04	0.362744570E+00	0.502443649E-01	0.555555522E-01	0.182535276E-01	0.736121535E-01	0.247090340E+01
0.398104883E+04	0.287584782E+00	0.398562886E-01	0.555555522E-01	0.170351824E-01	0.584722832E-01	0.311068058E+01
0.501184766E+04	0.228590131E+00	0.316942260E-01	0.555555522E-01	0.158981457E-01	0.464461595E-01	0.391611767E+01
0.630953125E+04	0.182265818E+00	0.252801068E-01	0.555555522E-01	0.148370378E-01	0.368935727E-01	0.493009186E+01
0.794323438E+04	0.145641744E+00	0.202059299E-01	0.555555522E-01	0.138467140E-01	0.293055773E-01	0.620662212E+01
0.999994922E+04	0.116451740E+00	0.161597319E-01	0.555555522E-01	0.129225217E-01	0.232782215E-01	0.781368160E+01

FSC-049 SHUTTLE LAUNCH, DOF FAST, MAX Q, MACH NO. 1.33, NOMINAL DI . DINF

EXPONENTIAL DECAY SCALES OF CORRELATION FUNCTIONS

FREQUENCY	ATT BL, LONG.	ATT BL, LAT.	SEP FLOW LONG.	SEP FLOW LAT.	PRST FLOW LONG.	STROUHAL NO.
0.100000000E+01	0.369254780E+01	0.499020100E+00	0.111111104E+00	0.111111104E+00	0.872928619E+02	0.781372190E-03
0.125892448E+01	0.369061947E+01	0.498766601E+00	0.111111104E+00	0.111111104E+00	0.693392639E+02	0.983688515E-03
0.158489227E+01	0.368819904E+01	0.498448431E+00	0.111111104E+00	0.111111104E+00	0.550781250E+02	0.123839057E-02
0.199526119E+01	0.368515396E+01	0.498047829E+00	0.111111104E+00	0.111111104E+00	0.437501068E+02	0.155904146E-02
0.251188374E+01	0.368132591E+01	0.497544467E+00	0.111111104E+00	0.111111104E+00	0.347519531E+02	0.196271599E-02
0.316227341E+01	0.367651844E+01	0.496912062E+00	0.111111104E+00	0.111111104E+00	0.276044617E+02	0.247091241E-02
0.398106480E+01	0.367047977E+01	0.496117890E+00	0.111111104E+00	0.111111104E+00	0.219270020E+02	0.311069330E-02
0.501186562E+01	0.366290474E+01	0.495121360E+00	0.111111104E+00	0.111111104E+00	0.174172516E+02	0.391612947E-02
0.630956078E+01	0.365340519E+01	0.493871391E+00	0.111111104E+00	0.111111104E+00	0.138350220E+02	0.493011251E-02
0.794326782E+01	0.364150715E+01	0.492306292E+00	0.109988093E+00	0.109988093E+00	0.109895439E+02	0.620664356E-02
0.999998760E+01	0.362662792E+01	0.490347564E+00	0.102646828E+00	0.102646828E+00	0.872929859E+01	0.781371027E-02
0.125892162E+02	0.360804844E+01	0.487901747E+00	0.957956314E-01	0.957956314E-01	0.693394184E+01	0.983686000E-02
0.158488903E+02	0.358489132E+01	0.484852493E+00	0.894017220E-01	0.894017220E-01	0.550782204E+01	0.123838820E-01
0.199525299E+02	0.355611038E+01	0.481060803E+00	0.834345222E-01	0.834345222E-01	0.437502766E+01	0.155903511E-01
0.251187897E+02	0.352044773E+01	0.476361275E+00	0.778656602E-01	0.778656602E-01	0.347520256E+01	0.196271241E-01
0.316227112E+02	0.347643948E+01	0.470557809E+00	0.726683736E-01	0.726683736E-01	0.276044941E+01	0.247091055E-01
0.398105621E+02	0.342239571E+01	0.463425398E+00	0.678181052E-01	0.678181052E-01	0.219270704E+01	0.311068632E-01
0.501185913E+02	0.335642052E+01	0.454711616E+00	0.632915497E-01	0.632915497E-01	0.174172592E+01	0.391612723E-01
0.630954590E+02	0.327648067E+01	0.444142103E+00	0.590671636E-01	0.590671636E-01	0.138350391E+01	0.493010357E-01
0.794325256E+02	0.318048000E+01	0.431432128E+00	0.555555522E-01	0.551247299E-01	0.109895611E+01	0.620663650E-01
0.999997253E+02	0.306642818E+01	0.416309059E+00	0.555555522E-01	0.514453799E-01	0.872931302E+00	0.781369805E-01
0.125892075E+03	0.293267155E+01	0.398540795E+00	0.555555522E-01	0.480116159E-01	0.693394721E+00	0.983685255E-01
0.158488800E+03	0.277816772E+01	0.377973080E+00	0.555555522E-01	0.448070392E-01	0.636021972E+00	0.123838723E+00
0.199525238E+03	0.260284328E+01	0.354577303E+00	0.555555522E-01	0.418163873E-01	0.578127801E+00	0.155903459E+00
0.251187683E+03	0.240789890E+01	0.328492165E+00	0.555555522E-01	0.390252955E-01	0.517142951E+00	0.196271062E+00
0.316226563E+03	0.219607735E+01	0.300043610E+00	0.555555522E-01	0.364205451E-01	0.456728778E+00	0.247090638E+00
0.398104980E+03	0.197172546E+01	0.269856215E+00	0.555555522E-01	0.339896455E-01	0.399386048E+00	0.311068118E+00
0.501185547E+03	0.174062729E+01	0.238635421E+00	0.555555522E-01	0.317209587E-01	0.346271694E+00	0.391612411E+00
0.630954102E+03	0.150958729E+01	0.207315385E+00	0.555555522E-01	0.296037570E-01	0.298112273E+00	0.493009984E+00
0.794324707E+03	0.128573227E+01	0.176866770E+00	0.555555522E-01	0.276278295E-01	0.255114734E+00	0.620663226E+00
0.999996338E+03	0.107576275E+01	0.148214459E+00	0.555555522E-01	0.257837661E-01	0.217193604E+00	0.781369328E+00
0.125891895E+04	0.885196626E+00	0.122132301E+00	0.555555522E-01	0.240628421E-01	0.184079766E+00	0.983684242E+00
0.158488574E+04	0.717811465E+00	0.991616249E-01	0.555555522E-01	0.224567503E-01	0.146875620E+00	0.123838520E+01
0.199524976E+04	0.575373590E+00	0.795692801E-01	0.555555522E-01	0.209578574E-01	0.116667569E+00	0.155903244E+01
0.251187524E+04	0.457652748E+00	0.633451939E-01	0.555555522E-01	0.195589960E-01	0.926721692E-01	0.196270943E+01
0.316226270E+04	0.362744570E+00	0.502443649E-01	0.555555522E-01	0.182535276E-01	0.736121535E-01	0.247090340E+01
0.398104883E+04	0.287544782E+00	0.398642886E-01	0.555555522E-01	0.170351826E-01	0.584722832E-01	0.311068058E+01
0.501184766E+04	0.228590131E+00	0.316942260E-01	0.555555522E-01	0.158981457E-01	0.464461595E-01	0.391611767E+01
0.630953125E+04	0.182265818E+00	0.252801068E-01	0.555555522E-01	0.148370378E-01	0.368935727E-01	0.493009186E+01
0.794323438E+04	0.145641744E+00	0.202059299E-01	0.555555522E-01	0.138467140E-01	0.293055773E-01	0.620662212E+01
0.999994922E+04	0.116451740E+00	0.161597319E-01	0.555555522E-01	0.129225217E-01	0.232782215E-01	0.781368160E+01

MSC-049 SHUTTLE LAUNCH, DOF FAST, MAX Q, MACH 1.8, 1.33, ORIGINAL WT, DINF

CORRELATION FUNCTIONS AT F= 0.251187683E+03 HZ

	ATT BL, LONG.	ATT BL LAT.	SEP FLOW LONG.	SEP FLOW LAT.	PART FLOW LONG.
0.000000000E+00	0.100000000E+01	0.100000000E+01	0.100000000E+01	0.100000000E+01	0.100000000E+01
0.199999988E+00	0.881852567E+00	0.543980360E+00	0.232587233E-01	0.594693422E-02	0.574210831E+00
0.399999976E+00	0.708382964E+00	0.295914531E+00	0.335348072E-03	0.353660143E-04	0.207251310E+00
0.599999964E+00	0.502497017E+00	0.160971820E+00	-0.176511458E-05	0.210320309E-06	-0.271190703E-01
0.799999952E+00	0.286296844E+00	0.875654221E-01	-0.332476986E-06	0.125078103E-08	-0.126987755E+00
0.999999940E+00	0.793553591E-01	0.476338603E-01	-0.141482204E-07	0.743826962E-11	-0.134338737E+00
0.119999981E+01	-0.102517545E+00	0.259118900E-01	-0.409916101E-09	0.442351098E-13	-0.967594385E-01
0.139999962E+01	-0.248020649E+00	0.140955746E-01	-0.850545155E-11	0.263064505E-15	-0.499102920E-01
0.159999943E+01	-0.350608706E+00	0.766771659E-02	-0.896083338E-13	0.156443594E-17	-0.130720921E-01
0.179999924E+01	-0.408310890E+00	0.417108834E-02	0.218167100E-14	0.930364285E-20	0.791197270E-02
0.199999905E+01	-0.423193574E+00	0.226899073E-02	0.168385372E-15	0.553278387E-22	0.151811130E-01
0.219999981E+01	-0.400571465E+00	0.123428344E-02	0.620402582E-17	0.329029249E-24	0.139051452E-01
0.239999962E+01	-0.348048476E+00	0.671426067E-03	0.162883650E-18	0.195672518E-26	0.905578306E-02
0.259999943E+01	-0.274629056E+00	0.365242595E-03	0.294500936E-20	0.116364499E-28	0.407930836E-02
0.279999924E+01	-0.189568758E+00	0.198685069E-03	0.153880383E-22	0.692015405E-31	0.529885758E-03
0.299999905E+01	-0.101748347E+00	0.108080800E-03	-0.148289442E-23	0.411539103E-33	-0.126944249E-02
0.319999981E+01	-0.188993029E-01	0.587936956E-04	-0.804682990E-25	0.244732988E-35	-0.171250128E-02
0.339999962E+01	0.528424121E-01	0.319825776E-04	-0.263611199E-26	0.145543371E-37	-0.139464624E-02
0.359999943E+01	0.109204113E+00	0.173979060E-04	-0.625473675E-28	0.865541227E-40	-0.822645845E-03
0.379999924E+01	0.147850096E+00	0.946420732E-05	-0.941449788E-30	0.514734156E-42	-0.307828654E-03
0.399999905E+01	0.168273985E+00	0.514834665E-05	0.290250622E-32	0.306110406E-44	0.235928164E-04
0.419999886E+01	0.171564937E+00	0.280060158E-05	0.837913495E-33	0.182040960E-46	0.169316685E-03
0.439999962E+01	0.160070896E+00	0.152345729E-05	0.368099398E-34	0.108257941E-48	0.184915523E-03
0.459999943E+01	0.137011826E+00	0.828732027E-06	0.108674037E-35	0.643806038E-51	0.135716778E-03
0.479999924E+01	0.106077313E+00	0.450814355E-06	0.230708658E-37	0.382865041E-53	0.716252107E-04
0.499999905E+01	0.710474849E-01	0.245234389E-06	0.261834895E-39	0.227688509E-55	0.202084630E-04
0.519999886E+01	0.354653820E-01	0.133402807E-06	-0.504442883E-41	0.135405543E-57	-0.967868527E-05
0.539999962E+01	0.237696408E-02	0.725693212E-07	-0.430129735E-42	0.805234234E-60	-0.205168617E-04
0.559999943E+01	-0.258449353E-01	0.394763404E-07	-0.162425381E-43	0.478870105E-62	-0.192603766E-04
0.579999924E+01	-0.475956462E-01	0.214743707E-07	-0.434438025E-45	0.284782362E-64	-0.128066858E-04
0.599999905E+01	-0.620556474E-01	0.116816459E-07	-0.808229954E-47	0.169359063E-66	-0.593305696E-05
0.619999886E+01	-0.691371560E-01	0.635458974E-08	-0.516198076E-49	0.100717209E-68	-0.940426673E-06
0.639999962E+01	-0.693796873E-01	0.345670337E-08	0.363276444E-50	0.598936263E-71	0.164534604E-05
0.659999943E+01	-0.638099313E-01	0.188038074E-08	0.207526189E-51	0.356192700E-73	0.233663195E-05
0.679999924E+01	-0.537811443E-01	0.102290199E-08	0.694151778E-53	0.211824251E-75	0.194296081E-05
0.699999905E+01	-0.408106633E-01	0.556438895E-09	0.167962177E-54	0.125971132E-77	0.114876618E-05
0.719999886E+01	-0.264281556E-01	0.302692094E-09	0.263076999E-56	0.000000000E+00	0.455089662E-06
0.739999866E+01	-0.120472014E-01	0.164658773E-09	-0.302411874E-59	0.000000000E+00	-0.130051312E-07
0.759999943E+01	0.113555463E-02	0.895712116E-10	-0.210469200E-59	0.000000000E+00	-0.225014844E-06
0.779999924E+01	0.122060925E-01	0.487250240E-10	-0.956467767E-61	0.000000000E+00	-0.254211386E-06
0.799999905E+01	0.205661319E-01	0.265054784E-10	-0.287796146E-62	0.000000000E+00	-0.190152718E-06
0.819999886E+01	0.259346925E-01	0.144181715E-10	-0.624662192E-64	0.000000000E+00	-0.102604076E-06
0.839999866E+01	0.283228159E-01	0.784320872E-11	-0.757104577E-66	0.000000000E+00	-0.309155759E-07
0.859999943E+01	0.279878415E-01	0.426655499E-11	0.114184220E-67	0.000000000E+00	0.115912364E-07
0.879999924E+01	0.253744349E-01	0.232092384E-11	0.109637141E-68	0.000000000E+00	0.276686514E-07
0.899999905E+01	0.210448178E-01	0.126255170E-11	0.424758896E-70	0.000000000E+00	0.266480562E-07
0.919999886E+01	0.156331658E-01	0.686803912E-12	0.115735346E-71	0.000000000E+00	0.180503661E-07
0.939999866E+01	0.974517316E-02	0.373608208E-12	0.221247759E-73	0.000000000E+00	0.857830074E-08
0.959999943E+01	0.394712389E-02	0.203235757E-12	0.165109269E-75	0.000000000E+00	0.159146163E-08

0.979999924E+01	-0.129206106E-02	0.110556367E+12	-0.883698095E-77	0.000000000E+00	-0.211755813E-08
0.999999905E+01	-0.562178716E-02	0.601392308E+13	0.000000000E+00	0.000000000E+00	-0.318310334E-08

MSC-049 SHUTTLE LAUNCH, DUF EAST, MAX Q, MACH NO. 1.33, NOMINAL UL = UINF

EXPONENTIAL DECAY SCALES OF CORRELATION FUNCTIONS

FREQUENCY	ATT BL, LONG.	ATT BL, LAT.	SEP FLOW LONG.	SEP FLOW LAT.	PROT FLOW LONG.	STROUHAL NO.
0.100000000E+01	0.369254780E+01	0.499020100E+00	0.1111 1104E+00	0.111111104E+00	0.872928619E+02	0.781372190E-03
0.125892448E+01	0.369061947E+01	0.498766601E+00	0.111111104E+00	0.111111104E+00	0.693392639E+02	0.983688515E-03
0.158489227E+01	0.368819904E+01	0.498448431E+00	0.111111104E+00	0.111111104E+00	0.550782150E+02	0.123839057E-02
0.199526119E+01	0.368515396E+01	0.498047829E+00	0.111111104E+00	0.111111104E+00	0.437501068E+02	0.155904144E-02
0.251188374E+01	0.368132591E+01	0.497544467E+00	0.111111104E+00	0.111111104E+00	0.347519531E+02	0.196271599E-02
0.316227341E+01	0.367651844E+01	0.496912062E+00	0.111111104E+00	0.111111104E+00	0.276044617E+02	0.247091241E-02
0.398106480E+01	0.367047977E+01	0.496117890E+00	0.111111104E+00	0.111111104E+00	0.219270020E+02	0.311069330E-02
0.501186562E+01	0.366290474E+01	0.495121360E+00	0.111111104E+00	0.111111104E+00	0.174172516E+02	0.391612947E-02
0.630956078E+01	0.365340519E+01	0.493871391E+00	0.111111104E+00	0.111111104E+00	0.138350220E+02	0.493011251E-02
0.794326782E+01	0.364150715E+01	0.492306292E+00	0.109988093E+00	0.109988093E+00	0.109898439E+02	0.620664656E-02
0.999998760E+01	0.362662792E+01	0.490347564E+00	0.102646828E+00	0.102646828E+00	0.872929859E+01	0.781371072E-02
0.125892162E+02	0.360804844E+01	0.487901747E+00	0.957956314E-01	0.957956314E-01	0.693394184E+01	0.983686000E-02
0.158488903E+02	0.358489132E+01	0.484852493E+00	0.894017220E-01	0.894017220E-01	0.550782204E+01	0.123838420E-01
0.199525299E+02	0.355611038E+01	0.481060803E+00	0.834345222E-01	0.834345222E-01	0.437502766E+01	0.155903511E-01
0.251187897E+02	0.352044773E+01	0.476361275E+00	0.778656602E-01	0.778656602E-01	0.347520256E+01	0.196271241E-01
0.316227112E+02	0.347643948E+01	0.470557809E+00	0.726683736E-01	0.726683736E-01	0.276044941E+01	0.247091055E-01
0.398105621E+02	0.342239571E+01	0.463425398E+00	0.678181052E-01	0.678181052E-01	0.219270706E+01	0.311068632E-01
0.501185913E+02	0.335642052E+01	0.454711616E+00	0.632915497E-01	0.632915497E-01	0.174172592E+01	0.391612723E-01
0.630954590E+02	0.327648067E+01	0.444142103E+00	0.590671636E-01	0.590671636E-01	0.138350391E+01	0.493010357E-01
0.794325256E+02	0.318048000E+01	0.431432128E+00	0.555555522E-01	0.551247299E-01	0.109895611E+01	0.620663650E-01
0.999997253E+02	0.306642818E+01	0.416309059E+00	0.555555522E-01	0.514453799E-01	0.872931302E+00	0.781369805E-01
0.125892075E+03	0.293267155E+01	0.398540795E+00	0.555555522E-01	0.480116159E-01	0.693394721E+00	0.983685255E-01
0.158488800E+03	0.277816772E+01	0.377973050E+00	0.555555522E-01	0.448070392E-01	0.636021972E+00	0.123838723E+00
0.199525238E+03	0.260284328E+01	0.354577303E+00	0.555555522E-01	0.418163873E-01	0.578127801E+00	0.155903459E+00
0.251187683E+03	0.240789890E+01	0.328492165E+00	0.555555522E-01	0.390252955E-01	0.517142951E+00	0.196271062E+00
0.316226563E+03	0.219607735E+01	0.300063610E+00	0.555555522E-01	0.364205651E-01	0.456788778E+00	0.247090638E+00
0.398104980E+03	0.197172546E+01	0.269856215E+00	0.555555522E-01	0.339896455E-01	0.399386048E+00	0.311068118E+00
0.501185547E+03	0.174062729E+01	0.238635421E+00	0.555555522E-01	0.317209587E-01	0.346271694E+00	0.391612411E+00
0.630954102E+03	0.150958729E+01	0.207315385E+00	0.555555522E-01	0.296037570E-01	0.298112273E+00	0.493009984E+00
0.794324707E+03	0.128573227E+01	0.176866770E+00	0.555555522E-01	0.276278295E-01	0.255114734E+00	0.620663226E+00
0.999996338E+03	0.107576275E+01	0.148214459E+00	0.555555522E-01	0.257837461E-01	0.217193604E+00	0.781369325E+00
0.125891895E+04	0.885196626E+00	0.122132301E+00	0.555555522E-01	0.240628421E-01	0.184079766E+00	0.983584242E+00
0.158488574E+04	0.717811465E+00	0.991616249E-01	0.555555522E-01	0.224567603E-01	0.146875620E+00	0.123838520E+01
0.199524976E+04	0.575373590E+00	0.795692801E-01	0.555555522E-01	0.209578574E-01	0.116667569E+00	0.1[illegible]903244E+01
0.251187524E+04	0.457652748E+00	0.633451939E-01	0.555555522E-01	0.195589960E-01	0.926721692E-01	0.196270343E+01
0.316226270E+04	0.362744570E+00	0.502443649E-01	0.555555522E-01	0.182535276E-01	0.736121535E-01	0.247090340E+01
0.398104883E+04	0.287584782E+00	0.398562886E-01	0.555555522E-01	0.170351826E-01	0.584722832E-01	0.311068055E+01
0.501184766E+04	0.228590131E+00	0.316942260E-01	0.555555522E-01	0.158981457E-01	0.464461595E-01	0.391611767E+01
0.630953125E+04	0.182265818E+00	0.252801068E-01	0.555555522E-01	0.148370378E-01	0.368935727E-01	0.493009186E+01
0.794323438E+04	0.145641744E+00	0.202059299E-01	0.555555522E-01	0.138467140E-01	0.293055773E-01	0.620662212E+01
0.999994922E+04	0.116451740E+00	0.161597319E-01	0.555555522E-01	0.129225217E-01	0.232782215E-01	0.781368160E+01

MSC-049 SHUTTLE LAUNCH, DUE EAST, MAX Q, MACH NO. 1.33, NOMINAL UL = UINF

CORRELATION FUNCTIONS AT F= 0.251187683E+03 HZ

X	ATT BL, LONG.	ATT BL LAT.	SFP FLOW LONG.	SFP FLOW LAT.	PROT FLOW LONG.
0.000000000E+00	0.100000000E+01	0.100000000E+01	0.100000000E+01	0.100000000E+01	0.100000000E+01
0.199999988E+00	0.881852567E+00	0.543980360E+00	0.232587233E-01	0.594693422E+02	0.578210831E+00
0.399999976E+00	0.708382964E+00	0.295914531E+00	0.335348072E-03	0.353660143E+04	0.207251310E+00
0.599999964E+00	0.502497017E+00	0.160971820E+00	-0.176511458E-05	0.210320309E+06	-0.271190703E-01
0.799999952E+00	0.286296844E+00	0.875654221E-01	-0.332476986E-06	0.125078103E+08	-0.126987755E+00
0.999999940E+00	0.793553591E-01	0.476338603E-01	-0.141482204E-07	0.743826962E+11	-0.134338737E+00
0.119999981E+01	-0.102517545E+00	0.259118900E-01	-0.409916101E-09	0.442351098E+13	-0.967594385E-01
0.139999962E+01	-0.248020649E+00	0.140955746E-01	-0.850545155E-11	0.263064505E+15	-0.499102920E-01
0.159999943E+01	-0.350608706E+00	0.766771659E-02	-0.896083338E-13	0.156443594E+17	-0.130720921E-01
0.179999924E+01	-0.408310890E+00	0.417108834E-02	0.218167100E-14	0.930364285E+20	0.791197270E-02
0.199999905E+01	-0.423193574E+00	0.226899073E-02	0.168385372E-15	0.553278387E+22	0.151811130E-01
0.219999981E+01	-0.400571465E+00	0.123428344E-02	0.620402582E-17	0.329029249E+24	0.139051452E-01
0.239999962E+01	-0.348068476E+00	0.671426067E-03	0.162883650E-18	0.195672518E+26	0.907557830E-02
0.259999943E+01	-0.274629056E+00	0.365242595E-03	0.294500936E-20	0.116364499E+28	0.407930836E-02
0.279999924E+01	-0.189568758E+00	0.198685069E-03	0.153880383E-22	0.692015405E+31	0.529885758E-03
0.299999905E+01	-0.101748347E+00	0.108080800E-03	-0.148289442E-23	0.411539103E+33	-0.126944249E-02
0.319999981E+01	-0.183993029E-01	0.587936956E-04	-0.804682990E-25	0.244732988E+35	-0.171250128E-02
0.339999962E+01	0.528424121E-01	0.319825776E-04	-0.263611199E-26	0.145543371E+37	-0.139464624E-02
0.359999943E+01	0.109204113E+00	0.173979060E-04	-0.625473675E-28	0.865541227E+40	-0.822645845E-03
0.379999924E+01	0.147850096E+00	0.946420732E-05	-0.941469788E-30	0.514734156E+42	-0.307828654E-03
0.399999905E+01	0.168273985E+00	0.514834665E-05	0.290250622E-32	0.306110406E+44	0.235928164E-04
0.419999886E+01	0.171564937E+00	0.280060158E-05	0.837913495E-33	0.182040960E+46	0.169316685E-03
0.439999962E+01	0.160070896E+00	0.152345729E-05	0.368099398E-34	0.108257941E+48	0.184915523E-03
0.459999943E+01	0.137011826E+00	0.828732027E-06	0.108674037E-35	0.643806038E+51	0.135716778E-03
0.479999924E+01	0.106077313E+00	0.450814355E-06	0.230708658E-37	0.382865041E+53	0.716252107E-04
0.499999905E+01	0.710474849E-01	0.245234389E-06	0.261834895E-39	0.227688509E+55	0.202084630E-04
0.519999886E+01	0.354653820E-01	0.133402807E-06	-0.504442883E-41	0.135405543E+57	-0.967848527E-05
0.539999962E+01	0.237696408E-02	0.725693212E-07	-0.430129735E-42	0.805234234E+60	-0.205168617E-04
0.559999943E+01	-0.258449353E-01	0.394763404E-07	-0.162425381E-43	0.478870105E+62	-0.192603766E-04
0.579999924E+01	-0.475956462E-01	0.214743707E-07	-0.434438025E-45	0.284782362E+64	-0.128066858E-04
0.599999905E+01	-0.620556474E-01	0.116816459E-07	-0.808229954E-47	0.169359063E+66	-0.592305696E-05
0.619999886E+01	-0.691371560E-01	0.635458974E-08	-0.516198076E-49	0.100717209E+68	-0.940426673E-06
0.639999962E+01	-0.693796873E-01	0.345670337E-08	0.363276444E-50	0.598936263E+71	0.164534504E-05
0.659999943E+01	-0.638099313E-01	0.188038074E-08	0.207526189E-51	0.356192700E+73	0.233663195E-05
0.679999924E+01	-0.537811443E-01	0.102290199E-08	0.694151778E-53	0.211824251E+75	0.194296081E-05
0.699999905E+01	-0.408106633E-01	0.556438895E-09	0.147962177E-54	0.125971132E+77	0.116876618E-05
0.719999886E+01	-0.264281556E-01	0.302692094E-09	0.263076999E-56	0.000000000E+00	0.455089662E-06
0.739999866E+01	-0.120472014E-01	0.164658773E-09	-0.302411874E-59	0.000000000E+00	-0.130051312E-07
0.759999943E+01	0.113595463E-02	0.895712116E-10	-0.210469200E-59	0.000000000E+00	-0.225014844E-06
0.779999924E+01	0.122060925E-01	0.487250240E-10	-0.956467767E-61	0.000000000E+00	-0.254211386E-06
0.799999905E+01	0.205661319E-01	0.265054784E-10	-0.287796146E-62	0.000000000E+00	-0.190152718E-06
0.819999886E+01	0.259346925E-01	0.144181715E-10	-0.624662192E-64	0.000000000E+00	-0.102604076E-06
0.839999866E+01	0.283228159E-01	0.784320872E-11	-0.757104577E-66	0.000000000E+00	-0.309155759E-07
0.859999943E+01	0.279878415E-01	0.426655499E-11	0.114184220E-67	0.000000000E+00	0.115912364E-07
0.879999924E+01	0.253744349E-01	0.232092384E-11	0.109637141E-68	0.000000000E+00	0.276686514E-07
0.899999905E+01	0.210488178E-01	0.126255170E-11	0.424758896E-70	0.000000000E+00	0.266480562E-07
0.919999886E+01	0.156331658E-01	0.686803912E-12	0.115735346E-71	0.000000000E+00	0.180503861E-07
0.939999866E+01	0.974517316E-02	0.373608208E-12	0.221247759E-73	0.000000000E+00	0.857830074E-08
0.959999943E+01	0.394712389E-02	0.203235757E-12	0.165109269E-75	0.000000000E+00	0.159146163E-08
0.979999924E+01	-0.129206106E-02	0.110556367E-12	-0.883698095E-77	0.000000000E+00	-0.211765513E-08
0.999999905E+01	-0.562178716E-02	0.601392308E-13	0.000000000E+00	0.000000000E+00	-0.318310334E-08

WYLE LABORATORIES

COMPUTER PROGRAM DESCRIPTION

Program Number:	73/005P-1
Author:	K. Plotkin
Date:	May 1973
Source Language:	Fortran IV-H

1.0 PROGRAM TITLE

Transonic Flow

2.0 PURPOSE

To compute fluctuating pressure environments on the cylindrical portion of a cone cylinder at transonic Mach numbers $0.6 \leq M_\infty \leq 0.98$.

3.0 METHOD

The program uses the prediction schemes presented in Reference 1 thru 3 for overall fluctuating pressure levels and terminal shock wave oscillation. There are three basic cases, as a function of Mach number and cone angle. For $M < .6$, attached flow fluctuating pressure level is computed from Equation 1 of Reference 1. For $6 \leq M \leq M_a$ (M_a = attachment Mach number), overall level is computed from Steven's prediction scheme (Reference 2) as cited in Reference 3. For attached flow and shock wave oscillation, overall level and shock location (relative to cylinder diameter) are computed from data presented in Figures 13 thru 16 of Reference 3.

4.0 COMPUTER CONFIGURATION

The required hardware is: XDS Sigma 5 Computer with 16 K core.

5.0 CALL SEQUENCE

The program is entered by a call:

```
CALL TRANS (THETA, EMINF, XOVERD, CP, NTYPE)
```

where

THETA	=	Cone half angle
EMINF	=	Free stream Mach number
XOVERD	=	Shock wave location divided by cylinder diameter

CP = Fluctuating pressure coefficient, $\sqrt{p^2}/q_\infty$

NTYPE = Signal parameter to indicate type of flow present

The program is entered with values of THETA and EMINF. Values of XOVERD, CP and NTYPE are returned. NTYPE may attain the following values:

0 : $M_\infty < 0.6$ attached flow exists and has been computed. XOVERD is set equal to 0.

1 : $0.6 < M_\infty < M_a$. Separated flow exists and has been computed. XOVERD is set equal to 0.

2 : $M_a < M_\infty < 0.98$. Attached flow and shock oscillation exists and has been computed.

3 : An unacceptably high value of M_∞ (>0.98) has been specified.

6.0 INPUT AND OUTPUT

This subroutine contains no READ or WRITE statements; values returned are to be handled by a main program provided by the user.

7.0 REFERENCES

1. Robertson, J. E., "Prediction of In-Flight Fluctuating Pressure Environments Including Protuberance Induced Flow," Wyle Laboratories Research Staff Report WR 71-10 , March 1971.

2. Himelblow, Harry, "Aeroacoustic, Vibration and Shock Environments for the Space Shuttle Orbiter," Paper presented at Space Shuttle Dynamics and Aeroelasticity Technology Working Group Meeting, Ames Research Center, Moffet Field, California, November 8-9, 1971.

3. Robertson, J. E., "Preliminary Estimates of Space Shuttle Fluctuating Pressure Environments," Wyle Laboratories Research Staff Report WR 72-10, August 1972.

WYLE LABORATORIES

COMPUTER PROGRAM DESCRIPTION

Program Number:	71/004S-1
Author:	D.M. Lister
Date:	July 1971
Source Language:	FORTRAN IV-H
Computer:	XDS Sigma 5

1.0 PROGRAM TITLE

Power Spectral Density.

2.0 PURPOSE

Given the local velocity, the free-stream dynamic pressure, the local boundary layer thickness and the frequency range of interest, the program prints and plots, the pressure spectral density, the normalized pressure spectral density and the fluctuating pressure level.

3.0 METHOD

The method employed is given in Section 3.2.2.4, page 31 of Reference 1.

4.0 COMPUTER CONFIGURATION

The required hardware is: XDS Sigma 5 computer with 16 K core, card reader, line printer and calcomp plotter.

5.0 PUNCHED CARD INPUT

This is best illustrated in tabular form as shown on the following page.

Note	Card #	Variable	Fortran Symbol	Description	Format	Columns
1,5	1	f_b	FB	Initial frequency of interest	F10.0	1-10
1	1	f_e	FE	Final frequency of interest	F10.0	11-20
2	1	npd	ANN	Number of frequency pts/decade	F10.0	21-30
3	1		XDECADE	Length in inches of decade of n axis	F10.0	31-40
3	1		YDECADE	Length in inches of decade of y axis	F10.0	41-50
3	1		YTDB	Length in inches of 10 dB on y axis	F10.0	51-60
4,5	2	Title	TI(I), I=1, 20	A Title card	20A4	1-80
5,6	3		IA	Zone parameters	I 1	5
6	3		IB		I 1	10
6	3		IC		I 1	15
6	3		ID		I 1	20
7	3		IP1	Plot parameters	I 1	25
7	3		IP2		I 1	30
7	3		IP3		I 1	35
8	4	q_∞	QS	Free-stream dynamic pressure	F10.0	1-10
	4	δ_ℓ	DB	Local boundary layer thickness	F10.0	11-20
	4	U	[illegible]	Local velocity	F10.0	21-30
9	5	$(P^2/q_\infty^2)_A$	QSA	Normalized mean square FPL Attached Flow	F10.0	1-10
	5	$(f_0\delta_\ell/U_\ell)_A$	FDUA	Normalized characteristic frequency Attached Flow	F10.0	11-20
9	6	$(P^2/q_\infty^2)_B$	PQSB	Normalized mean square FPL Separated Flow	F10.0	1-10
	6	$(f_0\delta_\ell/U_\ell)_B$	FDUB	Normalized characteristic frequency Separated Flow	F10.0	11-20
9	7	$(P^2/q_\infty^2)_T$	PQST	Normalized total mean square FPL Shock Oscillation	F10.0	1-10
	7	$(f_0\delta_\ell/U_\ell)_C$	FDUT	Normalized characteristic frequency Shock Oscillation	F10.0	11-20
	7	$(P^2/q_\infty^2)_B$	PQSB	Normalized mean square FPL Separated Flow	F10.0	21-30

Note	Card #	Variable	Fortran Symbol	Description	Format	Column
9	8	$(P^2/q_\infty^2)_T$	PQST	Normalized total mean square FPL Shock Oscillation	F10.0	1-10
9	8	$(f_0\delta_\ell/U_\ell)_C$	FDUT	Normalized characteristic frequency Shock Oscillation	F10.0	11-20
9	8	$(P^2/q_\infty^2)_A$	PQSA	Normalized mean square FPL Attached Flow	F10.0	21-30

NOTES:

1 The various output quantities are computed for values of frequency lying between f_b and f_e. The ith frequency point from f_b is given by the formula:

$$\log(f_i) = \log(f_b) + \frac{i}{npd}\log(10)$$

2 For third octave band frequencies, input npd = 10.

3 XDECADE is used by all three plots. It is suggested that XDECADE is selected such that XDECADE multiplied by the number of x decades is less than ten. (e.g., for frequency range 1 Hz to 10^4 Hz then XDECADE is best chosen to be two.)

4 The program inputs this card and prints its contents prior to the main output table. (i.e., a title card.)

5 At the end of processing the program returns to read a new title card and a new parameter card. If the sum of the zone parameters is zero a new card type one is read. If FE is not greater than FB then the program stops.

6 The zone parameters must be equal to zero or one. A one indicates that the structure is subjected to the indicated flow condition (see Reference 1, page 32). Possible combinations of the four zone parameters are: (1,0,0,0), (1,0,0,1), (0,1,0,0), (0,1,1,0), (0,0,1,0) and (0,0,0,1).

7 The plot parameters must be zero or unity. A unity indicates that a particular plot is required. IP1 = 1 then a plot of normalized pressure spectral density against frequency (log/log) is obtained. IP2 = 1 then a plot of pressure spectral density against frequency (log/log) is obtained. IP3 = 1 then a plot of fluctuating pressure level (dB; re: 0.0002 dynes/cm^2) against frequency (lin./log) is obtained.

8 Units of these variables must be consistent. Note FPL is referenced assuming ft. lb. sec units and P_{ref} equal 0.0002 dynes/cm^2.

9 If IA = 0 then no card type five required.

If IB = 0 then no card type six required.

If IC = 0 then no card type seven required.

If ID = 0 then no card type eight required.

6.0 OUTPUT

The line printer output is adequately annotated.

7.0 STORAGE

Just over a quarter of the available core is used.

8.0 REFERENCE

Robertson, J.E., "Prediction of In-Flight Fluctuating Pressure Environments Including Protuberance Induced Flow," NASA CR 119,947, March 1971 (N71-26677).

TYPICAL COMPUTER PRINT-OUT

```
INITIAL FREQUENCY =     0.10000E+01
  FINAL FREQUENCY =     0.10000E+05
 POINTS PER DECADE =    0.10000E+02


MSC-040 SHUTTLE LAUNCH, MACH NO. 0.86, TRANS. SHOCK BSC. H/O TANK

IA = 0     IB = 1     IC = 1     ID = 0

              DYNAMIC PRESSURE =     0.39500E+03
     BOUNDARY LAYER THICKNESS =     0.10000E+01
        LOCAL STREAM VELOCITY =     0.14600E+04

                   P.P/Q.Q  B =     0.40000E-03
            STROUHAL NUMBER B =     0.17000E+00
   CHARACTERISTIC FREQUENCY B =     0.24820E+03
OVERALL FLUCTUATING PRESSURE LEVEL =  0.14553E+03

                   P.P/Q.Q  T =     0.18200E-01
            STROUHAL NUMBER C =     0.10000E-01
   CHARACTERISTIC FREQUENCY T =     0.14600E+02
                   P.P/Q.Q BA =     0.40000E-03
OVERALL FLUCTUATING PRESSURE LEVEL =  0.16211E+03
```

TYPICAL COMPUTER PRINT-OUT (continued)

MSC-049 SHUTTLE LAUNCH, MACH NO. 0.86, TRANS. SHOCK OSC. H/B TANK

FREQUENCY.	STR.	PHI.	PHI*	FPI.
0.100000E+01	0.684931E-03	0.185504E+03	0.173585E+01	0.143897E+03
0.125892E+01	0.862277E-03	0.183437E+03	0.171650E+01	0.144849E+03
0.158489E+01	0.108554E-02	0.180545E+03	0.168945E+01	0.145780E+03
0.199526E+01	0.136662E-02	0.176539E+03	0.165196E+01	0.146682E+03
0.251188E+01	0.172047E-02	0.171054E+03	0.160064E+01	0.147545E+03
0.316227E+01	0.216594E-02	0.163675E+03	0.153158E+01	0.148354E+03
0.398106E+01	0.272676E-02	0.153976E+03	0.144083E+01	0.149088E+03
0.501187E+01	0.343278E-02	0.141623E+03	0.132524E+01	0.149725E+03
0.630956E+01	0.432162E-02	0.126522E+03	0.118393E+01	0.150235E+03
0.794327E+01	0.544059E-02	0.108997E+03	0.101994E+01	0.150588E+03
0.999999E+01	0.684930E-02	0.899063E+02	0.841296E+00	0.150752E+03
0.125892E+02	0.862275E-02	0.705898E+02	0.660542E+00	0.150701E+03
0.158489E+02	0.108554E-01	0.525707E+02	0.491929E+00	0.150421E+03
0.199525E+02	0.136661E-01	0.371256E+02	0.347402E+00	0.149910E+03
0.251188E+02	0.172046E-01	0.249384E+02	0.233361E+00	0.149182E+03
0.316227E+02	0.216594E-01	0.160284E+02	0.149986E+00	0.148263E+03
0.398106E+02	0.272675E-01	0.993343E+01	0.929518E-01	0.147185E+03
0.501186E+02	0.343278E-01	0.598677E+01	0.560211E-01	0.145986E+03
0.630955E+02	0.432161E-01	0.353963E+01	0.331221E-01	0.144703E+03
0.794325E+02	0.544058E-01	0.207057E+01	0.193753E-01	0.143375E+03
0.999997E+02	0.684929E-01	0.120841E+01	0.113077E-01	0.142036E+03
0.125892E+03	0.862274E-01	0.709357E+00	0.663779E-02	0.140722E+03
0.158489E+03	0.108554E+00	0.422061E+00	0.394943E-02	0.139467E+03
0.199525E+03	0.136661E+00	0.256222E+00	0.239759E-02	0.138300E+03
0.251188E+03	0.172046E+00	0.159428E+00	0.149185E-02	0.137239E+03
0.316227E+03	0.216594E+00	0.101852E+00	0.953074E-03	0.136293E+03
0.398105E+03	0.272675E+00	0.667140E-01	0.624275E-03	0.135456E+03
0.501186E+03	0.343278E+00	0.446283E-01	0.417608E-03	0.134710E+03
0.630954E+03	0.432160E+00	0.303293E-01	0.283806E-03	0.134032E+03
0.794325E+03	0.544058E+00	0.208258E-01	0.194877E-03	0.133400E+03
0.999996E+03	0.684929E+00	0.143800E-01	0.134560E-03	0.132791E+03
0.125892E+04	0.862273E+00	0.994739E-02	0.930525E-04	0.132191E+03
0.158489E+04	0.108554E+01	0.687574E-02	0.643396E-04	0.131587E+03
0.199525E+04	0.136661E+01	0.474095E-02	0.443633E-04	0.130972E+03
0.251188E+04	0.172046E+01	0.325789E-02	0.304857E-04	0.130343E+03
0.316226E+04	0.216593E+01	0.223028E-02	0.208698E-04	0.129697E+03
0.398105E+04	0.272675E+01	0.152092E-02	0.142320E-04	0.129035E+03
0.501185E+04	0.343277E+01	0.103335E-02	0.966959E-05	0.128356E+03
0.630953E+04	0.432160E+01	0.699694E-03	0.654737E-05	0.127663E+03
0.794323E+04	0.544057E+01	0.472315E-03	0.441968E-05	0.126956E+03
0.999995E+04	0.684928E+01	0.317964E-03	0.297534E-05	0.126237E+03
f, Hz	$\frac{f\delta}{U}$	$\phi(f)$, psf^2/Hz	$\frac{\phi(f)\ U}{q_\infty^2\ \delta}$	OAFPL,dB

WYLE LABORATORIES
COMPUTER PROGRAM DESCRIPTION

Program Number:	73/003P-1
Author:	K. J. Plotkin
Date:	February 1973
Source Language:	FORTRAN IV-H
Computer:	XDS Sigma V

1.0 PROGRAM TITLE

Plume Separation

2.0 PURPOSE

Given axisymmetric launch vehicle and trajectory parameters, the program computes properties relative to plume-induced separation. This includes separation length and plateau pressure, plus various properties of the plume and parameters describing the coupling to the unsteady pressure field.

3.0 METHOD

The analytic models incorporated in this program are described in detail in Wyle Laboratories Research Staff Report WR 73-3.

4.0 COMPUTER CONFIGURATION

The required hardware is: XDS Sigma V computer with 16 k core, card reader, and line printer.

5.0 PUNCHED CARD INPUT

Vehicle and trajectory parameters are input in metric units. Specific format for each card is as follows:

Card 1 — Descriptive title of vehicle. Up to 80 alphameric characters

Card 2 — Columns 1-10: Vehicle radius, meters
Columns 11-20: Total thrust, Newtons
Columns 21-30: Plume drag to thrust ratio
Columns 31-40: Exhaust gamma
Columns 41-50: Exhaust Mach number
Columns 51-60: Engine chamber pressure, N/m^2

Format for each item on this card is F10.0.

Card 3 — Descriptive title of trajectory. Up to 80 alphameric characters

Card 4 — N, the number of trajectory points to be read and computations performed for. Format I5.

Cards 5 through 4+N — Trajectory parameters

Columns 1-15: Time After Lift-Off, seconds
Columns 16-30: Altitude, kilometers
Columns 31-45: Flight Mach number
Columns 46-60: Free-stream dynamic pressure, N/m^2

Format for each item on these cards is E15.10.

6.0 OUTPUT

The first items output are a table of atmospheric properties and a table of separation conditions contained in the program. This is followed by output of the vehicle parameters contained in Card 2, prefaced by the title input in Card 1. The title input in Card 3 is then printed, followed by a listing of the trajectory parameters input. Five (5) tables of computed properties are then printed. Each of these tables consists of the time after lift-off, followed by various properties. The printout is sufficiently annotated so as to be self-explanatory; the column headings are FORTRAN representations of various expressions defined in WR 73-3. A sample output list is presented herein. Written below each column is the exact notation used in WR 73-3, or a definition for those items not specifically denoted in the report.

It should be noted that the program does not explicitly indicate whether or not the flow is separated. The output listing must be examined to determine this. The computed values represent separated flow when the plume angle is greater than the separation angle. In the sample output, flow is not separated at 84 seconds, but is at all other computation times.

ATMOSPHERE TABLE

ALTITUDE	PINF	RHOINF
0.	0.620000000E+05	0.122499943E+01
2000.	0.795013750E+05	0.100659943E+01
4000.	0.616604102E+05	0.819349945E+00
6000.	0.472184570E+05	0.660109997E+00
8000.	0.356516016E+05	0.525789976E+00
10000.	0.264998242E+05	0.413509965E+00
12000.	0.193993750E+05	0.311939955E+00
14000.	0.141703984E+05	0.227859974E+00
16000.	0.103527773E+05	0.166469991E+00
18000.	0.756521094E+04	0.121649981E+00
20000.	0.552930469E+04	0.889099836E-01
22000.	0.404748755E+04	0.645099878E-01
24000.	0.297174023E+04	0.469379984E-01
26000.	0.218837646E+04	0.342569984E-01
28000.	0.161619409E+04	0.250759982E-01
30000.	0.119703296E+04	0.184099972E-01
32000.	0.889062988E+03	0.110649988E-01
34000.	0.663410689E+03	0.988739729E-02
36000.	0.498521729E+03	0.725789741E-02
38000.	0.377137695E+03	0.536659732E-02
40000.	0.287143799E+03	0.399569795E-02
42000.	0.219966415E+03	0.299479999E-02
44000.	0.169496445E+03	0.225889985E-02
46000.	0.131340485E+03	0.137140985E-02
48000.	0.102295685E+03	0.131669990E-02
50000.	0.797790222E+02	0.102689979E-02
52000.	0.622283173E+02	0.800969778E-03
54000.	0.484916992E+02	0.631369883E-03
56000.	0.376572266E+02	0.497619854E-03
58000.	0.291372986E+02	0.390859786E-03
60000.	0.224606018E+02	0.305919908E-03

SEPARATION CONDITIONS - CONE

MACH NO	THETA SEP	P SEP	M SEP
1	0.261999965E+00	0.200000000E+01	0.100000000E+01
2	0.226999998E+00	0.200000000E+01	0.152999973E+01
3	0.193959946E+00	0.221199989E+01	0.242999935E+01
4	0.208999991E+00	0.287999916E+01	0.311999989E+01
5	0.226999998E+00	0.400000000E+01	0.369999981E+01
6	0.252999961E+00	0.570999908E+01	0.400000000E+01
7	0.278999984E+00	0.829699993E+01	0.434999943E+01
8	0.349999964E+00	0.118669996E+02	0.434999943E+01

SATURN V S-1

VEHICLE RADIUS = 5.03000 THRUST = 0.36000000E+08 D/T = 0.66400

EXHAUST GAMMA = 1.23000 EXHAUST M = 3.70000 CHAMBER PRESSURE = 0.75000000E+07

APOLLO NOMINAL TRAJECTORY

TIME	ALTITUDE	MACH NUMBER	DYNAMIC PRESSURE
84.	0.155999994E+02	0.209999943E+01	0.358640000E+05
96.	0.212999878E+02	0.275999928E+01	0.242770000E+05
108.	0.280000000E+02	0.352999973E+01	0.142600000E+05
116.	0.330000000E+02	0.409999943E+01	0.926300000E+04
124.	0.385000000E+02	0.470999908E+01	0.573900000E+04
132.	0.443999939E+02	0.537999916E+01	0.345000000E+04
140.	0.508999939E+02	0.625000000E+01	0.207900000E+04
146.	0.561999969E+02	0.706999969E+01	0.135200000E+04

TIME	PLATEAU PRESSURE	SEPARATION ANGLE	PLUME ANGLE	PLUME RADIUS	SEPARATION LENGTH
84.	0.224682578E+05	0.223699987E+00	0.151439667E+00	0.463399315E+01	0.189401436E+01
96.	0.986794922E+04	0.201919913E+00	0.300406456E+00	0.591540432E+01	0.394262433E+00
108.	0.414721484E+04	0.201949894E+00	0.441606522E+00	0.797319221E+01	0.538860703E+01
116.	0.232249878E+04	0.210799932E+00	0.528182983E+00	0.100266342E+02	0.106239071E+02
124.	0.130336914E+04	0.221779943E+00	0.608844757E+00	0.128696766E+02	0.174737854E+02
132.	0.752641113E+03	0.236879885E+00	0.680773735E+00	0.167162933E+02	0.253306396E+02
140.	0.456930908E+03	0.259499907E+00	0.742449760E+00	0.216619415E+02	0.331582947E+02
146.	0.314571045E+03	0.283969879E+00	0.786437988E+00	0.269578094E+02	0.388448181E+02
	p_{sep}	θ_{sep}	θ_{pl}	r_p	ℓ_s

TIME	PRESSURE RATIO	DECIBEL LEVEL	CP PLATEAU
84.	0.202119923E+01	0.175101395E+03	0.316351473E+00
96.	0.216111946E+01	0.168488480E+03	0.218388557E+00
108.	0.256603509E+01	0.162065887E+03	0.177490890E+00
116.	0.299139772E+01	0.157785645E+03	0.166928828E+00
124.	0.367519855E+01	0.153542816E+03	0.165312767E+00
132.	0.466979744E+01	0.149428421E+03	0.171239257E+00
140.	0.635674858E+01	0.145710312E+03	0.185208976E+00
146.	0.854689749E+01	0.142873550E+03	0.205447912E+00

$\frac{p_{sep}}{p_\infty}$ $\quad 20 \log_{10} \frac{p_{sep}}{p_{ref}}$ $\quad \frac{p_{sep}}{q_\infty}$

$p_{ref} = 2 \times 10^{-5}\ N/m^2$

TIME	D(THETA)/D(P/G)	ROUT	D(LS/R)/D(TH)	D(LSEP)/D(P/G)
84.	0.304861069E+00	-0.877964020E+00	0.439383850E+02	-0.117604179E+02
96.	0.422470927E+00	0.237953186E+00	0.114205112E+02	0.114803369E+01
108.	0.531207035E+00	0.194610596E+01	0.547453022E+01	0.565948582E+01
116.	0.575587213E+00	0.358976173E+01	0.393731403E+01	0.813535786E+01
124.	0.594765842E+00	0.582362652E+01	0.305723953E+01	0.105893402E+02
132.	0.562625263E+00	0.878054428E+01	0.252437782E+01	0.129052601E+02
140.	0.547040522E+00	0.123869772E+02	0.218768406E+01	0.148241367E+02
146.	0.496226549E+00	0.159960012E+02	0.199585056E+01	0.158423433E+02

$$\frac{d\theta_{pl}}{d(p/q_\infty)} \qquad r_p \cos\left(\theta_{sep} + \theta_{reat}\right) - r_v \qquad \frac{1}{ROUT}\frac{d\ell_s}{d\theta_{pl}} \qquad \frac{d\ell_s}{d(p/q_\infty)}$$

TIME	D(TH)/D(PC)	D(LSEP)/D(RP)	D(LSEP)/D(PC)
84.	0.162083015E+01	-0.193291283E+01	-0.438583984E+02
96.	0.918365657E+00	0.147554111E+01	0.685991192E+01
108.	0.826199412E+00	0.242265129E+01	0.184604645E+02
116.	0.771784842E+00	0.254424381E+01	0.236635132E+02
124.	0.722375810E+00	0.253046703E+01	0.291444702E+02
132.	0.679276109E+00	0.240221119E+01	0.351344452E+02
140.	0.642588861E+00	0.215229702E+01	0.407356720E+02
146.	0.617461205E+00	0.189406109E+01	0.452426758E+02

NSTOP

$$\frac{d\theta_{pl}}{d\left(P_c/\langle P_c\rangle\right)} \qquad \frac{\partial l_s}{\partial r_p} \qquad \frac{d l_s}{d\left(P_c/\langle P_c\rangle\right)}$$